



Fakultät für Medizin

Abteilung für diagnostische und interventionelle Neuroradiologie

Spectral analysis of resting-state fMRI BOLD signal in healthy subjects and patients suffering from major depressive disorder

Anja Kaja Ries

Vollständiger Abdruck der von der Fakultät für Medizin der Technischen Universität München zur Erlangung des akademischen Grades eines

Doctor of Philosophy (Ph.D.)

genehmigten Dissertation.

Vorsitzende: Prof. Dr. Agnes Görlach

Betreuer: Prof. Dr. Claus Zimmer

Prüfer der Dissertation:

1. Prof. Dr. Gil Westmeyer
2. Priv.-Doz. Dr. Christine Preibisch

Die Dissertation wurde am 10.12.2018 bei der Fakultät für Medizin der Technischen Universität München eingereicht und durch die Fakultät für Medizin am 27.02.2019 angenommen.

To Mia Sophie.

Abstract

Ongoing brain activity manifests itself in fluctuations of the signal measured via resting-state functional magnetic resonance imaging (rs-fMRI). The use of rs-fMRI in humans has attracted enormous interest, as it allows the investigation of the ongoing (or resting-state) brain activity at a macroscopic level while mapping the brain in a non-invasive and in vivo way. Rs-fMRI measurements have shown that the ongoing brain activity is organized into characteristic large-scale patterns of coherent signal fluctuations (i.e., functional connectivity; FC) known as resting-state networks (RSNs). The brain's functional organization at rest is considered to underlie higher cognition and plays a crucial role in its healthy functioning. Respectively, altered resting-state activity has been observed in various neuropsychiatric disorders, including major depressive disorder (MDD)—one of the world's most burdensome diseases. MDD has been associated with alterations in FC across a wide range of RSNs. Crucially, rs-fMRI analysis holds the potential to complement and improve current diagnostic, therapeutic, and prevention strategies. To this end, the organizational principles of resting-state activity assessed via fMRI need to be understood in more detail, and the underlying causes of altered rs-fMRI FC in MDD need to be investigated from a more mechanistic perspective.

In this thesis, I perform spectral analyses on the rs-fMRI signal in healthy subjects and patients suffering from MDD, with the aim of contributing to a deeper understanding of the organizational principles of ongoing neural processes, and their breakdown in MDD. Specifically, I investigate what information is carried within distinct frequencies of the rs-fMRI signal—especially in its higher frequencies (i.e., > 0.1 Hz)—with regards to: (i) specialized, local processing (i.e., the spectral content of ongoing RSN signal fluctuations), and (ii) communication and information integration across brain regions (i.e., FC). I introduce a measure novel to the field of rs-fMRI analysis—the spectral centroid (SC)—which serves as an aggregate measure describing spectral characteristics of rs-fMRI signal fluctuations within RSNs and which can be applied to detect key changes associated with brain disorders. Using the SC, I examine whether spectral underpinnings of network fluctuations are distinct across RSNs and whether MDD is associated with spectral alterations within RSNs. Furthermore, I investigate frequency-specific FC patterns in healthy subjects and the respective aberrations related to MDD.

The results of this work reveal frequency-specific organizational principles of resting-state activity measured via fMRI regarding both specialized local processing as well as information integration across brain regions. MDD is found to be associated with altered spectral properties of a core RSN and with altered FC patterns of distinct brain regions at distinct frequency regimes. Importantly, these results stress the benefit of considering higher frequencies in rs-fMRI analysis, as they hold unique information about the functional organization of the brain at rest. Combined, my findings highlight the relevance of the frequency content to the organizational properties of resting-state activity and reveal frequency-dependent alterations in MDD. Shifting the focus of future rs-fMRI investigations towards frequency-resolved analyses has the potential to largely improve our understanding of ongoing neural processes and strengthen the validity of rs-fMRI in the clinical scenario.

Zusammenfassung

Intrinsische Gehirnaktivität unter Ruhebedingungen bildet sich ab in der funktionellen Magnetresonanztomographie, abgekürzt rs-fMRT. Das Verfahren der rs-fMRT hat im letzten Jahrzehnt immer weiter steigendes Interesse ausgelöst, da es ermöglicht, Hirnaktivität beim Menschen auf makroskopischer Ebene zu untersuchen und gleichzeitig das Gehirn auf nicht-invasive Weise, in vivo zu kartieren. Die mit fMRT gemessene Signalaktivität unter Ruhe organisiert sich in charakteristischen Mustern kohärenter Signalschwankungen, den sogenannten Resting-State-Netzwerken (RSNs vom Englischen resting-state networks). Bei diesen Kohärenzen zwischen unterschiedlichen Hirnarealen spricht man von der sogenannten funktionellen Konnektivität (abgekürzt FK). Die funktionelle Architektur des Gehirns im Ruhezustand gilt als Basis für höhere Kognition und spielt eine entscheidende Rolle für gesunde Hirnfunktion. Die depressive Störung (abgekürzt MDD, für englisch Major Depressive Disorder) stellt eine der weltweit prävalentesten schwerwiegenden Krankheiten dar. Zahlreiche Studien belegen, dass die Ruheaktivität des Gehirns bei MDD signifikante Veränderungen aufweist. Aufbauend auf diesen Befunden besteht die Hoffnung durch rs-fMRT-Analyse, die derzeitigen Diagnose-, Therapie- und Präventionsstrategien zu ergänzen und zu verbessern. Zu diesem Zweck müssen jedoch die organisatorischen Prinzipien der rs-fMRT-Signale genauer verstanden und die zugrundeliegenden Ursachen für Veränderungen in der FK bei MDD aus einer eher mechanistischen Perspektive untersucht werden.

In der vorliegenden Arbeit führe ich Spektralanalysen von rs-fMRT-Signal bei gesunden Probanden und Patienten mit MDD durch. Ziel dabei ist es, zu einem besseren Verständnis der Organisation laufender neuronaler Prozesse und deren Störungen bei MDD beizutragen. Hierfür untersuche ich, welche Informationen des rs-fMRT-Signals, insbesondere in den höheren Frequenzbereichen (d.h. > 0.1 Hz) ausschlaggebend sind in Bezug auf: (i) spezialisierte, lokale Signalverarbeitung (z.B. der Spektralgehalt laufender RSN-Signalschwankungen) und (ii) Kommunikation und Informationsintegration zwischen den Hirnarealen (bezüglich FK). Ich verwende ein—auf dem Gebiet der rs-fMRT-Analyse—neues Verfahren das auf dem Spectral Centroid (SC) beruht. Der SC dient als aggregiertes Maß, das die spektralen Eigenschaften von rs-fMRT-Signalschwankungen innerhalb von RSNs zusammenfasst. Gleichzeitig kann man wichtige Veränderungen verbunden mit Hirn-

erkrankungen mittels des SC erkennen. Ich untersuche die spektralen Eigenschaften von Signalschwankungen in RSNs, sowie frequenzspezifische funktionelle Konnektivitätsmuster bei gesunden Probanden und vergleiche sie mit den entsprechenden Veränderungen im Zusammenhang mit MDD.

Die Ergebnisse der vorliegenden Arbeit offenbaren frequenzabhängige Organisationsprinzipien der mit rs-fMRT erfassten Hirnaktivität, sowohl in Bezug auf die spezialisierte, lokale Signalverarbeitung innerhalb der RSNs, als auch auf die Informationsintegration zwischen unterschiedlichen Gehirnregionen. MDD ist sowohl mit veränderten spektralen Eigenschaften in einem Kern-RSN, als auch mit differenziell veränderten FK-Mustern über verschiedene Hirnregionen hinweg in den unterschiedlichen Frequenzregimen assoziiert. Die Ergebnisse machen deutlich, dass höhere Frequenzen des rs-fMRT-Signals zusätzliche Informationen über die funktionelle Organisation des Gehirns im Ruhezustand beinhalten und in die Analyse einbezogen werden sollten. Insgesamt betonen meine Ergebnisse die Relevanz des gesamten Frequenzspektrums des rs-fMRT-Signals, um Aussagen über die organisatorischen Eigenschaften der Ruheaktivität zu treffen und zeigen frequenzabhängige Veränderungen bei MDD. Eine Verlagerung des Fokus von künftigen Forschungsarbeiten bezüglich rs-fMRT von Standard- hin zu verstärkt frequenz aufgelösten Analysen könnte wesentlich dazu beitragen, unser Verständnis für laufende neuronale Prozesse zu verbessern und insbesondere auch die Validität der rs-fMRT im klinischen Szenario zu stärken.

Acknowledgements

First and foremost, I would like to express my deepest gratitude to my direct supervisor Dr. Afra Wohlschläger, who guided my research and continuously challenged me for the better. She has always been thoughtful and caring with her advice and she drove my passion and curiosity towards understanding the human brain. Her outstanding knowledge and her respectful attitude towards students shaped an excellent working environment.

I would also like to thank my advisor Prof. Dr. Claus Zimmer for providing me the unique opportunity to work at the Neuroradiology Department of the Klinikum rechts der Isar and to capitalize on the expertise of the outstanding scientists affiliated with this department, as well as on the advanced technical equipment. I wish to recognize the support of Dr. Christian Sorg who has always provided insightful feedback on my research. I would like to thank the members of my thesis committee Dr. Christine Preibisch and Prof. Dr. Gil Westmeyer for their guidance throughout this PhD project. I thank all my colleagues at the TUM-NIC for the good team spirit. Big thanks to Martin for his IT & coffee support. I would like to extend my appreciation to the Studienstiftung des deutschen Volkes for their financial support which enabled me to fully focus on my research. The broad repertoire of cultural and educational activities offered by the Studienstiftung was of equivalent importance.

My immense gratitude goes to my friends, scattered all around the world. The time spent with you was always a great remedy for the daily routine and the challenges associated with the PhD training. To my dear friends in Warsaw: Agatka, Dorka, Krzys, Mafa, Mateusz, Matylda, Zosia. Kocham! To Mari, Natalia, and the whole Boroni family, for making Brazil feel like home to me. Muito obrigada! To my "Munich" friends: Adriana, Amanda, Ebru, Francois, Jairo, Juci, Kyveli, Melanie, Natan, Siyi, for all the fun times and countless good memories. To Yue for keeping me company both during the long hours spent in the StaBi and the adventurous travels around the world!

From the bottom of my heart, I would like to thank my family for their love, their continuous support, and for shaping me to the person I am today. To my parents, who raised me and my brother Oliver to become independent and taught us what is

important in life. I am genuinely thankful to Oliver and Zhana for being there for me and for the time we spend together. To my niece, Mia Sophie, for bringing lots of love and joy to my life with every inch of her being. To Andi and Joana, and their newborn son Andreas, for being such a good company.

Last but by far not least, a very special thank you goes to my partner Immanuel, for being a truly open-hearted and caring person. He has always been there for me, knowing how to raise my spirits. Thank you for your countless small and big gestures, our memorable travels, and your tremendous support. All of it has been boosting my power to continue this work!

Thanks for all your encouragement!

Contents

1	Introduction	1
1.1	Timescales of brain activity	4
1.2	Resting-State fMRI	9
1.2.1	Organizational principles of rs-fMRI activity	9
1.2.2	Significance of rs-fMRI activity	11
1.2.3	Limitations of conventional rs-fMRI analyses	12
1.3	Mapping timescales of brain activity via rs-fMRI	13
1.3.1	Frequency range of neural contributions to the rs-fMRI signal	13
1.3.2	The relevance of high-frequency rs-fMRI signal to the healthy brain function	15
1.3.3	Multiple timescales of rs-fMRI signal dynamics shape functional integration	16
1.4	Major Depressive Disorder	19
1.5	New and noteworthy: the Spectral Centroid	22
2	Objectives	25
2.1	Project 1: Grading of frequency spectral centroid across resting-state networks in the healthy brain, and alterations in major depressive disorder	25
2.2	Project 2: Frequency-specific organization of functional hubs in the healthy brain, and alterations in major depressive disorder	26
3	Project 1	27
3.1	Materials and methods	27
3.1.1	Dataset 1: Human Connectome Project	27
	Participants & Data Acquisition	28
	Data Preprocessing	28
	Data Analysis	29
3.1.2	Dataset 2: Healthy Controls & MDD patients	32
	Participants	32
	Data Acquisition	33
	Data Preprocessing	33
	Data Analysis	36
3.1.3	Correspondence of network dynamics across datasets	41

3.2	Results	42
3.2.1	Dataset 1: Human Connectome Project	42
	Resting-State Networks	42
	Spectral Centroid	43
	Spectral Centroid and RSN size	43
3.2.2	Dataset 2: Healthy Controls & MDD patients	47
	Resting-State Networks	47
	Spectral Centroid	47
	Percent Signal Change	47
	Spectral Centroid corrected for PSC	49
	Saliency Network: spectral differences between groups	52
	Spectral Centroid and symptom severity	53
3.2.3	Correspondence of network dynamics across datasets	55
4	Project 2	57
4.1	Materials and methods	57
4.1.1	Participants & Data Acquisition	57
4.1.2	Data Preprocessing	57
	Physiologic noise and motion correction	57
	Normalization	59
	Nuisance covariates regression	59
4.1.3	Data Analysis	59
	Degree Centrality Maps	59
	Construction of Gray Matter Volume Covariates	60
	Statistical Analysis	61
	Degree Centrality and symptom severity	61
4.2	Results	62
4.2.1	Brain Volumetric Analysis	62
4.2.2	Healthy Controls: frequency-resolved Degree Centrality	63
4.2.3	MDD patients: alterations in frequency-resolved Degree Centrality	64
4.2.4	Degree Centrality and symptom severity	68
5	Discussion	71
5.1	Project 1	71
5.1.1	Grading of Spectral Centroid across RSNs	71
5.1.2	Biological relevance of Spectral Centroid grading	75
5.1.3	Grading of BOLD activity levels across RSNs	77
5.1.4	Biological relevance of BOLD activity level grading	77
5.2	Project 2	79
5.2.1	Frequency-specific spatial distribution of hubs in healthy subjects	79

5.2.2	Frequency-specific decreases in regional hubness in major depressive disorder	81
5.3	Limitations	87
6	Conclusions and Outlook	89
Appendix A	Project 1	93
Appendix B	Project 2	97
	References	105
	List of Figures	131
	List of Tables	132
	Acronyms	133
	CV	139
	Publications	141

Introduction

” *When we take a general view of the wonderful stream of our consciousness, what strikes us first is the different pace of its parts. Like a bird’s life, it seems to be made of an alternation of flights and perchings.*

— **William James**

To meet the dynamic demands posed by our environment, the human brain performs complex processes that span distinct neuronal ensembles and multiple timescales. An intact execution of higher cognitive functions largely depends on the accurate reconciliation of different timescales of neural processing within and across distinct functional brain networks.

This dependence was already conceptualized at the turn of the 19th century by William James—a leading philosopher and psychologist of his time. In his apt metaphor, James compares the stream of consciousness to the pace of the individual elements comprising a bird’s life: the flights and the perchings (James, 1890). This metaphor has been further interpreted by Deco et al. (2017) in the context of modern dynamical systems: the flights have been associated with fast, segregative processes and the perchings with slower, integrative processes in the brain. Functional segregation refers to the specialized processing undertaken by local neuronal populations, while functional integration—facilitated by the brain’s connectivity—refers to the synthesis of these distinct specialized processes and is crucial for the execution of brain functions (Friston, 1994; Friston, 2011).

These dynamic processes, it seems, are being largely undertaken by the supposedly "resting" brain—extrapolating from the vast metabolic demands of ongoing (synonyms: intrinsic, spontaneous) brain activity. The human brain, although it represents on average only 2% of total body mass, accounts for 20% of the body’s energy consumption—most of which (ca. 80%) is used to support ongoing neuronal signaling (Ames, 2000; Attwell and Laughlin, 2001; Lennie, 2003; Shulman et al., 2004).

Resting-state functional magnetic resonance imaging (rs-fMRI) is a powerful tool to explore the architecture of ongoing brain processes and the timescales of activity that shape it. This architecture can be assessed via slow (< 1 Hz) fluctuations of the blood oxygen level dependent (BOLD) signal, which coherently evolve over time across distinct brain regions, forming characteristic functional systems (Biswal et al., 1995). An intact architecture of ongoing BOLD activity is crucial for healthy brain functioning, and deviations from it have been implicated in various neuropsychiatric disorders (Buckholtz and Meyer-Lindenberg, 2012), including major depressive disorder (MDD)—one of the world’s most burdensome and societally costly brain disorders (Kessler, 2012; Murray et al., 2012).

These realizations have made rs-fMRI an exciting and rapidly growing research branch. Yet, most rs-fMRI analyses focus mainly on mapping the spatial distribution and strength of temporal correlations within the BOLD signal, by viewing the signal in a constrained, single bandwidth of, conventionally, 0.01–0.1 Hz. Recently, however, it has been suggested that the coherent patterns of rs-fMRI BOLD fluctuations across distinct brain regions are governed both in a broadband (i.e., spanning a relatively wide range of frequencies) and multiband (i.e., exhibiting distinct coherence patterns at distinct frequency sub-bands of the signal) fashion (Gohel and Biswal, 2015; Thompson and Fransson, 2015). In consequence, the existing body of research, although highly informative, may have ignored potentially important information carried within higher BOLD frequencies, and overlooked contributions of different frequency sub-bands to the functional brain architecture. This might have resulted in blurred sources of understanding of the ongoing brain processes assessed via rs-fMRI, and hindered the gain of a clearer picture of the functional alterations associated with brain disorders.

In this work, I examine whether spectral analysis of rs-fMRI BOLD signal within the full width of accessible frequencies offers more understanding of the architecture of ongoing neural processes. Specifically, I investigate what information is contained in selective frequencies of the rs-fMRI BOLD signal—and especially in its higher frequencies (i.e., > 0.1 Hz)—with regards to:

- (i) specialized, local processing (i.e., the spectral content of ongoing BOLD fluctuations within characteristic large-scale functional systems),
- (ii) communication and information integration across brain areas (i.e., functional connectivity).

The scope of my investigations covers both the healthy mode of brain functioning and—by the example of MDD—its perturbed mode. I hypothesize that in healthy

subjects, distinct large-scale functional systems—formed by the coherent ongoing BOLD activity—exhibit characteristic spectral underpinnings; and that different frequency regimes facilitate different patterns of information integration. Furthermore, I hypothesize that in MDD, deviations from the healthy functioning of the brain are reflected in an imbalance between the contributions of relatively slow and fast processes shaping the activity within functional systems, as well as in disrupted communication patterns within specific frequency regimes. Just as alterations in the pace of individual elements in a bird's life would largely affect the animal's behavior.

In the following sections, I will briefly introduce the broad array of oscillatory processes governed by the brain. I will outline how these processes can be captured using selected neuroimaging techniques, and discuss the related advantages and shortcomings. I will focus on the relevance of the very slow (i.e., < 1 Hz) processes to brain function, assessed using rs-fMRI. To this end, I will explain the basis of fMRI technique; how it can be applied to study large-scale, ongoing brain activity; which frequencies contribute to the rs-fMRI signal; and how different frequency regimes differentially shape the brain's functional architecture at rest. I will delineate alterations in rs-fMRI activity which are associated with MDD, with the main focus on alterations within large-scale functional systems. I will stress the shortcomings of the conventional analysis approaches applied in rs-fMRI in healthy subjects and MDD patients, and highlight the remaining knowledge gap. Importantly, I will propose a novel method for rs-fMRI signal analysis—based on the Spectral Centroid measure—which allows the assessment of spectral characteristics reflecting the ongoing activity within large-scale functional systems in a compacted manner and, consequently, enables the detection of key changes associated with brain disorders. In particular, the Spectral Centroid reflects the relative contributions of slow and fast processes to the activity of the "resting" brain.

1.1 Timescales of brain activity

The human brain is a large, complex, and highly efficient network that operates on a multitude of oscillatory timescales in support of its functions. The term "neural oscillations" or "brain rhythms" refers to the rhythmic electrical activity generated spontaneously and in response to stimuli by neuronal assemblies in the cortex (Buzsáki, 2006; Draguhn and Buzsáki, 2004). The mammalian brain generates a plethora of neural oscillations which range from very slow ones, with periods of tens of seconds, to very fast ones, with frequencies exceeding 600 Hz (Buzsáki, 2006). Communication within and between neuronal modules is facilitated through oscillatory synchronicity, i.e., coordinated rhythmic neuronal activity and coherent signal development over time (Fries, 2005; Fries, 2015; Womelsdorf et al., 2007; Buzsáki, 2006).

To systematically classify the broad array of brain rhythms, Buzsáki and colleagues recorded electrophysiological signals in rats and grouped the observed neural oscillations into ten "oscillation classes"—each representing a distinct frequency band, as depicted in Figure 1.1 (Penttonen and Buzsáki, 2003; Draguhn and Buzsáki, 2004). They observed that neural oscillation classes are arrayed linearly when plotted on a logarithmic scale. From this observation and from empirical evidence at higher frequencies they concluded that independent frequency bands are generated by distinct oscillators—each with specific properties and unique physiological functions. Moreover, a spatial regularity associated with these oscillator classes has been noted: fast oscillations tend to be confined to small neuronal assemblies, while slow oscillations recruit large-scale networks. Additionally, slower oscillations appear to group and modulate faster ones (Steriade et al., 2001; Vanhatalo et al., 2004).

Neural oscillations at distinct frequency bands have been extensively studied in humans and animals using various electrophysiological techniques—as these provide precise temporal information in the range of milliseconds. Neural oscillations have been shown to play an important role in all aspects of cognition and behavior (Başar et al., 2001; Draguhn and Buzsáki, 2004; Knyazev, 2007; Wang, 2010) and to be frequently altered in pathology (Fitzgerald and Watson, 2018; Voytek and Knight, 2015). However, the exact role of different oscillations in cognitive functions is still a topic of debate and remains largely unknown. In the following section, some major functions associated with different frequency domains will be summarized. Frequently, neural oscillations are believed to relate to three main functional roles: (i) coding specific information, (ii) setting and modulating attentional states, and (iii) assuring the communication between neuronal assemblies such that specific dynamic workspaces may be created (Lopes da Silva, 2013). Usually, the brain oscillations studied using electrophysiological techniques are subdivided into the following main

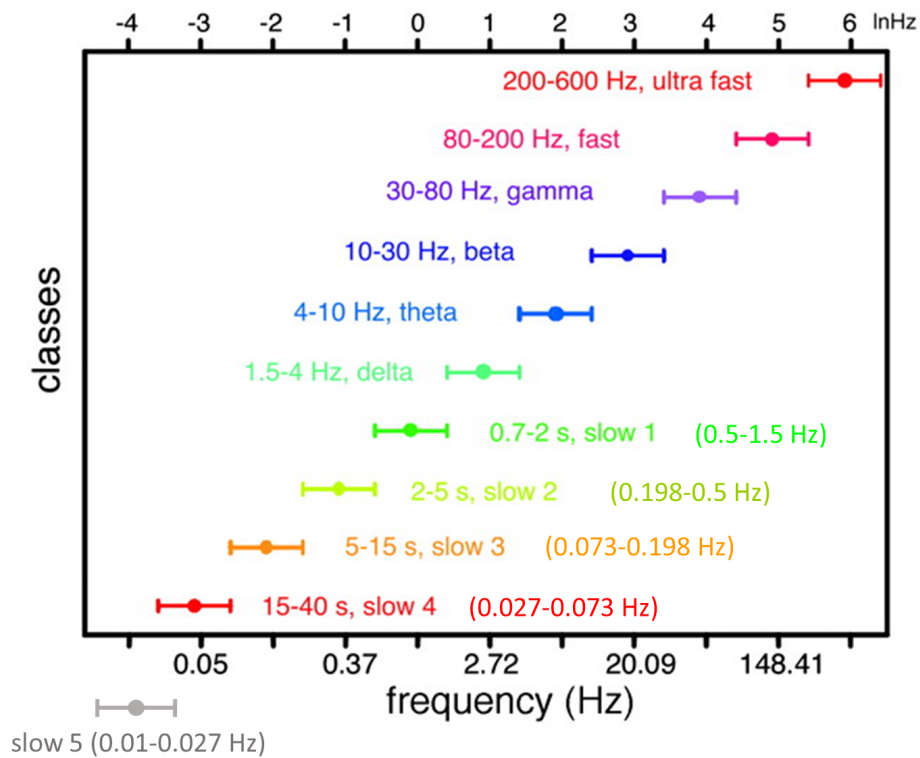


Fig. 1.1. | Rhythms of the brain. Oscillation classes in the cerebral cortex form a linear progression of the frequency bands on the logarithmic scale. For each band the frequency (Hz) ranges are shown together with their commonly used names. For the slow frequency bands (< 1.5 Hz) the period ranges are shown in addition. Modified figure and legend reprinted with permissions from Draguhn and Buzsáki (2004).

frequency bands (which complement and refine Buzsáki's nomenclature): delta (0.5–3.5 Hz), theta (4–7 Hz), alpha (8–12 Hz), beta (13–30 Hz), and gamma (30–80 Hz). The neural activity at individual frequency bands, as well as the complex cross-frequency interactions (Jensen and Colgin, 2007), have been associated with the following, selected functions. Delta oscillations are assumed to mediate signal detection and decision making (Başar et al., 2001; Schürmann et al., 2001), and are involved in motivational processes (Knyazev, 2007). Theta oscillations are often associated with memory processes and navigation (reviewed in Buzsáki and Moser, 2013; Colgin, 2013), as well as with emotional regulation (Knyazev, 2007). Specifically, theta rhythms have been shown to reflect processes of the working memory system (WMS) (Klimesch, 1996; Klimesch et al., 1997b; Klimesch et al., 2001; reviewed in Sauseng et al., 2010). Upper alpha oscillations (10–12 Hz) reflect information retrieval from the long-term memory system (LTMS), while

lower alpha oscillations (8–10 Hz) are being associated with transient increases in attentional demands (Başar et al., 1997; Klimesch, 1996; Klimesch et al., 1997a; Klimesch et al., 1997b). The exchange of information between WMS and LTMS is reflected by a specific interplay between theta and alpha rhythms (Sauseng et al., 2002). Beta oscillations are associated with preparation and inhibitory control in the motor system (Pfurtscheller et al., 1996). Gamma oscillations are believed to play a fundamental role in high-level cognitive functions such as attention (Fries et al., 2001; Gregoriou et al., 2009), memory (Carr et al., 2012; Colgin et al., 2009), and perception (Rodriguez et al., 1999; Melloni et al., 2007); leading to the hypothesis that gamma oscillations play a pivotal role for cortical processing (Fries, 2009; Tallon-Baudry, 2009). Moreover, gamma-frequency synchronization between neural ensembles is believed to play a crucial role for integration of sensory information (e.g., binding different attributes of a stimulus) (Singer and Gray, 1995; Singer, 1999; Uhlhaas et al., 2009). The coupling between theta and gamma oscillations is believed to integrate information into working memory representations (Sauseng et al., 2010).

On that note, much has been learned about the relevance of neural activity at different—although mostly high—frequency bands to brain function, using electrophysiology (for review see Lopes da Silva, 2013). Yet, these high-frequency sampling techniques suffer from either being—in terms of their spatial coverage—too narrow (e.g., single cell recordings; mostly applied in animal studies due to high invasiveness) or too unspecific (e.g., electroencephalography (EEG) recordings that capture the activity of millions of neurons only at the scalp surface, after which the inverse estimation of original sources remains problematic). As a consequence, the more precise spatial distribution of distinct oscillatory activity across functional systems remains ill-defined.

Furthermore, for a long time, EEG has been considered not to be suitable for the investigation of the very slow frequencies (< 0.5 Hz). The majority of EEG studies apply a band-pass filter of 0.5–50 Hz already during signal acquisition and thus discard the slow oscillations, as they are considered to represent noise. Only recently, a shift in EEG signal acquisition and analysis has been proposed, which expands the range of recorded frequencies both towards the lower end (i.e., slow oscillations < 0.5 Hz) and the higher end (i.e., fast oscillations > 50 Hz). This is known as direct-current-coupled full-band electroencephalography (DC fbEEG) (Vanhatalo et al., 2005). However, since this approach is relatively new, it is not yet being routinely applied, the literature is scarce, and standardized analysis pipelines are lacking. Thus, only very little information regarding these slow oscillations in humans is provided by EEG recordings.

Functional magnetic resonance imaging (fMRI), on the other hand, is well optimized for mapping brain functions across the whole brain at a good spatial resolution (1.5–3 mm voxels) in a non-invasive, in vivo manner. Although the temporal resolution of fMRI allows for the investigation of only a narrow range of frequencies, fMRI is highly optimized to capture the slow (0.1–1.5 Hz) and infra-slow (0.01–0.1 Hz) fluctuations of brain activity. These generally termed "slow" fluctuations represented in the rs-fMRI signal have become the focus of a large number of studies that map brain function, as they enable the investigation of the brain's large-scale functional architecture (Biswal et al., 1995; Greicius et al., 2003; Fox et al., 2005). Slow fluctuations in the rs-fMRI signal are temporally coherent within large-scale functional brain networks. These networks of coherent BOLD activity are believed to represent functional integration across distinct brain regions and thus appear to reflect a fundamental aspect of brain organization (Biswal et al., 1995; Fox and Raichle, 2007). In particular, the presence of low-frequency dynamics (i.e., 0.1–2 Hz) within specific brain networks is believed to constitute a key mechanism underlying attention, perception, and awareness (He and Raichle, 2009; Lakatos et al., 2008; Dehaene and Changeux, 2011). Combined, both the good spatial resolution of fMRI and its capacity to measure slow fluctuations in the brain, make this technique a powerful tool for exploring the spatial distribution of distinct, slow processes which lie at the core of large-scale information integration in the brain and, respectively, higher order brain processes.

fMRI is based on the BOLD contrast (Ogawa et al., 1990; Ogawa et al., 1992) which measures local changes in blood flow in response to elevated neuronal activity (hemodynamic response; Buckner et al., 1996; Buxton et al., 2004). The BOLD contrast capitalizes on the neurovascular coupling (i.e., the mechanism by which neuronal activity increases blood flow) (Buxton et al., 2004; Buxton, 2012) and the differences in magnetic properties of oxygenated and deoxygenated hemoglobin (Pauling and Coryell, 1936). Elevated neural activity within a brain region results in a brief, local "undershoot" in oxygenated hemoglobin—due to the energetic demands—and is subsequently followed by the dilation of blood vessels together with an increased inflow ("overshoot") of blood rich in oxygenated hemoglobin to that region. Thus, brain regions of elevated neural activity exhibit significant periods of increased blood flow and oxygenation. The oxygenated hemoglobin shows a slower MR signal decay rate ($T2^*$) compared to the deoxygenated hemoglobin, thus the signal from well-oxygenated regions results in a stronger MR signal intensity than areas lacking the increased blood flow. These are the electrophysiological underpinnings of the BOLD signal (Harris et al., 2011). Importantly, the BOLD signal is viewed as an indirect measure of neuronal activity.

Yet, the exact relation between hemodynamic responses, as measured with fMRI BOLD signal, and the underlying neural activity is not fully understood (Logothetis,

2008). The BOLD signal has been shown to strongly correlate with single-neuron activity, as well as with the local field potential (LFP) which reflects integrated electrical population-based activity in pre- and post-synaptic terminals (Goense and Logothetis, 2008; Logothetis et al., 2001; Logothetis, 2008; Lee et al., 2010; Mukamel et al., 2005). Importantly, infra-slow fluctuations (ISFs) observed both in the electrophysiological and BOLD signal were shown to correlate with the amplitude envelopes of simultaneously acquired, distinct EEG oscillations at higher frequencies, e.g., the gamma-, beta- and alpha-bands (Leopold et al., 2003; Shmuel and Leopold, 2008; Schölvinck et al., 2010; Jann et al., 2010; Goldman et al., 2002; Mantini et al., 2007; Sadaghiani et al., 2010). In addition to the correlation between the BOLD signal and the down-sampled, smoothed amplitude envelopes of high-frequency oscillations, the recent body of research revealed a direct relation between high-frequency neural activity and the BOLD signal (Kyathanahally et al., 2017; Lewis et al., 2016). On the other side, ISFs in the rs-fMRI BOLD signal also correlate with ISFs in scalp potentials (also termed slow cortical potentials; SCPs, 0.01–1 Hz) (He et al., 2008; He and Raichle, 2009; Hiltunen et al., 2014; Khader et al., 2008). Taken together, resting-state BOLD fluctuations of cortical and sub-cortical regions are believed to originate from intrinsic neural activity, and the temporal coherence between BOLD fluctuations of anatomically remote brain regions is believed to reflect the synchronization between the underlying neural activation patterns of these regions. Moreover, the BOLD signal seems to reflect distinct timescales of neuronal activity: the fast and slow processes—each playing a distinct role in the functioning of the brain. Thus, it is of high interest to investigate whether distinct frequency sub-bands of the BOLD signal also reflect differential contributions to the brain's functional architecture.

It is important to note, however, that fluctuations in the rs-fMRI BOLD signal are also largely driven by non-neuronal sources. Physiological noise, i.e., cardiac and respiratory rates, as well as head movement artifacts contribute to the rs-fMRI BOLD signal (for a review covering various noise sources in the fMRI signal, and approaches to mitigate noise effects, see Murphy et al., 2013 and Liu, 2016). Importantly, these non-neural sources may induce spurious patterns of BOLD signal coherence (Van Dijk et al., 2012; Murphy et al., 2013; Power et al., 2012). Despite the debate on whether coherent activity patterns in the BOLD signal originate solely from such non-neural noise contributions, evidence shows that large-scale functional systems do originate from neural processes (De Luca et al., 2006). However, special preprocessing procedures need to be applied to the BOLD signal to minimize the effects of noise artifacts, in order to identify the effects that are truly related to the underlying neuronal activity.

1.2 Resting-State fMRI

1.2.1 Organizational principles of rs-fMRI activity

BOLD time-series at rest (i.e., measured in the absence of external stimulation and response demands), assessed with fMRI at low frequencies (< 1 Hz), exhibit correlated activity between anatomically remote brain regions. Such temporal dependence is known as (resting-state) functional connectivity (FC) (Friston et al., 1996; Biswal et al., 1995). Consistent patterns of FC have been observed and categorized into different resting-state networks (RSNs) (Biswal et al., 1995; Fox et al., 2005; Fox and Raichle, 2007; Greicius et al., 2003; Beckmann et al., 2005; Damoiseaux et al., 2006; De Luca et al., 2006). RSNs closely relate to the underlying anatomical connectivity (Hagmann et al., 2008; Sporns et al., 2000), they strongly resemble task-related networks, and support brain functions such as attention, memory, task control, introspection, and sensory processes (Cole et al., 2013; Power et al., 2011; Yeo et al., 2011). RSNs show remarkable reproducibility across individuals (Damoiseaux et al., 2006), ages (Fransson et al., 2007), subject states (Liu et al., 2008; Greicius et al., 2008), or species (Vincent et al., 2007; Lu et al., 2012; Jonckers et al., 2011). Core RSNs include the default-mode network (DMN) (Buckner et al., 2008; Raichle et al., 2001; Greicius et al., 2003), the salience network (SN) (Menon and Uddin, 2010; Seeley et al., 2007), and the central executive network (CEN) (Seeley et al., 2007; Vincent et al., 2008). Additional RSNs such as the attentional, visual, auditory and sensorimotor networks have been identified (Fox et al., 2006; Biswal et al., 1995; Cordes et al., 2000; Eckert et al., 2008; Bianciardi et al., 2009). Examples of RSNs are shown in figure 1.2.A.

Independent component analysis (ICA) is a powerful signal analysis method used for the identification and exploration of consistent FC patterns of BOLD fluctuations in the resting brain (Beckmann et al., 2005; Calhoun et al., 2001; Calhoun et al., 2009; Kiviniemi et al., 2003). Spatial ICA—the ICA variant most commonly used in rs-fMRI—is a model-free, data-driven approach used to decompose the whole-brain fMRI data into systematically non-overlapping, temporally coherent components; each associated with a spatial map and a BOLD time course. These independent components (ICs) can be later categorized into components that represent RSNs and components that represent physiological and movement artifacts. The categorization of ICs into RSNs of interest can be facilitated by the use of established RSN templates (e.g. Allen et al., 2011; Yeo et al., 2011). Example BOLD power spectra of RSNs and physiological noise components are presented in Figure 1.2.B.

Brain function, particularly higher cognitive processes, require the integrated action of many, sometimes highly distributed specialized brain regions. Information

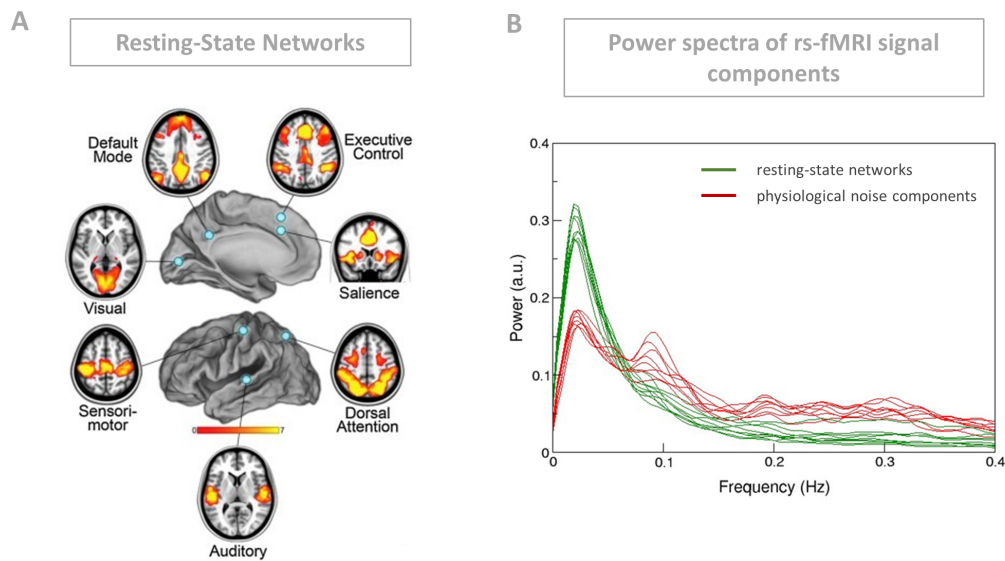


Fig. 1.2. | **Example RSNs and their power spectra.** (A) Example spatial maps of seven major resting-state networks (RSNs), assessed via measures of functional connectivity. Modified figure reprinted from Raichle, 2011, with permission of Mary Ann Liebert, Inc. Publishers, Copyright 2011, Mary Ann Liebert, Inc. (B) Comparison of the mean spectral distribution of diverse RSNs (shown in green) and various physiological noise components (shown in red). Modified figure and legend taken from Boubela et al. (2014), distributed under the terms of the Creative Commons Attribution License (CC BY).

needs to be efficiently integrated both between specialized regions within the same functional system (i.e., within a RSN) as well as between regions of functionally distinct systems (i.e., between RSNs). Such operations are facilitated by functional hubs—i.e., highly connected brain regions. Biological systems—including the brain—can be represented as complex networks and examined by use of graph theoretical measures. The brain can be viewed as a graph consisting of a number of nodes (i.e., brain regions) and edges linking the nodes (i.e., functional connectivity between brain regions) (Salvador et al., 2005; Sporns et al., 2000; Bassett and Bullmore, 2006; Bullmore and Sporns, 2009; Bullmore and Sporns, 2012). Examining the topological properties of such a graph provides essential information about the brain’s organization and function (Sporns et al., 2004), since the topology of a network is directly linked to its level of robustness, its capability to integrate information, and its communication efficiency (Draguhn and Buzsáki, 2004; Latora and Marchiori, 2001; Mathias and Gopal, 2001).

FMRI studies using graph-theoretical approaches revealed that the functional organization of large-scale brain activity at rest exhibits properties of a scale-free, small-world network (Bullmore and Sporns, 2009; van den Heuvel et al., 2008; Sal-

vador et al., 2005; Eguíluz et al., 2005; Achard et al., 2006). Small-world networks (Watts and Strogatz, 1998) are characterized by a high level of clustering (i.e., high probability that two nodes which are directly connected to a third node will also be directly connected to each other) and a short average path length (i.e., the average distance from node to node). Scale-free networks (Barabási and Albert, 1999; Barabási and Bonabeau, 2003; Barabási, 2009) are characterized by a low number of connections per node, on average, along with the occurrence of a small number of highly connected nodes (hubs) which ensure a high level of global connectivity.

The scale-free, small-world regime has been hypothesized to constitute an optimal topographic constellation for brain functioning, as it reflects a balance between local processing and global integration in the human brain (Sporns et al., 2004). Hubs are prominent in such a constellation and play an important role for information integration and flow—by mediating interactions among distinct brain regions and networks (Buckner et al., 2009; Fransson and Marrelec, 2008; Nijhuis et al., 2013; Power et al., 2013; Zuo et al., 2012). Hubs can be identified by means of their degree centrality (DC)—a graph theoretical measure that reflects the overall connectedness of a given region to the rest of the brain (Buckner et al., 2009; Takeuchi et al., 2015; Tomasi and Volkow, 2010). High-centrality hubs entail high energetic and metabolic demands (Bullmore and Sporns, 2012), possess the highest level of neural activity (Haan et al., 2012), and constitute points of increased vulnerability to brain damage and neurodegenerative disorders (Buckner et al., 2009; Crossley et al., 2014; Sperling et al., 2009).

1.2.2 Significance of rs-fMRI activity

Exploration of FC and network topology of the human brain by means of rs-fMRI has become a major topic in neuroscience (Deco et al., 2011; Fox and Raichle, 2007; Lowe, 2012; Raichle, 2015). Rs-fMRI FC patterns have been shown to underlie behavioral and cognitive variability (Fox et al., 2007; Hampson et al., 2006; Kasagi et al., 2017); relate to personality traits (Dubois et al., 2018; Nostro et al., 2018) and intelligence (Schultz and Cole, 2016). Rs-fMRI FC can even act as a "fingerprint" to accurately identify subjects from a large group of individuals (Finn et al., 2015). Alterations in the brain's functional architecture have been observed following pharmacological intervention (Tagliazucchi et al., 2016; Boveroux et al., 2010), throughout learning processes (Lewis et al., 2009), and across developmental stages (Hoff et al., 2013; Sala-Llonch et al., 2015). Importantly, RSN integrity has been shown to be essential to healthy brain function (Zhang and Raichle, 2010; Cole et al., 2014; Greicius et al., 2008; He et al., 2007; Alexander-Bloch et al., 2018). Aberrant rs-fMRI FC patterns have been widely observed in a number of neurological and psychiatric diseases, and summarized using meta-analytic approaches, including

Alzheimer's disease (Badhwar et al., 2017), schizophrenia (Dong et al., 2018), obsessive-compulsive disorder (OCD) (Gürsel et al., 2018), and MDD (Kaiser et al., 2015; Zhong et al., 2016). To conclude, rs-fMRI is highly suitable for investigating the ongoing, large-scale functional brain architecture, and proves to be a highly informative tool that could be used in a clinical context (Fischer et al., 2016; Fox and Greicius, 2010). However, there are some limitations concerning the conventionally applied analyses approaches, and overcoming them could provide a more detailed understanding of the brain's functional architecture and its alterations in brain disorders.

1.2.3 Limitations of conventional rs-fMRI analyses

A major caveat in rs-fMRI analyses is that studies examining resting-state FC employ an approach where the BOLD signal is investigated within a single, previously band-pass filtered frequency range of, typically, 0.01–0.1 Hz. Although these studies have contributed an exceptional understanding of the brain's functional organization at rest, their approach is limited in a twofold manner:

1. The frequency range of 0.01–0.1 Hz is a relatively narrow one, given the full frequency span accessible from the rs-fMRI signal (depending on acquisition parameters, frequencies can span up to 0.25 Hz and higher). As such, it neglects the information content carried in higher frequencies within the ongoing BOLD signal (i.e., > 0.1 Hz).
2. By analyzing FC patterns across one single frequency band (i.e., 0.01–0.1 Hz), the representation of different neural processes carried within distinct frequency sub-bands is being fused together.

Moreover, the majority of rs-fMRI studies focus solely on the spatial distribution of FC patterns and their respective alterations in disease, but usually do not examine the underlying spectral characteristics of the BOLD signal, and thus, do not delineate the mechanisms which underlie the FC formation and its breakdown. As a result, there are many, often divergent, reports of altered FC in a number of neurological and psychiatric disorders, but the mechanistic causes remain elusive.

In recent years, the need for a shift in rs-fMRI analysis has become prominent. A large body of research suggests that RSNs operate on a much broader frequency range than the one conventionally investigated. In particular, the spotlight has been placed on the higher frequencies of the ongoing BOLD signal (i.e., < 0.1 Hz), highlighting their relevance to healthy brain function. Additionally, the need for frequency-resolved analyses of the BOLD signal has been stressed, as different frequency sub-bands

of the BOLD signal differentially contribute to the functional organization of the brain. Importantly, it became clear that the spectral underpinnings of RSNs BOLD fluctuations need to be explored in a more systematic fashion. Especially, future work needs to explore which frequencies—and to what extent—contribute to the RSN BOLD fluctuations, and how these are changed in disease. In the following sections, I will introduce the range of frequencies in the rs-fMRI BOLD signal that shape RSN activity, and explain how distinct regional and network dynamics, as well as distinct FC patterns, are manifested through distinct sub-bands within this frequency range.

1.3 Mapping timescales of brain activity via rs-fMRI

1.3.1 Frequency range of neural contributions to the rs-fMRI signal

Usually, rs-fMRI data is acquired during scans of approximately 5–15 minutes, with a relatively long repetition time (TR) of commonly 2–3 seconds. Depending on the acquisition parameters, detected frequencies of resting-state BOLD fluctuations typically fall within the range of 0.001–0.25 Hz (as in the case of TR = 2 s). Technical advances in fMRI data acquisition, such as the introduction of multiband EPI sequences (Feinberg et al., 2010; Feinberg and Yacoub, 2012; Moeller et al., 2010), enable the mapping of brain function at a much shorter TR (e.g., < 1 s) and, respectively, widen the span of accessible frequencies of the BOLD signal towards higher frequencies (e.g., > 0.25 Hz).

Despite this relatively broad range of frequencies in the BOLD signal at rest, most rs-fMRI studies have focused on the single, narrowed-down frequency band of 0.01–0.1 Hz (or even 0.01–0.08 Hz) (Biswal et al., 1995; Cordes et al., 2001; Cordes et al., 2002; Fox and Raichle, 2007; Greicius et al., 2003; Lowe et al., 1998). Classically, the rs-fMRI signal is band-pass filtered into this frequency range; as the lowest frequencies (0.001–0.009 Hz) are largely influenced by scanner noise which cannot be fully accounted for, and higher frequencies (> 0.1 Hz) are believed to predominantly originate from non-neuronal sources (i.e., respiration and cardiac signals; Birn et al., 2006; Wise et al., 2004). Consequently, the majority of rs-fMRI studies which aim at investigating the functional organization of the brain at rest, ignore the high-frequency BOLD dynamics which, as later shown, contain meaningful features of neuronal activity.

This conventional approach was motivated by the following observations: Firstly, the power spectra of RSN BOLD fluctuations roughly follow a $1/f$ power-law scaling (He, 2011), exhibiting highest contributions of power at frequencies < 0.1 Hz, while the power continuously decreases with increasing frequencies (see figure 1.2.B). Secondly, early investigations on the relative contributions of different BOLD frequencies to the resting-state FC yielded that signal correlations within the auditory, sensorimotor and visual cortices were almost exclusively driven by frequencies < 0.1 Hz, while higher frequencies only contributed to the correlations between signals from major arteries and veins, as well as the cerebrospinal fluid (CSF) (Cordes et al., 2001). Lastly, the standard model of convolving neural activity with a hemodynamic response function (which is delayed by 3–10 s compared to neural activity) suggests that the signal of interest in fMRI should be carried by the low frequencies (Aguirre et al., 1998). Altogether, these observations have led to the general characterization of RSNs as networks of low-frequency fluctuations, conventionally between 0.01–0.1 Hz.

However, recent studies viewing spectral properties of rs-fMRI BOLD fluctuations show that characteristic connectivity patterns corresponding to RSNs can be detected at multiple frequency bands, including high frequencies up to 0.25 Hz (Wu et al., 2008; Niazy et al., 2011; van Oort et al., 2012), up to 0.75 Hz (Gohel and Biswal, 2015; Chen and Glover, 2015), or even higher (Boubela et al., 2013; Lee et al., 2013). An additional body of research further suggests that the conventionally discarded frequency bands might provide important insights on brain activity (Boyacioglu and Barth, 2013; Liao et al., 2013; Sasai et al., 2014; Thompson and Fransson, 2015; Lewis et al., 2016). Thus, convincing evidence is provided that the frequency range of fluctuations attributable to RSNs is broader than conventionally assumed, and higher frequencies also contain meaningful information of neuronal origin and should be investigated in more detail.

As a consequence, the application of classical band-pass filters in the rs-fMRI signal analysis should be reconsidered, as it eliminates potentially relevant information about ongoing activity at higher frequencies. On another note, accounting for high-frequency noise by using band-pass filters has been questioned. It has been shown that in rs-fMRI, without applying a sufficiently high sampling rate, a significant amount of high-frequency physiological noise is folded into the very low-frequency range (< 0.1 Hz) (Robinson et al., 2009; Bhattacharyya and Lowe, 2004) (see 1.2.B). Instead, more specific methods for the elimination of physiological noise have been proposed, for example, the regression of physiological signal components (Beall and Lowe, 2007; Glover et al., 2000).

1.3.2 The relevance of high-frequency rs-fMRI signal to the healthy brain function

Not only do higher frequencies of the BOLD signal represent meaningful processes of neuronal origin, they also largely contribute to the healthy functioning of the brain. Crucially, the intact balance between high and low frequencies of the BOLD signal has been shown to be essential for healthy brain functioning and consciousness.

Huang et al. (2018) examined timescales of neural processing acquired with rs-fMRI during wakefulness, under different states of unconsciousness, and in disorders of consciousness (DOC). Outcomes of their study indicate that states of light sedation resulted in the slowing of the BOLD signal, manifested by elevated power at the lower end of the frequency spectrum and decreased power at relatively "higher" frequencies (it is important to note, however, that the frequency range of analyzed frequencies lay in the classical band of 0.01–0.1 Hz). Conversely, under deep anesthesia and in DOC, a speeding up of intrinsic activity was observed, which was manifested by decreased power at lower frequencies and increased power at higher frequencies (see figure 1.3.A). Moreover, they observed that changes in the dynamics of BOLD fluctuations were followed by changes in local and global FC and brain topology.

Similarly, in various neuropsychiatric disorders, an imbalance between the contributions of low- and high-frequency power to the regional as well as network-wide resting-state BOLD signal has been revealed by studies investigating the full range of accessible frequencies (also > 0.1 Hz). A general tendency of increased power at the higher end of the frequency spectrum, often accompanied by decreased power at the lower end of the frequency spectrum has been observed. Such altered BOLD dynamics were observed in the insula and anterior cingulate cortex (ACC) (Malinen et al., 2010) (see figure 1.3.B), as well as in the DMN (Baliki et al., 2011) in chronic pain patients; as well as across several RSNs in schizophrenia and bipolar disorder (Calhoun et al., 2011; Garrity et al., 2007) (see figure 1.3.C). Further reports of altered high-frequency BOLD dynamics in diseased states have been made (Otti et al., 2013; Hong et al., 2013; Cauda et al., 2009). However, the contributions of low and high frequencies to the resting-state BOLD signal in MDD have not yet been investigated. Since many psychiatric disorders overlap with each other in terms of symptomatology and share common neurobiological substrates (Goodkind et al., 2015), it stands to reason to expect similar changes in MDD.

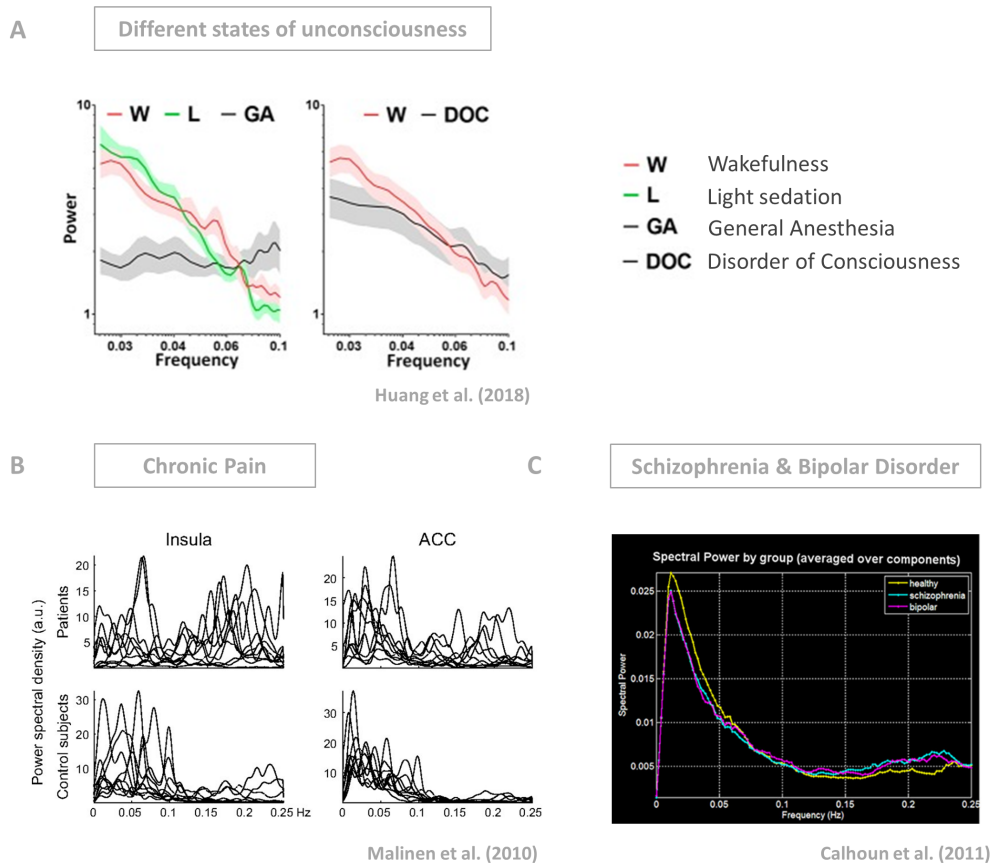


Fig. 1.3. | **BOLD power spectra under different pharmacologic and neuropathologic conditions.** Altered spectral distributions of the BOLD signal in: (A) different states of unconsciousness (modified figure taken from Huang et al. (2018), distributed under the terms of the CC BY); (B) chronic pain (modified figure taken from Malinen et al. (2010), Copyright (2010) National Academy of Sciences); and (C) schizophrenia and bipolar disorder (modified figure taken from Calhoun et al. (2011), distributed under the terms of the CC BY).

1.3.3 Multiple timescales of rs-fMRI signal dynamics shape functional integration

Having discussed the range of frequencies in the rs-fMRI BOLD signal which carry meaningful neural information, it is important to further reflect upon the different processes executed at distinct frequency sub-bands within the broad spectrum of rs-fMRI BOLD fluctuations. The second methodological restriction of the majority of rs-fMRI studies is that FC patterns are mostly analyzed across one single frequency band (typically 0.01–0.1 Hz), without distinction into specific frequency sub-bands. Given the differential role of distinct neuronal oscillation classes to brain function (Buzsáki, 2006; Penttonen and Buzsáki, 2003; Draguhn and Buzsáki, 2004; Knyazev,

2007)—combined with the assumption that BOLD fluctuations reflect the underlying neuronal dynamics—it stands to reason that different frequencies of the BOLD signal would differentially shape the brain’s large-scale organization.

In the nomenclature of Buzsáki and colleagues, slow neuronal oscillations were further subdivided into distinct frequency bands: slow-5: 0.01–0.027 Hz, slow-4: 0.027–0.073 Hz, slow-3: 0.073–0.198 Hz, slow-2: 0.198–0.5 Hz, slow-1: 0.5–1.5 Hz (see Figure 1.1), each believed to be generated by distinct oscillators and serving different functions. The span of neurally meaningful frequencies detected in the rs-fMRI BOLD signal covers the slow-5 to slow-2 classes as well as part of slow-1 (given a sufficiently high sampling rate). Thus, at least five distinct frequency bands of rs-fMRI BOLD fluctuations could also reflect distinct neuronal processes, and differentially shape the brain’s functional architecture. Indeed, recent studies investigating spectral contributions to the BOLD signal in distinct brain regions, as well as the frequency-specific FC, shed more light on the resting-state functional architecture which evolves over multiple timescales.

A hierarchy of timescales of neural dynamics has been observed in the human brain. Prior work revealed that during various task demands, information integration across spatially distinct neural circuits evolves on different timescales (Baldassano et al., 2017; Ding et al., 2016; Hasson et al., 2008; Hasson et al., 2015; Lerner et al., 2011). Primary sensory areas were found to encode instantaneous, rapidly changing information (in the order of milliseconds to seconds), whereas transmodal association areas were shown to encode information accumulated over a longer time (in the order of seconds, minutes, or longer). Such spatial distribution of oscillatory timescales has been termed "sensorimotor-to-transmodal gradient" (for review see Huntenburg et al., 2018). Importantly, such temporal hierarchy of information integration during tasks relates to timescales of ongoing (i.e., resting-state) cortical dynamics, as shown in human electrocorticography (ECoG) (Honey et al., 2012) and fMRI (Stephens et al., 2013) studies, as well as in single-cell recordings in primates (Murray et al., 2014). Respectively, early sensory areas that accumulate information over shorter timescales were found to exhibit faster resting-state fluctuations, while transmodal areas that accumulate information over longer timescales showed slower resting-state fluctuations. Numerous other studies in humans and primates further support the notion of a hierarchy of resting-state timescales across individual cortical regions (Baria et al., 2011; Chaudhuri et al., 2015; Cocchi et al., 2016).

With respect to the spatial organization of ongoing dynamics of individual cortical regions, the ongoing activity of large-scale networks, assessed with rs-fMRI, was also shown to be largely shaped by the temporal domain. Both FC within- and between-RSNs, as well as the resulting network topology and presence of functional hubs were shown to be governed in a frequency-specific manner (De Domenico

et al., 2016; Gohel and Biswal, 2015; Salvador et al., 2008; Sasai et al., 2014; Thompson and Fransson, 2015; Wu et al., 2008; Zuo et al., 2010; Chen and Glover, 2015). In particular, BOLD signals from different brain regions and networks were shown to exhibit different power contributions at distinct frequency sub-bands. Graph properties were found to alternate across different frequencies, with small-world network topology peaking at specific frequencies, and stronger information integration or segregation being promoted at distinct frequency regimes.

More recently, Gollo et al. (2017) suggested that a hierarchy of timescales organizes activity between RSNs (with higher order networks showing a slower regime of activity and sensory networks faster neural dynamics) and within RSNs (with highly connected regions of a network showing slower dynamics than less interconnected, peripheral regions). Furthermore, a relation between the frequency regime and directionality of information flow has been made (Cocchi et al., 2016; Neufang et al., 2014). Altogether, the hierarchy of neural timescales is believed to enable the brain to link multiple timescales of perception and to construct a temporal continuum of conscious experience (Northoff and Huang, 2017). Correspondingly, frequency specific alterations in rs-fMRI activity and FC have been reported in a number of brain disorders (Meda et al., 2015; Qian et al., 2017; Wang et al., 2015; Wang et al., 2017; Zhang et al., 2015; Zhang et al., 2017; Chen et al., 2015; Xu et al., 2016), including MDD (Luo et al., 2015; Xue et al., 2016; Wang et al., 2016).

Thus, a large body of evidence hints at differential functional contributions of processes reflected by segregated spectral ranges of rs-fMRI BOLD fluctuations. Functional integration between distinct brain areas occurs over multiple frequency bands in the rs-fMRI BOLD signal, and distinct connectivity patterns are promoted at distinct frequency bands. Considering these findings, it is crucial to investigate the brain's functional organization in a frequency-resolved fashion.

However, the current literature does not provide a unified picture regarding the frequency-specific functional architecture of the brain. Firstly, there are some discrepancies in terms of which frequencies were investigated; whether the classical band of 0.01–0.1 Hz was used, or whether higher frequencies were also considered. Secondly, the division of the frequency width of the BOLD signal into distinct sub-bands also varies between studies. Most frequently, studies investigating frequency-resolved rs-fMRI activity divide the BOLD signal into distinct frequency sub-bands according to the low-frequency intervals defined by Buzsáki and colleagues. However, as these frequency intervals were derived from electrophysiological studies in animals, and not from the BOLD signal itself, they may not constitute the optimal division in the context of the BOLD signal. Moreover, these frequency intervals are rather broad and applying them might still merge distinct processes together. Thus, applying much narrower frequency sub-bands could reveal different, more fine-grained functional

organizational principles of the brain (Baria et al., 2011; Thompson and Fransson, 2015).

In MDD specifically, only three studies report frequency-dependent alterations in FC. One of these three studies operates on the conventional, narrow frequency band of 0.01–0.08 Hz (Xue et al., 2016), and the other two—although they consider higher frequencies (i.e., > 0.1 Hz)—use rather broad frequency intervals (Luo et al., 2015; Wang et al., 2016) when dividing the BOLD signal into frequency sub-bands. Thus, more research investigating the architecture of ongoing brain activity in MDD is needed, especially under consideration of the full span of accessible frequencies of the BOLD signal along with a frequency subdivision at a higher resolution.

1.4 Major Depressive Disorder

Major depressive disorder has been ranked as one of the most burdensome diseases in the world in terms of total disability-adjusted life years (Murray et al., 2012), affecting various aspects of life and work in more than 300 million people worldwide (WHO, 2017). MDD is a complex, heterogeneous disorder comprised of many symptoms, each of which likely involves distinct neural circuits. MDD is characterized by single or recurrent major depressive episodes during which patients experience depressed mood, impaired cognition, energy loss, vegetative symptoms, and suicidal thoughts (American Psychiatric Association, 2013). From the societal and economic perspective, MDD is considered the most costly psychiatric disorder and is accompanied by an alarmingly high personal cost in terms of death by suicide (Alonso et al., 2004; Nordentoft et al., 2011; Murray et al., 2012). Up to date, the predominant method of diagnosis in MDD is based on psychiatric interviews and patients' self-reports, and there is still the need for more objective and quantifiable procedures. The ever-increasing amount of brain imaging studies viewing depression highlights the relevance of the functional organization of large-scale brain systems to MDD pathophysiology. Neuroimaging approaches are used in the attempt to reveal informative and putatively more accurate diagnostic, therapeutic, and prevention strategies in MDD—by investigating the underlying neural circuitry and disease mechanisms—which could supplement the currently available procedures (Drysdale et al., 2017; Fischer et al., 2016).

Neuroimaging studies in MDD report alterations in brain structure (Bora et al., 2012; Koolschijn et al., 2009), neurochemistry (Dunlop and Nemeroff, 2007; Savitz and Drevets, 2013; Sanacora et al., 2002; Belujon and Grace, 2017) and function (Diener et al., 2012; Hamilton et al., 2012; Pizzagalli, 2011); for an integrative summary of neuroimaging studies in MDD see Treadway and Pizzagalli (2014).

Structural changes brought by MDD are reflected in, for example, gray matter volume (GMV) abnormalities, predominantly in the hippocampus, anterior cingulate cortex (ACC), medial prefrontal cortex (mPFC), orbitofrontal cortex (OFC), dorsolateral prefrontal cortex (dlPFC), the striatum, and the amygdala (Hamilton et al., 2008; Kempton et al., 2011). From the neurochemical perspective, the brain's monoaminergic systems (serotonergic, noradrenergic and dopaminergic) have been the center of attention in neurobiological studies of depression, and most therapeutics target these systems. In recent years, however, the pivotal role of both the glutamatergic (Jun et al., 2014; Mathews et al., 2012; Sanacora et al., 2012) and GABAergic (Luscher et al., 2011; Tunnicliff and Malatynska, 2003) systems to the neurobiology and treatment of MDD has been highlighted. These are, respectively, the major excitatory and inhibitory neurotransmitter systems in the brain. Furthermore, MDD affects the proper execution of a number of brain functions such as emotion regulation, reward processing, cognitive control and affective cognition (Hamilton et al., 2012; Kerestes et al., 2014). Such a broad spectrum of brain functional abnormalities further suggests that MDD is a complex brain disorder and that its pathophysiology entails multiple brain circuits and networks (Pandya et al., 2012).

Importantly, widely distributed aberrations in rs-fMRI FC patterns and the resulting network topology were shown to underlie MDD (Belleau et al., 2015; Greicius et al., 2007; Manoliu et al., 2013; Northoff et al., 2011; Sheline et al., 2009; Hamilton et al., 2011; Meng et al., 2014; Veer et al., 2010). Findings of altered rs-fMRI FC in MDD have been thoroughly reviewed (Dichter et al., 2015; Dutta et al., 2014; Mulders et al., 2015; Wang et al., 2012) and several meta-analyses have been performed (Kaiser et al., 2015; Zhong et al., 2016). These studies highlight a large number of RSNs which exhibit aberrant FC in MDD. Observations are often discrepant and even contradictory—potentially owing to the heterogeneous profile of MDD which is somewhat used as an umbrella term, encompassing distinct disease sub-types, each with different symptom characteristics (Drysdale et al., 2017). Another potential explanation for the inconsistent reports of aberrant FC patterns in MDD could be that these are mostly assessed under the assumption of the stationarity of the FC. However, RSN FC has been shown to be highly variable both in its spatial and temporal domain (Allen et al., 2014; Calhoun et al., 2014; Deco et al., 2017; Hutchison et al., 2013a; Hutchison et al., 2013b; Irajil et al., 2018; Yaesoubi et al., 2017). Alterations in dynamic FC have been reported in MDD (Kaiser et al., 2016; Demirtaş et al., 2016; Zhi et al., 2018). Thus, more focus should be placed on the temporal and frequency aspects of resting-state activity in MDD.

Nonetheless, the major body of evidence points toward functional abnormalities in mostly three RSNs: the DMN, the SN, and the CEN (Belleau et al., 2015; Kaiser et al., 2015; Manoliu et al., 2013; Sambataro et al., 2013; Wei et al., 2013). Alterations in functional integration across these three RSNs have been consistently

observed in a number of other psychiatric disorders, leading to the conceptualization of the "triple network model of psychopathology" (Menon, 2011). This model suggests that both the aberrant functional organization within each functional network and the interplay among them are characteristic of many psychiatric and neurological disorders. These three networks are generally referred to as the "core neuro-cognitive networks", as they are involved in a broad spectrum of cognitive tasks (Greicius et al., 2003; Greicius et al., 2004; Menon and Uddin, 2010; Menon, 2011). Specifically, the CEN and the SN are believed to facilitate externally-driven cognitive and affective processing, while the DMN is involved in self-referential, internally-driven intellectual activity (Greicius et al., 2003; Greicius et al., 2004). The DMN has been proposed to play a role in depressive rumination, due to its importance for self-referential processes (Berman et al., 2011; Berman et al., 2014; Cooney et al., 2010; Hamilton et al., 2011; Jacobs et al., 2014).

Interestingly, several studies in MDD report on the normalization of altered rs-fMRI FC patterns after antidepressant treatment. Specifically, the normalization of abnormal FC in the posterior DMN has been reported after antidepressant treatment, while persistent abnormal FC in the anterior DMN has been associated with asymptomatic depression and potential for relapse (Li et al., 2013; Wu et al., 2011b). Another study further reported widespread effects of antidepressant treatment on the FC within multiple networks and pointed to an integrative role for the precuneus and posterior cingulate (parts of the posterior DMN) (Klaassens et al., 2015). Moreover, the efficacy of depression treatment using transcranial magnetic stimulation (TMS) targeting the dlPFC was found to depend on the resting-state FC of the stimulation site with the subgenual cingulate (part of the anterior DMN) (Fox et al., 2012a).

Investigation of aberrant resting-state FC in MDD has become a promising endeavor for the understanding of maladaptive processes underlying its psychopathology. Traditional rs-fMRI analysis methods that focus on changes in FC have been successful in identifying differences between healthy control subjects and individuals with MDD. Nonetheless, such analyses do not explain the mechanisms behind the observed FC aberrations. FC is calculated as a measure reflecting signal covariance, i.e. synchronous signal development over time. This can only occur when dominant frequencies of the time courses are identical, because otherwise the signal would naturally diverge at significant periods of time. Thus, the intact temporal organization of neural dynamics determines the healthy regime of brain functioning. Deviations from this healthy regime could be reflected in malfunctioning neural processes, as is the case in several other neurological disorders. Aberrant FC patterns could relate to shifts in frequency distribution of regional and network BOLD signal fluctuations. Nonetheless, spectral properties of rs-fMRI BOLD fluctuations in MDD have not been investigated yet. In order to understand how FC is generated, and what mechanisms lead to FC breakdown, the investigatory focus needs to be placed on broadband

spectral properties of the BOLD signal. Especially, studies need to investigate which frequencies—and to what extent—contribute to the ongoing activity within distinct RSN; how the orchestration of these frequencies contributes to functional integration in the brain; and whether MDD is associated with alterations in spectral properties of RSNs. If the latter holds true, studies need to examine the implications of such altered spectral properties on FC patterns. In the next section, I will introduce a novel aggregate measure which can be used to assess the spectral characteristics of broadband RSN BOLD fluctuations, in an attempt to answer the aforementioned questions.

1.5 New and noteworthy: the Spectral Centroid

RSNs represent complex processes that evolve through coherence on various temporal scales within the broad term of slow rs-fMRI BOLD fluctuations. Investigation of broadband processes is needed to preserve the richness of RSNs operating regime, i.e., information content across the broad frequency spectrum. The more detailed architecture of frequency spectra across networks is, however, poorly understood. In particular, it is unknown to what extent brain disorders affect such architecture.

Identifying key features of broadband spectra of BOLD network fluctuations—which might also be sensitive to pathological change—bears a challenge, given the relatively wide frequency span of meaningful resting-state BOLD fluctuations (e.g., 0.01–0.75 Hz) and the need for frequency-resolved analysis (e.g., dividing the full frequency band into 2–10 sub-bands). Moreover, the vast amount of literature on aberrant resting-state BOLD activity in various diseases—often involving divergent results—points toward a large set of regions or networks that are implicated in specific diseases. Thus, investigating group differences in spectral properties of regions or networks-of-interest within several frequency sub-bands would involve many statistical tests, possibly inflating false-positive results; and if strictly corrected for multiple comparisons—reduce the statistical power of the analysis. I propose that in order to circumvent this problem, complex measures can be summarized into meaningful aggregate measures, which may improve the detection of systematic patterns and emphasize major disease-related alterations. These can be subsequently followed-up by post-hoc tests and targeted investigations yielding detailed information on the underlying changes in power spectra.

As part of this thesis, I propose a measure novel to the field of rs-fMRI—the spectral centroid (SC)—which is an aggregate measure describing the properties of the power spectrum of BOLD fluctuations. The SC of RSN BOLD fluctuations represents the “center of gravity” of the full power spectrum within a network (Ries et al., 2018).

Pictorially, it can be understood as a midpoint within the spectral density function at which the distribution is divided into two equal parts so that, figuratively speaking, if put on the tip of a pin at this midpoint—the spectral distribution would be perfectly balanced (see Figure 1.4). In mathematical terms, it represents a weighted mean, as explicitly given by the equation in figure 1.4 as well as in the methods section 3.1.1. In practice, the SC is a compact measure for statistical analysis¹.

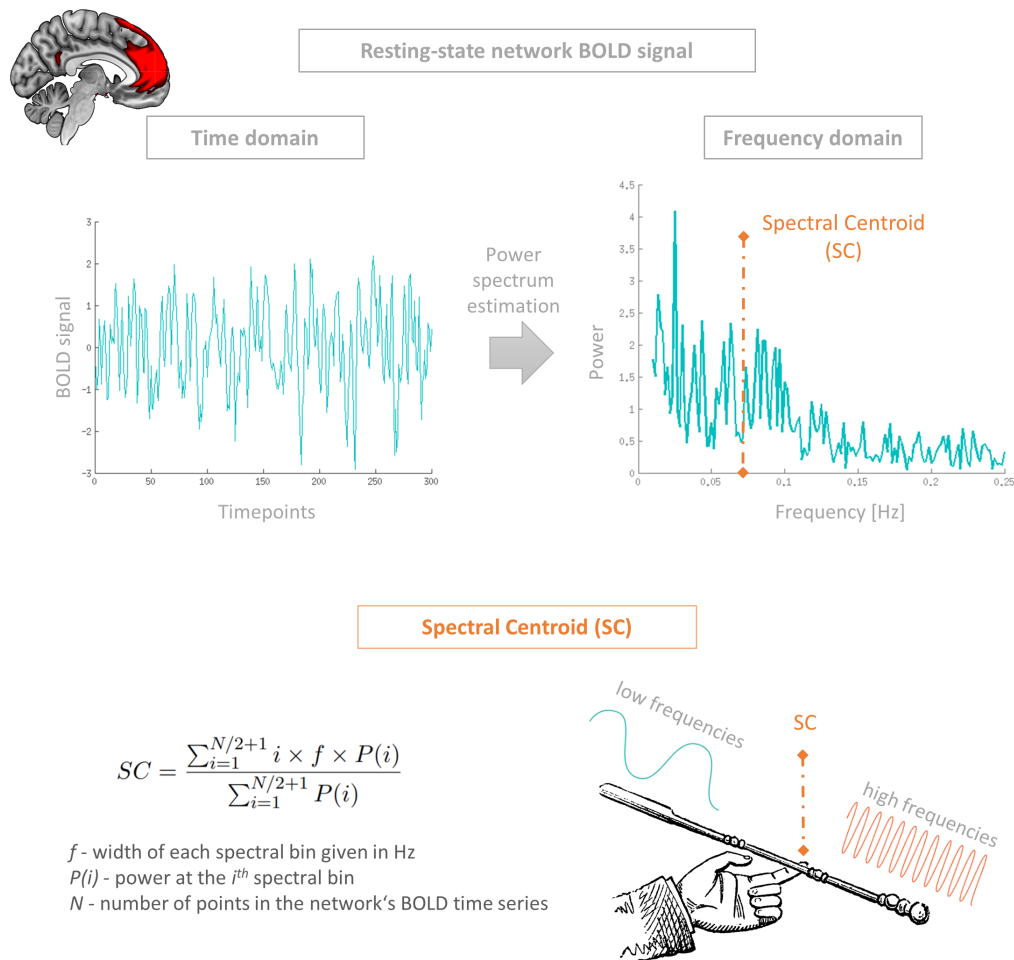


Fig. 1.4. | SC: calculation workflow. The spectral centroid (SC) is an integral measure obtained by evaluating the "center of gravity" of the full power spectrum of BOLD network fluctuations. The SC is based on the frequency and magnitude information obtained via a power estimation method of one's choice (e.g., fast Fourier transform (FFT), periodogram, or modified periodogram). The SC is calculated as the weighted mean of the frequencies present in the signal with their power as the weight, as expressed by the formula in the lower left corner. The spectral centroid can be conceptualized as a midpoint within the power spectrum that divides it into two equally weighted parts so that, figuratively speaking, if put on the tip of a pin at this midpoint, the spectral distribution would be perfectly balanced (see lower right corner).

¹Portions of this section have been published as an original article; see Ries et al. (2018).

Objectives

This thesis comprises two consecutive projects. The objective of the first project is to systematically evaluate the spectral content of RSN BOLD activity, and particularly, to determine whether the BOLD spectral content is characteristic for individual RSNs and whether MDD is associated with altered spectral properties of specific RSNs. The objective of the second project is to investigate the brain's frequency-resolved FC structure in a higher spectral resolution and under consideration of higher frequencies, as well as to determine frequency-dependent aberrations in FC patterns associated with MDD.

2.1 Project 1: Grading of frequency spectral centroid across resting-state networks in the healthy brain, and alterations in major depressive disorder

Ongoing, slowly fluctuating brain activity is organized into RSNs of spatially coherent fluctuations. Beyond spatial coherence, RSN activity is governed in a frequency-specific manner. The more detailed architecture of broadband frequency spectra across RSNs is, however, poorly understood. In the first project, I propose a novel measure—the spectral centroid—which represents the "center of gravity" of the full power spectrum of broadband RSN signal fluctuations. I examine whether spectral underpinnings of network fluctuations are distinct across RSNs. I hypothesize that spectral content differs across networks in a consistent way, thus, the aggregate representation—the SC—systematically differs across RSNs. To this end, I test for a significant grading (i.e., ordering) of SC across RSNs in a high-quality dataset comprising 820 healthy subjects of the Human Connectome Project (HCP). Subsequently, to validate the reliability and replicability of the results, I further examine the SC based on an independent dataset comprising 25 healthy subjects. Moreover, I hypothesize that such grading is biologically relevant, by demonstrating its RSN-specific change through brain disease, namely MDD. I examine the SC values in 25 MDD patients and test for significant deviations of network SC from healthy controls.

This study provides a systematic characterization of RSNs in terms of their spectral content. In particular, it highlights the distinct contributions of slow and fast BOLD fluctuations to the overall RSN activity regime. Moreover, this study provides a more detailed understanding about the mechanistic causes underlying alterations in rs-fMRI activity in MDD, as it delineates the disrupted balance between slow and fast fluctuations in specific RSNs and the respective alterations in FC. Altogether, this study provides a new methodological framework by means of which characteristic properties of RSNs can be assessed, and key changes related to brain disease detected.

Parts of the results and argumentation presented in this project have been previously published (Ries et al., 2018). However, the published results were based on a slightly different spectral estimation method than the one presented in this thesis.

2.2 Project 2: Frequency-specific organization of functional hubs in the healthy brain, and alterations in major depressive disorder

Empirical evidence highlights the importance of frequency information when investigating functional brain organization with rs-fMRI. Particularly, higher frequencies within the BOLD signal have been shown to largely contribute to the healthy function of the brain. The investigation of the frequency-specific functional architecture of the brain at rest has gained substantial attention in recent years. The objective of this project is to investigate frequency-specific FC structure in a higher spectral resolution (i.e., dividing the BOLD signal into fine-grained, narrow-band frequency intervals) and also under consideration of higher frequencies (i.e., > 0.1 Hz). In this project, I calculate frequency-specific degree centrality—a measure of overall FC of a brain region—within 10 distinct frequency bands accessible from the full range of resting-state functional MRI BOLD fluctuations (i.e., 0.01–0.25 Hz) in 24 healthy controls and 24 MDD patients. This project highlights a frequency-dependent spatial organization of functional hubs in healthy controls and reveals frequency associated changes in regional hubness in MDD. Importantly, the outcome of this project shows that frequency-resolved analysis within the full frequency range accessible from the BOLD signal, including higher frequencies, reveals unique information about brain organization and its changes, which can otherwise be overlooked.

The results and argumentation of Project 2 have been summarized in form of a manuscript and submitted for publication.

Project 1

3.1 Materials and methods

In Project 1, I operate on two datasets: (i) Dataset 1: rs-fMRI data of 820 healthy subjects from the Human Connectome Project (HCP), and (ii) Dataset 2: rs-fMRI data of 25 healthy controls and 25 MDD patients, acquired at my research facility, the Department of Diagnostic and Interventional Neuroradiology of the Klinikum rechts der Isar, Technische Universität München.

3.1.1 Dataset 1: Human Connectome Project

The Human Connectome Project¹ is a consortium led by the Washington University, University of Minnesota, and Oxford University and its overarching objective is to map macroscopic human brain circuits—via multimodal imaging techniques—and their relationship to behavior and genetics in a large population of healthy adults (Van Essen et al., 2013). The HCP set itself a goal to acquire data from 1200 healthy subjects within five years. Throughout the acquisition process batches of already collected data have been released quarterly (for example the 500 subjects release or the 900 subjects release). The HCP data is characterized by its exceptionally high quality—to which the customized scanner, the large population size, and the tailored preprocessing procedures significantly redound.

Another objective of the HCP is to make imaging data freely accessible, in an optimized way. Accordingly, the HCP data can be easily downloaded from the ConnectomeDB database², which has specifically been established for handling the large amounts of unprocessed and processed HCP data.

Information about the HCP study population, data acquisition protocols, as well as preprocessing and analysis steps are described in great detail in previous publications (Van Essen et al., 2013; Smith et al., 2013; Uğurbil et al., 2013), as well as in the

¹<http://www.humanconnectomeproject.org/>

²<https://db.humanconnectome.org>

HCP 900 Subjects Data Release Reference Manual³. Below, I will briefly describe these procedures with the specific focus on aspects related to my further analyses.

Participants & Data Acquisition

In this project, the 900 subjects release (S900) HCP data was used. The S900 release comprises rs-fMRI scans of 900 young and healthy adults (aged 22–35), together with task-based MEG and fMRI, and structural MRI scans. Subjects of the HCP were drawn from a population of adult twins and their non-twin siblings. All subjects were scanned at Connectome Skyra—the HCP-customized Siemens Skyra 3 Tesla (3T) scanner at the Washington University. Within two scanning sessions, four rs-fMRI runs and two pairs of anatomical images were collected per subject. Out of 900 subjects, the complete acquisition of all four rs-fMRI runs with 100% of collected time points was obtained only from 820 subjects. The following analysis is based on rs-fMRI scans of those 820 subjects. The data of 820 HCP healthy subjects will hereafter be referred to as Dataset 1.

Functional Images Rs-fMRI images were acquired in four runs of approximately 15 minutes each. Two runs were acquired in one session and two in another session, for a total of 1h of resting-state functional data. Participants were instructed to keep their eyes open with relaxed fixation on a projected bright cross-hair on a dark background, presented in a dimmed room. Within each session, oblique axial acquisition alternated between phase encoding in right-to-left (RL) direction in one run and phase encoding in a left-to-right (LR) direction in the other run. Resting-state functional images were collected with the following parameters: gradient-echo EPI sequence, TR = 720 ms, TE = 33.1 ms, flip angle = 52°, field of view = 208 x 180 (RO x PE), matrix 104 x 90 (RO x PE), slice thickness = 2 mm, 72 slices, 2.0 mm isotropic voxels, multiband factor = 8, echo spacing 0.58 ms, bandwidth = 2290 Hz/Px.

Structural Images Structural scans were acquired as a pair of T1-weighted and a pair of T2-weighted images, all acquired at 0.7 mm isotropic resolution.

Data Preprocessing

Anatomical images and functional resting-state images were preprocessed by the HCP using the minimal preprocessing pipelines (MPP) (Glasser et al., 2013). The

³https://www.humanconnectome.org/storage/app/media/documentation/s900/HCP_S900_Release_Reference_Manual.pdf

MPP are procedures specifically designed to capitalize on the high-quality data of HCP. These procedures include: the removal of spatial artifacts and distortions, anatomical image segmentation, within-subject cross-modal image registration, and normalization into standard space. Particularly, the MPP are designed to minimize the amount of information removed from the functional data. Respectively, the MPP do not include such steps as temporal filtering, nuisance regression, motion censoring (scrubbing), or significant spatial smoothing. Instead, the minimally preprocessed rs-fMRI images are denoised using ICA in combination with FMRIB's ICA-based Xnoiseifier (FIX), so that artifactual (i.e., non-neural) spatial components are automatically removed from the signal (ICA-FIX) (Smith et al., 2013; Griffanti et al., 2014; Salimi-Khorshidi et al., 2014). The procedure goes as follows: ICA with an automatic dimensionality estimation is run on the minimally preprocessed rs-fMRI images (with high-pass filtered time courses) using the MELODIC software from FSL⁴. The resulting ICs are subsequently fed into FIX⁵ for an automated classification into “good” vs. “bad” components. Bad components are then removed from the data in a non-aggressive way, which means that only variance unique to the bad components is regressed out from the data while global variance shared across good and bad components remains intact.

Data Analysis

Determination of resting-state networks Within the HCP analysis framework, an ICA was performed on the preprocessed and denoised rs-fMRI images using the MELODIC software. Different ICA parcellation scenarios were used with a varying number of ICs (i.e., 15, 25, 50, 100, 300). For each scenario, the time courses per IC and subject, as well as group-averaged spatial maps of the ICs are publicly available for download.

Subsequent analyses were performed by me and are based on the spatial maps and BOLD time courses of ICs obtained from the IC = 50 parcellation scenario. Previous studies have demonstrated that a high model order ICA reveals refined components that correspond to known anatomical and functional segmentations (Kiviniemi et al., 2009; Smith et al., 2009; Abou-Elseoud et al., 2009; Ystad et al., 2010; Ray et al., 2013). Specifically, the model order of around 70–75 ICs has been found to be optimal and has been widely used in previous studies, next to the model order of 20 ICs. Thus, in Dataset 1, when following the 70–75 model order standard, I had to choose between the option of 50 and 100 ICs, as the HCP does not provide results of ICA with 75 ICs. I have decided to choose the 50 ICs model order, as it resembles to

⁴<https://fsl.fmrib.ox.ac.uk/fsl/fslwiki/MELODIC>

⁵<https://fsl.fmrib.ox.ac.uk/fsl/fslwiki/FIX>

a higher extent the settings of previous studies, compared to the model order of 100 ICs.

From the set of 50 ICs provided by the HCP, a number of RSNs was identified in an automated way, using the *fslcc* function. This function is implemented in FSL and was used to calculate cross-correlations between spatial maps of the ICs and the well-established templates defined by Allen et al. (2011) which represent canonical RSNs. These templates are freely available for download⁶. A correlation threshold of $r > 0.2$ was applied when using *fslcc*. Next, ICs of the highest correlation with the canonical RSN templates were selected and represented the corresponding RSNs. This selection procedure was accompanied by a careful visual inspection of compliance between the spatial maps of the selected ICs and the canonical RSN templates from Allen et al. (2011).

Spectral Centroid Each RSN is characterized by its spatial map, representing the span of the FC within the network, and the corresponding BOLD signal. The BOLD signal can be transformed from its time domain into the frequency domain using the Fast Fourier Transform (FFT). As a result, the power spectral density (or simply the power spectrum) is obtained. Based on the power spectrum, the contributions of different frequencies to the RSN BOLD signal can be investigated, with respect to their power.

An in-house, Matlab-based script was used to perform the FFT on the time courses of each RSN, in each participant and run. With a TR of 720ms, the full spectrum of accessible frequencies spans between 0–0.69 Hz. For the subsequent analysis, the FFT results were restricted to the frequency range of 0.01–0.69 Hz, omitting the very low frequencies below 0.01 Hz, as these are largely affected by the slow drifts occurring due to scanner hardware, and cannot fully be separated from the neural signal drifts.

The spectral properties of RSN BOLD fluctuations were examined at the subject level, by means of the spectral centroid (SC). The SC is an aggregate measure obtained by evaluating the "center of gravity" of the full power spectrum of RSN BOLD fluctuations, based on the frequency and magnitude information obtained from the FFT. The SC is calculated as the weighted mean of the frequencies present

⁶http://mialab.mrn.org/data/hcp/RSN_HC_unthresholded_tmaps.nii

in the signal with their power as the weight. The formula for the calculation of the SC is described below:

$$SC = \frac{\sum_{i=1}^{N/2+1} i \times f \times P(i)}{\sum_{i=1}^{N/2+1} P(i)} \quad (3.1)$$

where f is the width of each spectral bin in Hz, $P(i)$ is the power at the i^{th} spectral bin given in Hz, and N is the number of points in the network's BOLD time series. In Dataset 1 the respective parameters are: $f = 0.0012$ Hz, and $N = 1200$.

The SC of the power spectrum of network BOLD fluctuations was calculated within the frequency range of 0.01–0.69 Hz for each of the 24 RSNs in each participant and per run. Thus, the analysis resulted in four SC values per subject and per RSN. Next, for each RSN and subject, the mean SC of all four runs was calculated and represents the final SC value. As such, one mean SC value was obtained per subject and per RSN.

Statistical analysis In Matlab, Lilliefors normality tests were carried out on the set of SC values for each RSN, to determine whether the SC values follow a normal distribution ($p < 0.05$, Bonferroni-corrected for 24 RSNs). SC values did not significantly deviate from a normal distribution. To test for significant differences in SC values between RSNs, a one-way repeated measures ANOVA was performed, with the factor network. Subsequently, post-hoc tests were performed as Wilcoxon signed rank test to investigate significant pairwise differences in SC between specific RSNs ($p < 0.05$, Bonferroni-corrected for 24 networks).

Assessment of SC dependence on RSN size The relation between the size of a RSN and its corresponding SC value was examined. This was motivated by the possibility that, despite the high-quality data and the careful artifact removal, spatially smaller networks would be differently affected by local, high-frequency motion artifacts when compared to more distributed networks. The network size was estimated from group-averaged IC spatial maps. The spatial maps were first binarized (at a threshold of $z > 10$, which corresponds to $p < 0.001$ under familywise error (FWE) correction). Next, all non-zero voxels were counted and their sum indicated the network size. Lastly, Pearson's correlation was computed between the RSN size and SC values.

3.1.2 Dataset 2: Healthy Controls & MDD patients

Participants

Twenty-five MDD patients and 25 age- and sex-matched healthy controls (HC) took part in the study. The data were previously analyzed in a different context, the results of which were published in Manoliu et al. (2013) and Meng et al. (2014). Patients with MDD were recruited from the Department of Psychiatry of the Klinikum rechts der Isar, Technische Universität München, by practicing psychiatrists. HC subjects were recruited from the area of Munich via advertising. All participants provided informed consent in accordance with the Human Research Committee guidelines of the Klinikum rechts der Isar, Technische Universität München. All participants were examined for their medical history, underwent psychiatric interviews and psychometric assessments. Psychiatric diagnoses were based on the Diagnostic and Statistical Manual of Mental Disorders–IV (DSM–IV) (American Psychiatric Association, 2013). The Structured Clinical Interview (SCID) was used to determine the presence of psychiatric diagnoses (First et al., 1996). The severity of depression symptoms was assessed with the Hamilton Rating Scale for Depression (HAM–D) (Hamilton, 1960), as well as the Beck Depression Inventory (BDI) (Beck et al., 1961). The global level of occupational, psychological, and social functioning was assessed with the GAF scale (Spitzer et al., 1992). The clinical-psychometric assessment was performed by psychiatrists who have been professionally trained for the SCID interviews. Inter-rater reliability for diagnoses and scores was higher than 95%. For all patients, recurrent MDD was the primary diagnosis. Moreover, all patients met the criteria for a current major depressive (MD) episode. The average MD episode length was 16.4 weeks (SD = 6.70), the average HAM–D score was 21.38 (SD = 7.06), and the average BDI score was 23.58 (SD = 5.93). The mean duration of MDD was 16.92 years (SD = 10.38), with a mean number of MD episodes of 5.46 (SD = 2.47). The average GAF-score was 50.17 (SD = 10.60). Fourteen MDD patients had psychiatric co-morbidities, including avoidant or dependent personality disorder (n = 5), generalized anxiety disorder (GAD) (n = 6), and somatization disorder (n = 3). Exclusion criteria for the patients included substance abuse, bipolar disorder, psychotic symptoms, schizophrenia, and schizoaffective disorder. The following issues constituted additional exclusion criteria for both groups: pregnancy, neurological or severe internal systemic diseases, and general contraindications for MRI. One MDD patient was not undergoing psychotropic medication treatment by the time of the MRI assessment. Seven patients were treated by antidepressant mono-therapy [three cases: citalopram 30 mg/d (mean dose); three cases: sertraline 200 mg/d; one case: mirtazapine 30 mg/d]; 11 patients by dual-therapy (five cases: citalopram 37.5 mg/d + mirtazapine 30 mg/d; two cases: citalopram 40 mg/d + venlafaxine 225 mg/d; one case: citalopram 30 mg/d

+ quetiapine 200 mg/d; one case: sertraline 200 mg/d + mirtazapine 30 mg/d; two cases: venlafaxine 225 mg/d + mirtazapine 30 mg/d); and five patients by triple-therapy (two cases: citalopram 30 mg/d + venlafaxine 187.5 mg/d + amisulpride 200 mg/d; two cases: citalopram 30 mg/d + mirtazapine 30 mg/d + quetiapine 200 mg/d; 1 case: venlafaxine 22 mg/d + mirtazapine 30 mg/d + quetiapine 200 mg/d). All HC subjects were free of any current or past neurological or psychiatric disorders or psychotropic medication. Detailed information on demographic and clinical characteristics of the study group is presented in Table 3.1.

Data Acquisition

MRI data were collected on a 3T Philips Achieva scanner with an 8-channel phased-array head coil. An anatomical image, as well as 10 minutes of rs-fMRI data were acquired from all participants. Participants were explicitly instructed to keep their eyes closed, not to fall asleep, and not to think about anything during the resting-state condition. Directly after the scanning session, a subjective verification that participants stayed in a state of alertness during the rs-fMRI scan was obtained by interrogating them via intercom. All participants successfully completed the scanning sessions.

Functional images The resting-state functional images were acquired using a gradient echo EPI sequence (TE = 35 ms, TR = 2000 ms, flip angle = 82°, field of view = 220 mm × 220 mm, matrix = 80 × 80, 32 slices, slice thickness = 4 mm, and 0 mm interslice gap, voxel size = 2.75 mm × 2.75 mm × 4 mm; 300 volumes).

Structural images The T1-weighted structural images were acquired with a MPRAGE sequence (TE = 4 ms, TR = 9 ms, inversion time = 100 ms, flip angle = 5°, field of view = 240 mm × 240 mm, matrix = 240 × 240, 170 slices, slice thickness = 1 mm, and 0 mm interslice gap, voxel size = 1 mm × 1 mm × 1 mm).

Data Preprocessing

The first three volumes of rs-fMRI data were discarded due to the magnetization effects. The remaining images were preprocessed using the statistical parametric mapping (SPM12)⁷ software. The preprocessing steps included head motion correction, spatial normalization into the Montreal Neurological Institute (MNI) standard space, and spatial smoothing with a 6-mm full width at half maximum (FWHM)

⁷<http://www.fil.ion.ucl.ac.uk/spm/>

Tab. 3.1. | **Demographic and clinical characteristics.** Information about major depressive disorder patients and healthy controls.

Measure	MDD (n = 25)	HC (n = 25)	MDD vs. HC ^{a,b}
	Mean (SD)	Mean (SD)	p-value
Age [years]	48.76 (14.38)	44.08 (14.78)	>0.05 ^a
Gender (m/f)	12/13	11/14	>0.05 ^b
Duration of MDD [years]	16.72 (10.20)	NA	
Number of episodes	5.56 (2.47)	NA	
Duration of current episode [weeks]	16.56 (6.62)	NA	
GAF	49.80 (10.53)	99.50 (1.10)	<0.001 ^{a,*}
HAM-D	22.12 (7.06)	0	<0.001 ^{a,*}
BDI	24.08 (6.31)	0	<0.001 ^{a,*}

^a two-sample t-test

^b χ^2 -test

* significant for $p < 0.05$, Bonferroni-corrected for multiple comparisons.

Gaussian kernel. No slice-timing correction was performed, as this procedure has been shown to have minimal effects on rs-fMRI data acquired at a TR of 2 s (Wu et al., 2011a).

Numerous head motion parameters were investigated and were compared between MDD patients and HC to control for potential differences in head motion between groups, as they could affect the results of the main analyses. For each subject, the temporal signal-to-noise ratio and the point-to-point head motion was estimated (Murphy et al., 2007; Van Dijk et al., 2012). Excessive head motion (i.e., cumulative motion translation or rotation > 3 mm or 3° , and mean point-to-point translation or rotation > 0.15 mm or 0.1°) constituted an exclusion criterion. The point-to-point motion was defined as the absolute displacement of each brain volume compared with its preceding volume. None of the participants had to be excluded with respect to this procedure. Furthermore, the two-sample t-tests showed no significant differences between groups regarding the mean point-to-point translation or rotation of any direction ($p > 0.1$), as well as the temporal signal-to-noise ratio ($p > 0.5$).

Nuisance covariates regression The main data analysis (which will be described in the "Data Analysis" section) is based on two branched sets of data: (1) the ICA-derived time courses of RSNs—which are used in the examination of RSN spectral properties via the SC; and (2) the "native" preprocessed whole-brain fMRI EPI time courses—which are used for the calculation of percent signal change (PSC) (an analysis complementary to the SC analysis), as well as for the estimation of the seed-based FC of a given RSN. In this section, I will describe the procedure of nuisance signal regression (i.e., regressing out the signal of no interest originating from the WM and CSF) from the preprocessed whole-brain fMRI EPI time courses (i.e., the second branch of data).

The PSC is analyzed in the context of the SC—as it provides information complementary to that of SC and may help to elucidate observed differences in the SC. PSC has been shown to differ between different RSNs (van den Heuvel et al., 2016), and might be impacted by disease (Brambilla et al., 2003; Sanacora et al., 2002; Tunnicliff and Malatynska, 2003). Thus, when investigating between-group differences in the SC values of RSN BOLD fluctuations, it is important to control for the overall PSC.

Coming back to the two branched datasets: since these two datasets are used for analyses which are complementary to each other, it is crucial to maintain the signal quality and properties as consistent as possible across the datasets. The ICA-derived data is largely cleaned from non-neural sources of variance such as head-movement distortions, cardiac and respiratory signals, as well as contributions of the WM and CSF signals. Fluctuations of the aforementioned origins are being captured as individual ICs and are—to a great extent—separated from the remaining ICs which represent selected RSNs. Regarding the preprocessed whole-brain rs-fMRI EPI data, these are corrected for head movement distortions, yet their variance may still be affected by other sources of artifacts. To reduce the influence of these sources on the fMRI signal, nuisance covariates (i.e., WM and CSF signals) were regressed out—as it is highly important to exclude non-neural variance from the signal on which the PSC will be calculated later.

The regression of nuisance covariates was performed as follows: For each subject, binarized masks of the WM and CSF were created from the T1 segmentation compartments (applying a binarization threshold of $i > 0.9$). In each participant, averaged signals corresponding to the WM and CSF were separately extracted from the preprocessed (realigned and normalized, but not smoothed) whole-brain fMRI EPI signal, and served as covariable signals in the regression. Subsequently, the nuisance covariates regression was performed, in each participant individually, on the previously realigned and normalized, but not smoothed data, using Resting-State

fMRI Data Analysis Toolkit (REST)⁸. In the final step, the cleaned data (i.e., with reduced contributions of the WM and CSF) were spatially smoothed in SPM12, using a 6-mm FWHM Gaussian kernel.

Estimation of cardiac and respiratory rates As part of an additional signal control procedure, Physiologic Estimation by Temporal ICA (PESTICA)⁹ (Beall and Lowe, 2007) was applied on raw (i.e., not preprocessed) whole-brain fMRI data to detect heartbeat and breathing cycles in individual subjects. PESTICA is a powerful tool which enables the detection of physiological contributions to the fMRI signal, directly from the signal (i.e., without the need for external physiological recordings). In Matlab, FFT was used to calculate peak frequencies of cardiac and respiratory rate time courses obtained from PESTICA (with a temporal resolution of TR/slice number = 2 s/32). Precisely, a Gaussian fit in a search window was applied which corresponded to expectation values for the physiological rhythms (cardiac 55–70 bpm, beats per minute; respiratory 10–24 bpm). A visual check of fit quality was performed. Next, group differences in cardiac and respiratory rates were tested with two-sample t-tests. No significant difference between the groups regarding the cardiac rate ($p > 0.5$), as well as the respiratory rate ($p > 0.5$), was revealed by the tests.

Data Analysis

Determination of resting-state networks For the determination of RSNs, an established approach proposed by Allen et al. (2011) was followed. Group-ICA (Calhoun et al., 2001) was used to decompose the whole-brain fMRI data into 75 ICs. This procedure was based on the Infomax algorithm implemented in the Group ICA of fMRI Toolbox (GIFT)¹⁰. The ICA procedure was the following: First, rs-fMRI data from all subjects (both HC and MDD patients) were concatenated into one dataset. Next, the concatenated data were reduced by two-step principal component analysis (PCA) to lower the computational burden. Subsequently, ICA was run, based on the Infomax algorithm and using a model order of 75 ICs. The ICA was run 20 times using the ICASSO algorithm, to reach an estimate of component reliability. At the final step, the set of 75 group-averaged ICs were back-projected into the single-subject space. In result, 75 ICs were obtained, each described by a spatial map of z-scores (reflecting the component's FC pattern across space) and an associated time course (reflecting the component's BOLD activity across time). With regards to the spatial maps, high z-scores of voxels reflect their strong FC within the IC, while

⁸<http://restfmri.net/forum/REST>

⁹<https://www.nitrc.org/projects/pestica/>

¹⁰<http://icatb.sourceforge.net>

z-scores of approximately 0 reflect the lack of or a very low FC of the voxel within the IC. A threshold of $z > 1$ was set on the z-values, to omit the very weak as well as the negative FC patterns within the ICs. The variance of the time course associated with an IC after back projection is by default normalized to 1.

The identification of meaningful RSNs from obtained ICs was performed in an automated way. Within the GIFT toolbox, multiple spatial regression analyses on the 75 ICs were run, using established templates from Allen et al. (2011) which reflect canonical RSNs. ICs of the highest correlation coefficient with RSNs templates (at a threshold of $r > 0.2$) were selected for further analysis. This resulted in a selection of 24 RSNs of interest.

Percent Signal Change (PSC) When investigating differences in the SC values of RSN BOLD fluctuations between groups, it is important to control for the overall RSN BOLD activity level, as it might influence the spectral properties of the fMRI signal. More precisely, the spectral characteristics of BOLD fluctuations would be affected by the relative balance between the signal of neuronal origin and the noise present in the acquired rs-fMRI time series. The spectrum of resting-state BOLD fluctuations has an approximately $1/f^\beta$ distribution, with frequency f and power-law exponent β (He, 2011), due in part to the low-pass character of the hemodynamic response. Thus, assuming that the low-frequency noise sources (e.g., slow head motion, scanner drifts, and aliased physiological noise) are adequately removed, RSNs with smaller BOLD signal fluctuations may exhibit a distribution skewed toward higher frequencies (i.e., a more shallow $1/f^\beta$ slope) and thus a reduced overall variance (which would be reflected in a smaller PSC value in this RSN). Since there might be systematic differences in PSC related to pathology, which in turn would amplify changes in the SC, it is important to control for the influence of the PSC on the SC. To this end, I investigated the impact of controlling for BOLD signal variance (i.e., PSC) in the analysis of SC.

PSC was calculated individually for each participant and each network in the following way: First, network binary masks were created from spatial maps of each RSN in each participant at a threshold of $z > 2.32$, which corresponds to a p-value of 0.01. Next, these masks served as regions of interest (ROIs) to extract averaged signals from: (i) preprocessed whole-brain rs-fMRI EPI data, and (ii) preprocessed whole brain rs-fMRI EPI data with nuisance covariates regression (i.e., WM and CSF). As a result, for each mask representing a RSN and in each participant, two time courses were obtained. These time courses are hereafter called *network_EPI* and *network_EPI_nuisance*, and represent the network time courses of preprocessed rs-fMRI EPI data without and with nuisance regression, respectively. Next, the PSC was calculated by dividing the standard deviation of the GM-based signal

(i.e., *network_EPI_nuisance*) by the mean of the *network_EPI* signal (which reflects the combined contributions of GM, WM, and CSF), adhering to the established standard procedures for task-based fMRI (see e.g., Gläscher, 2009), as by equation below:

$$PSC = \frac{SD[network_EPI_nuisance]}{mean[network_EPI]} \times 100 \quad (3.2)$$

Subsequently, statistical analyses were performed on the PSC values. Differences in PSC between individual RSNs and between groups were examined via a repeated measures ANOVA with the factors network and group. Post-hoc tests were performed as Wilcoxon ranksum test ($p < 0.05$).

Spectral Density In Matlab, and adequately to the procedure executed in Dataset 1, FFT was used to compute the power spectra of ICA-derived BOLD signals of each RSN in every participant. Subsequent SC calculation was based on these power spectra.

For direct comparisons of the spectral power between groups, the full power spectra were then split into 10 frequency sub-bands (freq1: 0.01–0.025; freq2: 0.025–0.05; freq3: 0.05–0.075; freq4: 0.075–0.1; freq5: 0.1–0.125; freq6: 0.125–0.15; freq7: 0.15–0.175; freq8: 0.175–0.2; freq9: 0.2–0.225; freq10: 0.225–0.25 Hz). These frequency sub-bands (or bins) were chosen in an exploratory manner and constitute a compromise between the averaging for better power and the sufficient spectral resolution.

For each RSN, the mean power at each frequency band was computed across groups. Subsequently, the mean power values for each RSN were re-scaled by multiplication with the corresponding group-averaged PSC value. Wilcoxon ranksum tests were performed on the power values at each frequency band to test for group-differences within the original as well as the re-scaled power spectrum of a given RSN.

Spectral Centroid Spectral properties of BOLD network fluctuations were examined at the subject level by means of the SC. The SC values were calculated as described in equation 3.1 (with the following parameters: width of each spectral bin $f = 0.0017$ Hz; number of points in the network's BOLD time series $N = 300$). Next, the results of the FFT were restricted to the frequency range of 0.01–0.25 Hz, omitting the very low frequencies below 0.01 Hz. For each RSNs and in each participant, a SC value of the full power spectrum (i.e., 0.01–0.25 Hz) of BOLD network

fluctuations was calculated. In total, SC values for 24 RSNs and 50 participants (25 HC and 25 MDD patients) were obtained.

Subsequently, statistical analyses were performed on the SC values. In Matlab, Lilliefors normality tests were carried out on the set of SC values, separately for each RSN and in each group, to determine whether they follow a normal distribution ($p < 0.05$, Bonferroni-corrected for 24 RSNs). No significant deviations from the normal distribution were found. Next, a repeated measures ANOVA with the factors network and group was performed on the SC values. Post-hoc tests were performed as Wilcoxon ranksum tests ($p < 0.05$).

Correction of Spectral Centroid with PSC As previously explained, it is crucial to rule out any group differences in RSN spectral properties which could be attributed to the absolute BOLD activity level within a network (assessed via the PSC). Thus, a regression analysis of the SC values and the PSC values was conducted. In each group separately, a global regression was performed. Precisely, SC values corresponding to all RSNs in all participants within a given group were pooled together and regressed against the corresponding PSC values. The resulting regression residuals were taken to represent the "new" (corrected for PSC) SC values and are later referred to as the corrected spectral centroid (SCcorr).

Subsequently, statistical analyses were performed on the SCcorr values. A repeated measures ANOVA with the factors network and group was performed on the SCcorr values. Post-hoc analyses were performed as Wilcoxon ranksum tests ($p < 0.05$) to examine group differences in SCcorr of specific RSNs, and as Wilcoxon signed rank tests to investigate significant pairwise differences in SCcorr between RSNs in the HC group ($p < 0.05$, Bonferroni-corrected for 24 RSNs).

To facilitate the comprehension of the SC and PSC calculation procedures performed on the two branched sets of fMRI data in Dataset 2, a schematic analysis workflow is displayed in Figure 3.1.

Assessment of SC dependence on RSN size Accordingly to the procedure performed in Dataset 1, the link between the size of a RSN and its corresponding SC and SCcorr values was examined. The network size was determined from the group-averaged and binarized spatial maps of RSNs of HC subjects (obtained in an earlier step of PSC calculation). Non-zero voxels within the spatial maps of each RSN were counted, and their sum indicated the network's size. No significant correlation between the RSN size and the SC, or the SCcorr was found (Pearson's correlation RSN size x SC: $r = -0.119$, $p = 0.58$; RSN size x SCcorr: $r = -0.197$, $p = 0.36$).

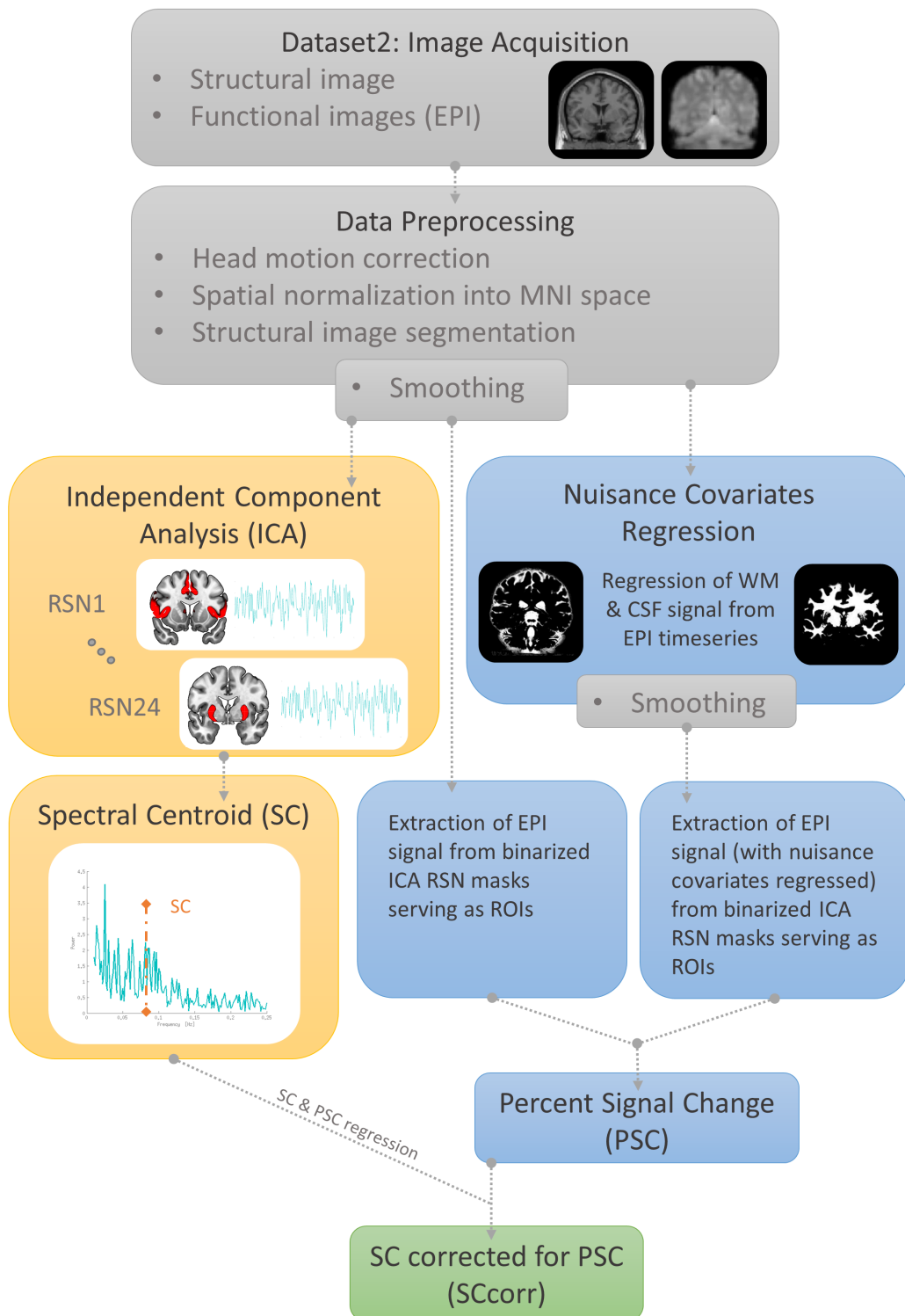


Fig. 3.1. | Schematic analysis workflow for Dataset 2. Analysis steps for the calculation of the spectral centroid (SC), percent signal change (PSC), and SC corrected for PSC (SCcorr). Methods adapted from Ries et al. (2018).

Assessment of SC dependence on clinical scores To examine whether spectral properties of BOLD network fluctuations relate to the symptomatic and pathophysiology of MDD, correlation analyses between the SCcorr values and the symptom characteristics were conducted. Pearson's correlation was calculated between the SCcorr values of each RSN and measures of MDD symptom severity, such as the HAM-D and BDI scores, as well as the number of MD episodes, the length of current episode, and the GAF score ($p < 0.05$, Bonferroni-corrected for 24 multiple comparisons for 24 RSNs were investigated).

Seed-based FC of the Salience Network In a subsequent analysis, the seed-based FC of the SN was determined. ICA-derived BOLD time courses of the SN served as regressors in a 1st level general linear model (GLM) analysis. The GLM analysis enables the identification of the FC pattern of the SN towards the whole brain. In the 1st level analysis, seed-based FC maps of the SN were determined in each participant individually, based on the BOLD signal fluctuations within the full power spectrum (i.e., 0.01–0.25 Hz). In the 2nd level analysis, the SN FC maps obtained per participant were subjected to a one-sample t-test, separately for HC and MDD patients ($p < 0.05$, FWE-corrected) and represented SN FC at the group level. Subsequently, to test for group differences in the SN connectivity patterns, a two-sample t-test was applied (p cluster-level corrected < 0.05 , on underlying voxel-level correction of $p < 0.001$, with voxels restricted to GM).

For the determination of seed-based FC patterns of the SN at the 10 distinct frequency sub-bands (defined in previous sections), the same procedure as described above was performed, but this time the BOLD signal was previously band-pass filtered into the 10 distinct sub-bands. The REST toolbox was used to perform the band-pass filtration. The REST toolbox utilizes an ideal filter which transforms the BOLD time series into the frequency domain via the discrete Fourier Transform and adds zeros to extend the frequency coverage; the information in the frequency domain is then transformed back to the time domain, by using the inverse discrete Fourier Transform (Song et al., 2011). For each frequency sub-band, the 1st and 2nd level analyses described in the paragraph above were performed on the corresponding band-pass filtered BOLD time series.

3.1.3 Correspondence of network dynamics across datasets

In this project, spectral properties of RSN signal fluctuations were examined via the SC in two independent datasets (i.e., Dataset 1 of the HCP and Dataset 2 of HC and MDD patients). It is of high interest to compare the results in healthy subjects

in both datasets and examine whether findings are generally replicable. In the following analysis, the accord between the obtained SC values of the corresponding RSNs across the two datasets was examined. A correlation analysis was performed between the SC values of corresponding RSN obtained from Dataset 1 and from healthy subjects in Dataset 2. For a clear overview of RSN correspondence across study sites (i.e., the study of Allen et al. (2011), the HCP study, and the HC & MDD study) see Table A.1 in the Appendix. In total, 22 RSNs from Dataset 1 and Dataset 2 could be matched as representing the same networks as in Allen et al. (2011).

The SC depends on the overall measurement length as well as on the sampling frequency, as these two parameters determine which part of the signal spectrum is accessible to analysis. E.g., with a higher sampling rate, higher frequencies can be measured, which in turn shifts the SC to slightly higher values, depending on the power within these additional frequencies. To enable an accurate comparison of the SC values between corresponding RSNs obtained in the two independent datasets (which were acquired using different scanning parameters), the FFT results in Dataset 1 were restricted to the frequency range of 0.01–0.25 Hz (as this is the frequency range accessible from Dataset 2). Next, and only for comparison purposes, new SC values were computed on this range, so that they correspond to the frequency range accessible from Dataset 2.

The basal ganglia network was excluded from the correlation analysis, as in Dataset 1 its SC exceeded two standard deviations. This resulted in a Pearson's correlation analysis between 21 RSNs from Dataset 1 and 21 RSNs from Dataset 2.

3.2 Results

3.2.1 Dataset 1: Human Connectome Project

Resting-State Networks

RSNs were identified by applying an ICA on the rs-fMRI data of 820 healthy subjects from the HCP. The resulting spatial maps of ICs were correlated with established spatial templates from Allen et al. (2011) which represent canonical RSNs. Components of the highest correlation coefficient (at a threshold of $r > 0.2$) were selected to represent RSNs of interest and were used in further analysis. In total, 24 RSNs were identified and were categorized into the following functional systems: basal ganglia (BG; $n = 1$), auditory (AUD; $n = 1$), sensorimotor (SM; $n = 5$), visual (VIS; $n = 5$), default-mode (DMN; $n = 4$), attentional (ATT; $n = 5$), and frontal (FRONT; $n = 3$).

Within the attentional system, the salience network (SN) and the central executive network (CEN) were identified. Four subdivisions of the default-mode system were identified: the anterior default-mode network (DMN_ant), the anterior-medial DMN (DMN_antmed), the posterior DMN (DMN_post) and the posterior-lateral DMN (DMN_postlat). Spatial maps of selected RSNs are displayed in Figure 3.2, and the peak activation sites within RSNs are summarized in Table 3.2.

Spectral Centroid

The SC is an aggregate measure that represents the "center of gravity" of the broad power spectrum of BOLD network fluctuations. SC values were calculated for each participant and each RSN. Mean SC values (averaged across 820 subjects) for each RSN are depicted in Figure 3.3.A and summarized in Table 3.2.

Statistical analysis on the SC values was performed as a one-way repeated measures ANOVA and revealed a significant effect of the factor network ($F(1,23) = 2182.3$, $p < 0.001$). Next, significant pairwise differences in SC between RSNs were examined, and are displayed in form of a matrix in Figure 3.3.B. Columns and rows of the matrix, respectively, represent the individual RSNs and are ordered according to increasing SC magnitude. From the matrix, it can be deduced that most RSNs significantly differ from one another regarding their SC values.

Altogether, these results indicate a significant grading of SC values across RSNs, where most networks can be distinguished from each other based on their characteristic SC value. The term "grading" refers to the observation that each RSN takes a distinct position in an ordering of all SC values.

Spectral Centroid and RSN size

The relationship between the size of a RSN and its corresponding SC value was examined. Pearson's correlation analysis between the RSN size and SC value revealed a significant negative relation ($r = -0.54$, $p = 0.007$). Next, a regression analysis was performed on the SC and network size values, to rule out possible differences in spectral properties due to differences in network size. Regression residuals represented the "new" SC values—corrected for network size. A one-way repeated measures ANOVA with the factor network was performed on the SC values which were corrected for the network size. The ANOVA outcome yielded a significant effect of the factor network ($F(1,23) = 1554.7$, $p < 0.001$), and thus revealed an intact grading of SC values also after controlling for network size. In conclusion,

the grading of SC values across RSNs occurs independently of the relation between spectral properties of BOLD fluctuations of a given network and its size.

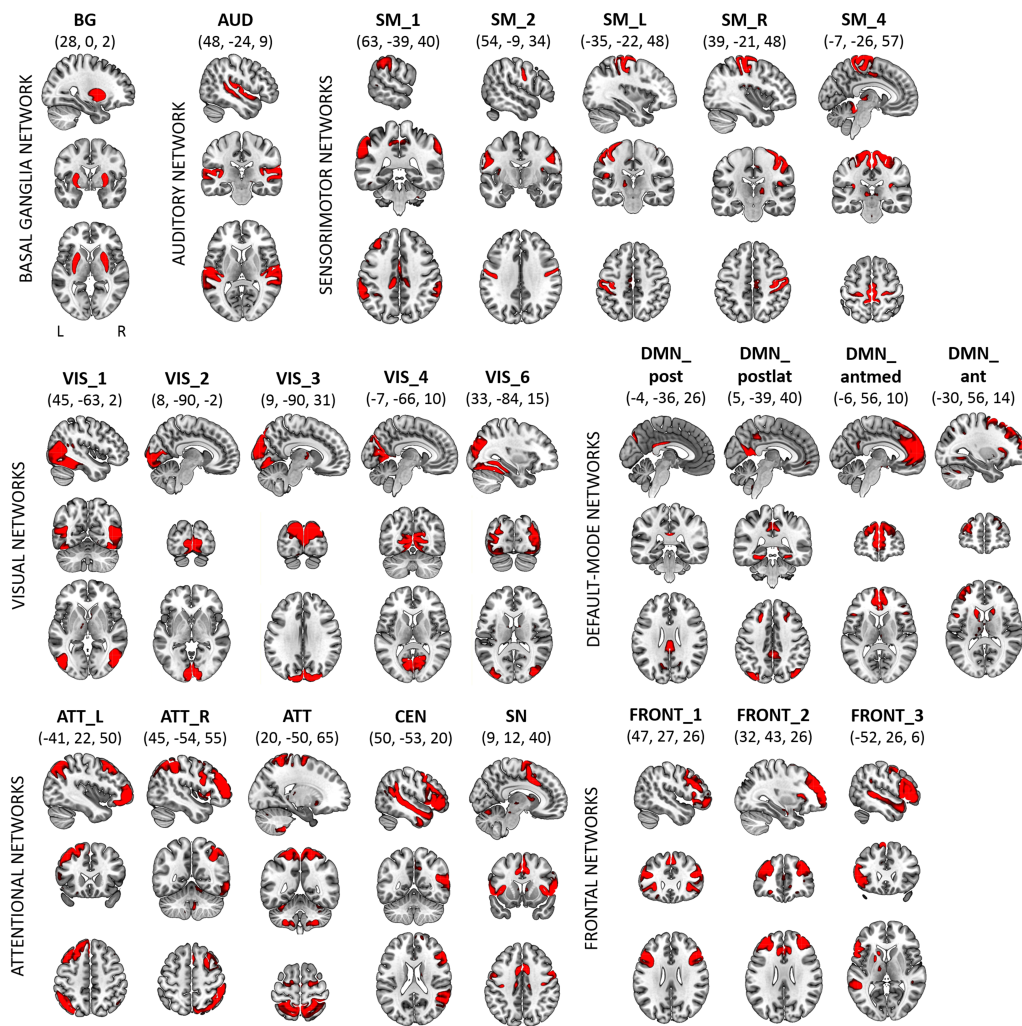


Fig. 3.2. | **Dataset 1: RSNs.** Spatial maps of 24 resting-state networks (RSNs) obtained via spatial ICA performed on the Human Connectome Project data of 820 healthy subjects. The spatial maps are represented as z-scores and are displayed at the three most informative slices (MNI-space). RSNs are categorized into distinct groups according to their anatomical and functional properties. Figure and modified legend taken from Ries et al. (2018).

Tab. 3.2. | **Dataset 1: RSN FC profiles and results of SC analysis.** For each resting-state network (RSN) the corresponding spectral centroid (SC) value and the set of brain regions constituting the network's positive functional connectivity (FC) are presented in the table. RSNs are ordered according to their increasing SC values. Abbreviations: ACC, Anterior Cingulate Cortex; IFG, Inferior Frontal Gyrus; IPL, Inferior Parietal Lobule; MCC, Midcingulate Cortex.

Dataset 1: Human Connectome Project		
RSN	positive FC	SC [Hz]
SM_1	IPL, Supramarginal gyrus, IFG	0.083
DMN_postlat	Lingual Gyrus, Cuneus, Calcarine Gyrus, Precuneus, IPL, Angular Gyrus MCC, Superior Frontal Gyrus, Fusiform Gyrus	0.083
ATT_R	Superior Parietal Lobule, IPL, Middle Frontal Gyrus, IFG, Superior Frontal Gyrus	0.084
ATT_L	Superior Frontal Gyrus, Middle Frontal Gyrus, Angular Gyrus, IPL, Middle Orbital Gyrus, IFG, MCC	0.085
VIS_3	Cuneus, Superior Occipital Gyrus, Lingual Gyrus	0.086
DMN_post	PCC, Cuneus, Precuneus, IPL	0.086
VIS_6	Fusiform Gyrus, Lingual Gyrus, Middle Occipital Cortex, Lateral Occipital Cortex, Middle Temporal Gyrus, area V5/MT	0.086
SM_2	Postcentral Gyrus	0.087
VIS_4	V2, Calcarine Gyrus, Lingual Gyrus, Cuneus, Superior Occipital Gyrus, Dorsal and Ventral Extrastriate Cortex (V3)	0.087
FRONT_3	IFG, Posterior-Medial-Frontal	0.088
SN	ACC, Insula, MCC, Posterior-Medial-Frontal	0.088
FRONT_1	Insula, IFG, Middle Frontal Gyrus, Superior Medial Gyrus, Caudate Nucleus	0.088
VIS_2	Calcarine Gyrus, V1	0.089
ATT	Superior Parietal Lobule, Posterior-Medial-Frontal, MCC, Supramarginal Gyrus,	0.089
CEN	IFG, Middle Temporal Gyrus, Posterior-Medial-Frontal, Supramarginal Gyrus	0.089
DMN_ant	Middle Frontal Gyrus, Superior Frontal Gyrus, MCC	0.089
VIS_1	Middle Temporal Gyrus, area V5/MT	0.090
SM_L	Precentral Gyrus	0.090
FRONT_2	Middle Frontal Gyrus, ACC	0.090
DMN_antmed	Superior Medial Gyrus, Insula, IFG, MCC	0.091
SM_R	Precentral Gyrus	0.091
SM_4	Paracentral Lobule	0.091
AUD	Superior Temporal Gyrus	0.093
BG	Putamen, Caudate Nucleus	0.106

Dataset 1: Human Connectome Project

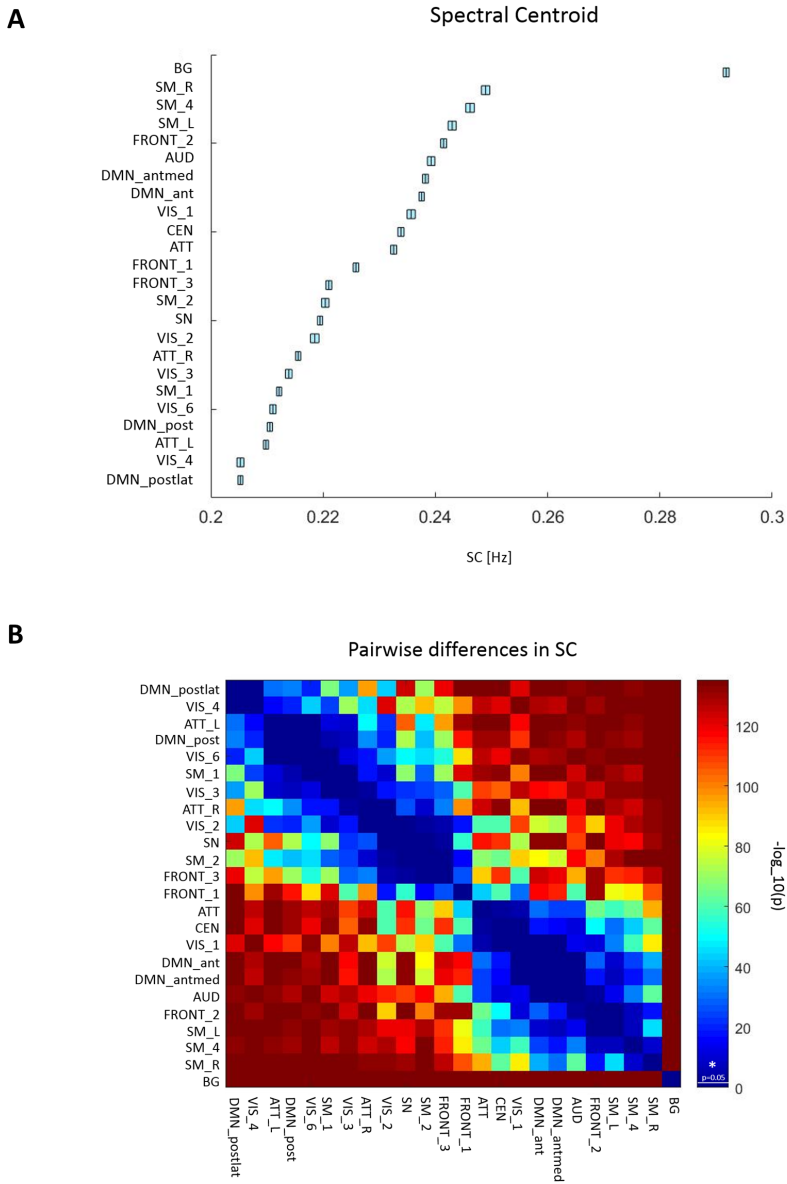


Fig. 3.3. | **Dataset 1: Results of the SC analysis.** (A) Mean spectral centroid (SC) values of each RSN obtained from the Human Connectome Project (HCP) data of 820 healthy subjects. For each RSN the mean SC value is indicated by the black vertical line, and the standard error of the mean (SEM) is depicted through the light blue box. RSNs are ordered according to their increasing SC magnitude. SCs were calculated based on the power spectra of BOLD network fluctuations within the frequency range of 0.01–0.69 Hz. (B) A matrix that represents p-values of pairwise differences in the SC between individual RSNs. The colors indicate the significance, where red stands for lower p-values and higher significance, and blue for higher p-values and thus lower significance. P-values were scaled with a $-\log_{10}(p)$ transform, the color bar value of 1.3 corresponds to $p = 0.05$ (as indicated by a vertical line across the color bar and an asterisk, which represent the significance threshold).

3.2.2 Dataset 2: Healthy Controls & MDD patients

Resting-State Networks

In Dataset 2, RSNs were identified by applying a group-ICA on rs-fMRI data pooled together from 25 HC and 25 MDD patients. The resulting spatial maps of ICs were correlated with established RSN templates from Allen et al. (2011). Components of the highest correlation coefficient (at a threshold of $r > 0.2$) were selected as RSNs of interest and were used in further analysis. In total, 24 RSNs were identified and were categorized into the following functional systems: basal ganglia (BG; $n = 1$), auditory (AUD; $n = 1$), sensorimotor (SM; $n = 6$), visual (VIS; $n = 5$), default-mode (DMN; $n = 4$), attentional (ATT; $n = 5$), and frontal (FRONT; $n = 2$). Within the attentional system, the salience network (SN) and the central executive network (CEN) were identified. Four subdivisions of the default-mode system were identified: the DMN_ant, the DMN_antmed, the DMN_post, and the DMN_postlat. Spatial maps of selected RSNs are displayed in Figure 3.4, and the peak activation sites within RSNs are summarized in Table A.2 of the Appendix.

Spectral Centroid

Repeated measures ANOVA on the SC values revealed a significant effect of the factor network ($F(1,23) = 24.64$, $p < 0.001$), and a significant interaction between the factors network and group ($F(1,23) = 1.76$, $p < 0.05$). What drives the interaction can be deduced from Figure 3.5.A, i.e., the bars representing the SC values in separate groups are apart with respect to the SN and the VIS_2 network. Post-hoc Wilcoxon ranksum tests yielded a significant group difference in the SC of the SN, where MDD patients showed significantly increased SC values when compared to HC ($p < 0.05$; MDD mean \pm std: 0.112 ± 0.013 Hz; HC mean \pm std: 0.103 ± 0.017 Hz). This test also revealed a trend towards statistical significance in one of the visual networks (VIS_2; $p = 0.07$; HC mean \pm std: 0.1 ± 0.016 Hz, MDD mean \pm std: 0.091 ± 0.018 Hz). Mean SC values for each RSN in both groups are depicted in Figure 3.5.A and summarized in Table 3.3.

Percent Signal Change

Repeated measures ANOVA on the PSC values revealed a significant effect of the factor network ($F(1,23) = 11.5$, $p < 0.001$) and a significant interaction between the factors network and group ($F(1,23) = 2.74$, $p < 0.001$). Post-hoc Wilcoxon

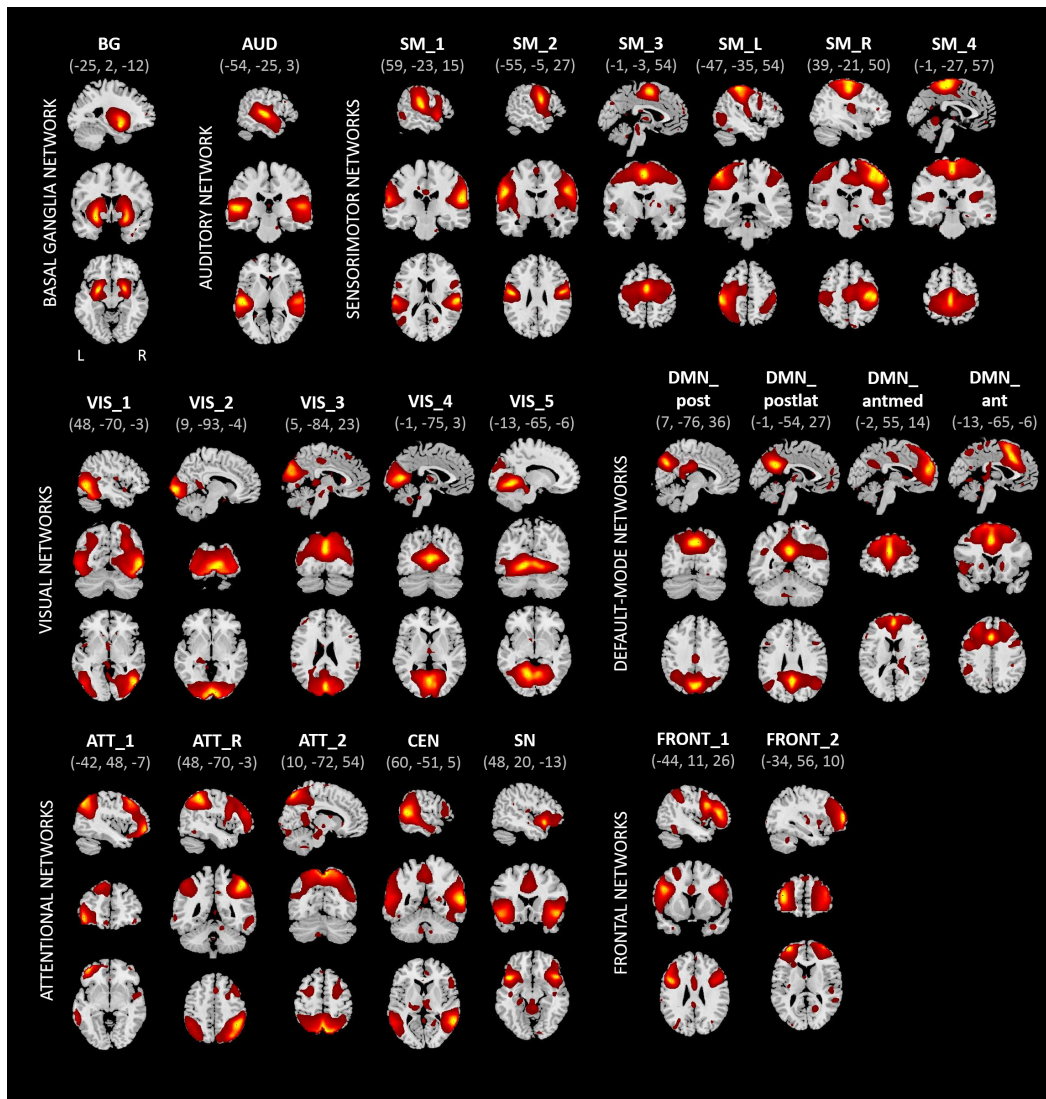


Fig. 3.4. | **Dataset 2: RSNs.** Spatial maps of 24 resting-state networks (RSNs) obtained from spatial group-ICA performed on the group data of 25 healthy controls and 25 MDD patients. Spatial maps are plotted as z-scores, thresholded at $z > 1$, and displayed at the three most informative slices (MNI-space). RSNs are categorized into groups according to their anatomical and functional properties. Modified figure and legend taken from Ries et al. (2018).

ranksum tests were carried out to identify the networks which show significant changes in PSC between groups. Accordingly, one of the visual networks (VIS_2) showed significantly increased PSC values in MDD patients when compared to HC ($p < 0.05$; MDD mean \pm std: $0.471 \pm 0.162\%$; HC mean \pm std: $0.374 \pm 0.119\%$). In another network, also associated with the visual system (VIS_4), a trend towards significance was observed, with higher PSC values in MDD patients than in HC ($p = 0.065$; MDD mean \pm std: $0.447 \pm 0.198\%$; HC mean \pm std: $0.327 \pm 0.078\%$).

Mean PSC values for each RSN in both groups are depicted in Figure 3.5.B and summarized in Table 3.3.

Spectral Centroid corrected for PSC

The original SC values were corrected for differences in PSC at the level of each RSN and participant. The repeated measures ANOVA performed on the SCcorr values revealed a significant effect of the factor network ($F(1,23) = 21.19, p < 0.001$). No significant interaction between the factors network and group was observed ($F(1,23) = 1.12, p = 0.3$). Mean SC values for each RSN, separately for HC and MDD patients are displayed in Figure 3.5.C and summarized in Table 3.3.

A matrix that represents pairwise differences in SCcorr between all RSNs in HC is displayed in Figure 3.5.D. Columns and rows of the matrix, respectively, represent the individual RSNs and are ordered according to increasing SCcorr magnitude. The results of Wilcoxon signed rank tests on the SCcorr values between each pair of RSNs in healthy controls showed significant pairwise differences in all networks with a minimum difference in SCcorr of 0.0001. At the given statistical power, only differences between networks from both ends of the SCcorr scale become statistically significant.

Post-hoc analysis was carried out to investigate group differences in SCcorr values of, specifically, the SN. This was motivated by the previous finding of significantly altered SC of the SN in MDD patients (before correction for PSC) and by the working hypothesis of altered dynamics of the SN in MDD—as it is widely implicated in depression. Additionally, since a trend towards significance in SC value of the visual network VIS_2 was observed—the post-hoc analysis also involved the investigation of significant group differences in the SCcorr of this visual network.

The Wilcoxon ranksum test revealed a significant difference in the SCcorr of SN between groups, where MDD patients showed higher SCcorr value than HC ($p < 0.05$; MDD mean \pm std: 0.013 ± 0.014 ; HC mean \pm std: 0.005 ± 0.017). Concerning the visual network VIS_2, after correction for PSC no significant difference in SC between groups remained. Thus, the previously reported shift in SC of the visual network VIS_2 could be fully attributed to differences in the absolute BOLD activity level within this network, as captured via PSC.

Dataset 2: Healthy Controls & MDD patients

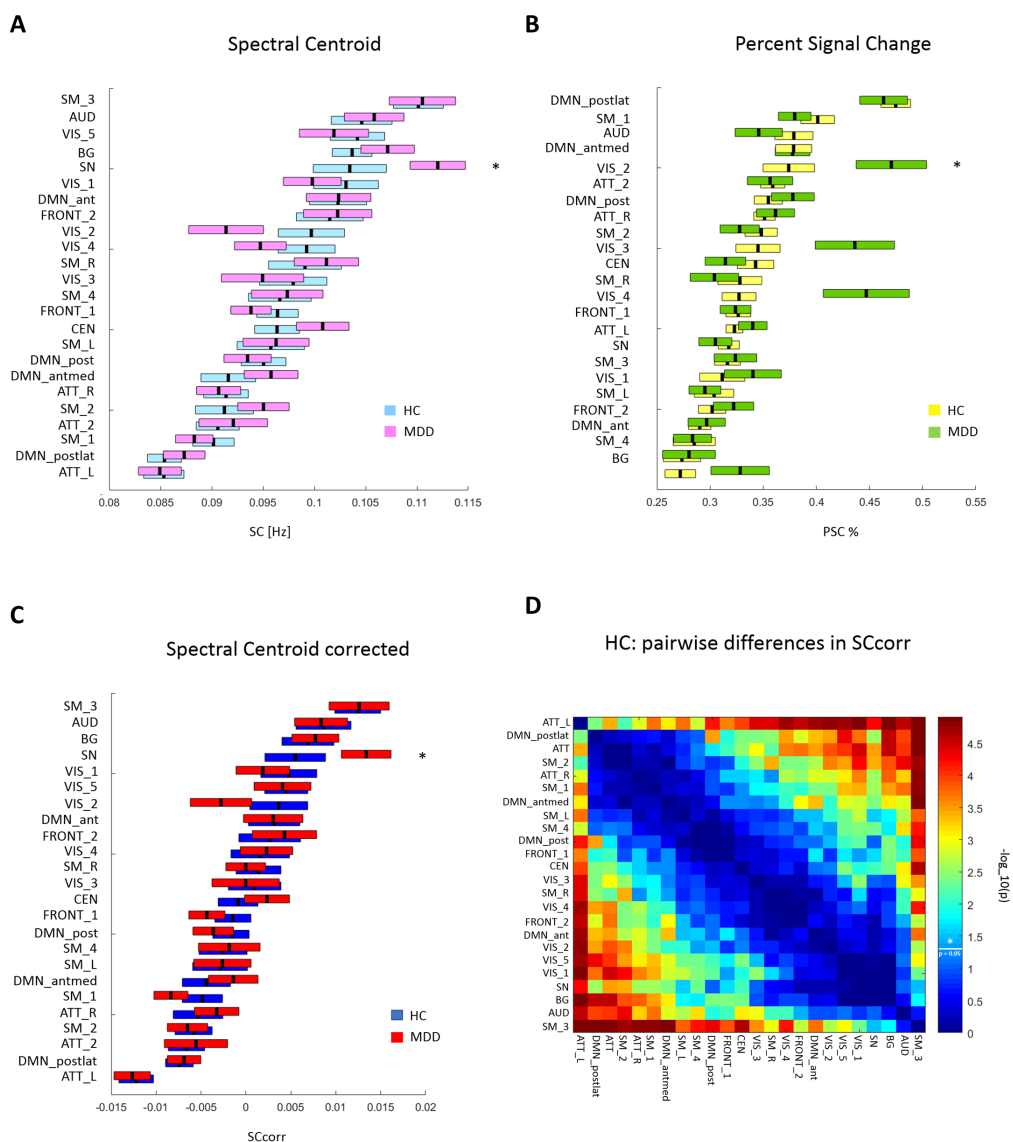


Fig. 3.5. | **Dataset 2: Results of SC and PSC analyses.** (A) Mean (\pm SEM) spectral centroid (SC) values of each RSN in healthy controls (HC) and major depressive disorder (MDD) patients. RSNs are ordered according to increasing SC magnitude in HC. SCs were calculated based on the power spectra of BOLD network fluctuations within the frequency range of 0.01–0.25 Hz. (B) Mean (\pm SEM) SC values corrected (SCcorr) for percent signal change (PSC) in HC and MDD, ordered according to increasing SCcorr magnitude in HC. (C) Mean (\pm SEM) PSC values of each RSN in HC and MDD patients. RSNs are ordered according to increasing PSC magnitude in HC. **Note:** the ordering on the y-axis differs between plots. (D) A matrix that represents p-values of pairwise differences in the SCcorr between individual RSNs in HC. The colors indicate the significance, where red stands for lower p-values and higher significance, and blue for higher p-values and thus lower significance. P-values were scaled with a $-\log_{10}(p)$ transform, the color bar value of 1.3 corresponds to $p = 0.05$ (as indicated by a vertical line across the color bar and an asterisk, which represent the significance threshold). Modified figure and legend taken from Ries et al. (2018).

Tab. 3.3. | **Dataset 2: Results of SC and PSC analyses.** For each resting-state network (RSN), the table represents group averaged values of the spectral centroid (SC), the SC corrected for percent signal change (SCcorr; PSC), and the PSC, separately for healthy controls (HC) and major depressive disorder (MDD) patients. RSNs are ordered according to the increasing SC magnitude in HC, the color scale represents the magnitude range, where green = low, yellow = middle, red = high.

Dataset 2: healthy controls and MDD patients						
RSN	SC [Hz]		SCcorr		PSC [%]	
	HC	MDD	HC	MDD	HC	MDD
ATT_L	0.085	0.085	-0.013	-0.013	0.32	0.34
DMN_postlat	0.085	0.087	-0.008	-0.007	0.47	0.46
SM_1	0.090	0.088	-0.005	-0.008	0.40	0.38
ATT	0.091	0.092	-0.006	-0.005	0.36	0.36
SM_2	0.091	0.095	-0.006	-0.003	0.35	0.33
ATT_R	0.091	0.091	-0.006	-0.006	0.35	0.36
DMN_antmed	0.092	0.096	-0.004	-0.001	0.38	0.38
DMN_post	0.095	0.093	-0.002	-0.003	0.35	0.35
SM_L	0.096	0.096	-0.003	-0.003	0.30	0.30
CEN	0.096	0.101	-0.001	0.002	0.34	0.31
FRONT_1	0.096	0.094	-0.001	-0.004	0.33	0.32
SM_4	0.097	0.097	-0.002	-0.002	0.29	0.28
VIS_3	0.098	0.095	0.001	0.000	0.35	0.44
SM_R	0.099	0.101	0.001	0.002	0.33	0.3
VIS_4	0.099	0.095	0.002	0.000	0.33	0.45
VIS_2	0.100	0.091	0.004	-0.003	0.37	0.47
FRONT_2	0.102	0.102	0.003	0.004	0.3	0.32
DMN_ant	0.102	0.102	0.003	0.003	0.29	0.3
VIS_1	0.103	0.100	0.005	0.002	0.31	0.34
SN	0.103	0.112	0.005	0.013	0.32	0.31
BG	0.104	0.107	0.007	0.008	0.35	0.28
VIS_5	0.104	0.102	0.005	0.004	0.27	0.33
AUD	0.105	0.106	0.009	0.008	0.38	0.35
SM_3	0.110	0.111	0.012	0.012	0.32	0.32

Salience Network: spectral differences between groups

The above results highlight disease-related alterations in the dynamic regime of BOLD fluctuations within the SN. Specifically, increased SCcorr values of the SN were observed in MDD patients, when compared to HC. To further investigate the causes of such increase, the spectral power of SN BOLD fluctuations was examined in both groups at 10 distinct frequency sub-bands. Specifically, group differences in the spectral power at each frequency sub-band were examined. The original power spectrum of the SN, as well as the power spectrum re-scaled by multiplication with PSC, are shown in Figure 3.6 (in the left and right panel, respectively). The analysis of the original power spectrum of the SN yielded a decrease in power at the lowest frequency band (freq1 0.01–0.025 Hz) in MDD patients, as supported by the significant outcome of the Wilcoxon ranksum test ($p < 0.01$). There was also a tendency of increased power at the higher frequency bands in MDD patients (freq7 0.15–0.175 Hz, $p = 0.06$; freq8 0.175–0.2 Hz, $p = 0.08$; freq10 0.225–0.25 Hz, $p = 0.08$). Within the re-scaled power spectrum of the SN, a significant decrease in the power at the lowest frequency band (freq1 0.01–0.025 Hz) was observed in MDD patients ($p < 0.05$). In conclusion, attenuated power at lower frequencies together with increased power at higher frequencies result in a shift of the SC in SN towards higher frequencies.

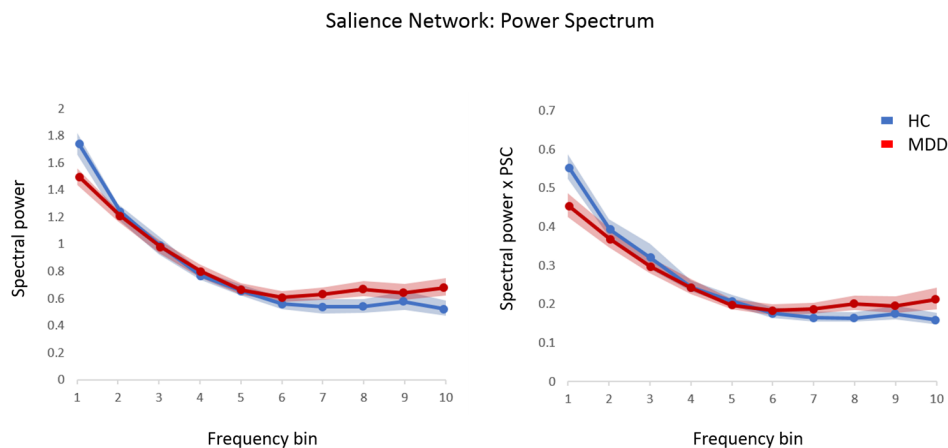


Fig. 3.6. | **Dataset 2: Power spectra of the salience network in HC and MDD.** Mean (\pm SEM) spectral power of the salience network (SN) at 10 distinct frequency bins in healthy controls (HC; in blue) and major depressive disorder (MDD) patients (in red). The left panel depicts the original power spectrum. The right panel depicts the power spectrum rescaled by the PSC, where the spectral power values for each frequency bin and each subject were multiplied by the corresponding PSC value of the SN BOLD fluctuations. Modified figure and legend taken from Ries et al. (2018).

Spectral Centroid and symptom severity

A possible link between the dynamical regime of BOLD network fluctuations and the symptomatology of MDD was examined. Pearson's correlation was calculated between the SCcorr values of each RSN and the symptom severity scores. A significant correlation between SCcorr and BDI scores was observed in one of the visual networks (VIS_4; $r = 0.61$, $p = 0.002$) and the anterior DMN (DMN_ant; $r = 0.57$, $p = 0.003$). Counter-intuitively, no significant correlation between the SCcorr values of the SN and scores of symptom severity was found. However, an indirect influence of altered SN activity on the severity of symptoms experienced by MDD patients could be deduced from the results of a subsequent whole-brain seed-based FC analysis of the SN. This analysis was motivated by the finding of altered SC of the SN in MDD patients. The logical conclusion is the following: FC is a measure of signal covariance, i.e., coherent signal development over time. Signals can evolve coherently only if their main frequencies are identical. If spectral properties of the signal from one source are significantly altered—which would be reflected in a change in the SC—then the coherence with the signal from the other source would be disturbed. As a result, FC between both sources would decrease. To this end, a subsequent seed-based FC analysis of the SN was performed, the results of which are presented in the following section.

Seed-based FC of the Salience Network The analysis of seed-based FC of the SN based on the rs-fMRI BOLD signal within the full spectrum of accessible frequencies (i.e., 0.01–0.25 Hz) revealed the following results: In HC, the SN exhibited functional connections to the insula, inferior frontal gyrus, superior temporal gyrus, thalamus, and cuneus (see Figure 3.7.A). In MDD patients, the SN exhibited significantly reduced FC towards the bilateral middle frontal gyrus and ACC, and the right cuneus (see Figure 3.7.B). The most prominent decreases in FC of the SN were observed in regions associated with the anterior DMN (DMN_ant) and one of the visual networks (VIS_4)—the exact two networks with SC values that significantly correlated with symptom severity scores (i.e., BDI). This observation is graphically summarized in Figure 3.7.C, where group-averaged, binarized masks of the DMN_ant and VIS_4 were overlaid on the clusters of significantly altered SN FC, derived from the MDD > HC contrast (as in panel B). At the bottom of Figure 3.7.C, correlation plots between the SCcorr values and BDI scores in each patient are displayed for each of the two RSNs. Subsequently, the analysis of frequency-resolved seed-based FC of the SN was performed, where the BOLD signal was band-pass filtered into 10 distinct frequency sub-bands beforehand. However, the statistical power within the band-limited regimes was too low to provide significant results. Band-specific group differences only appeared on a very liberal significance level ($p < 0.05$ uncorrected).

Seed-based FC of the Saliency Network

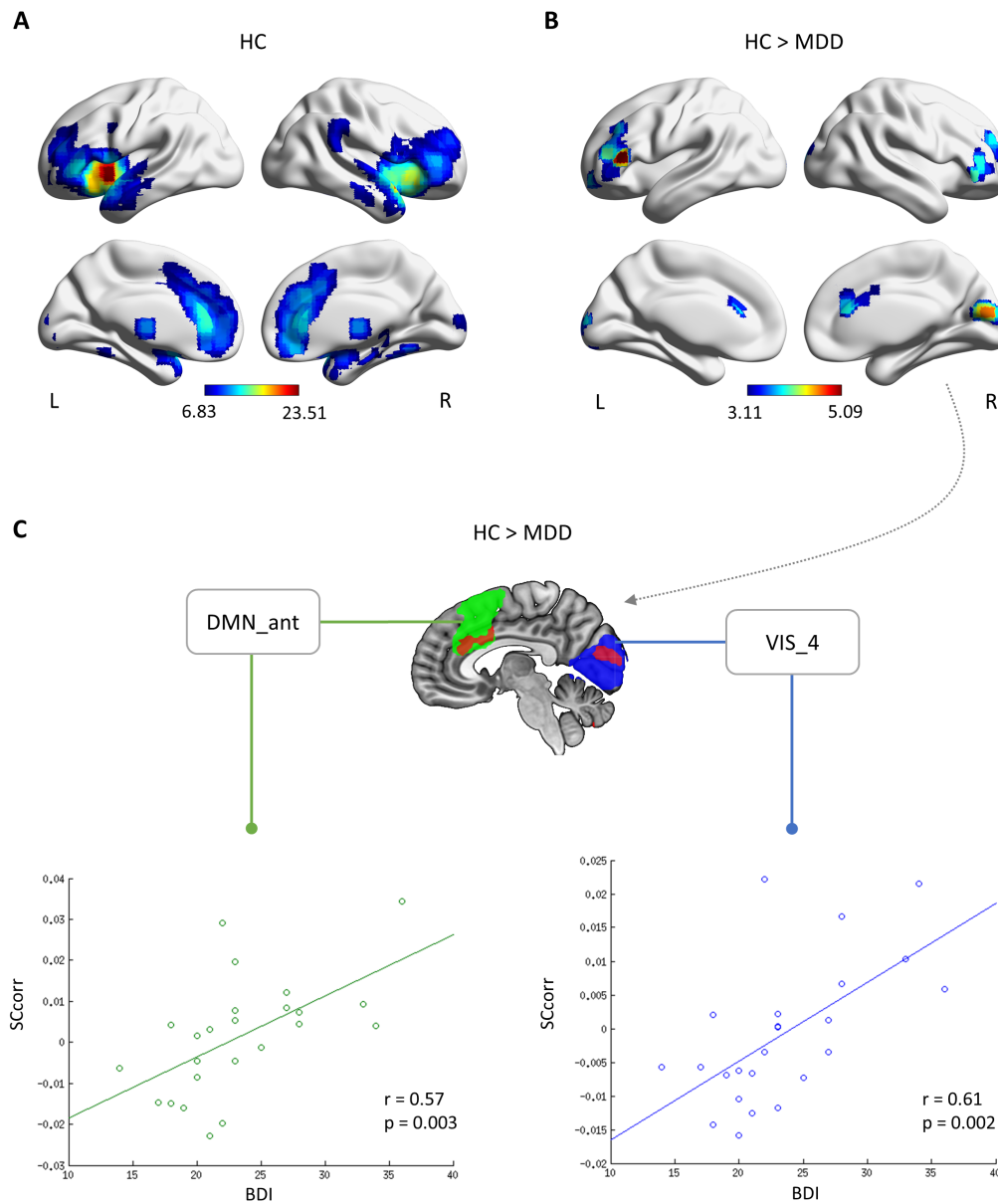


Fig. 3.7. | Dataset 2: Seed-based FC of the SN in HC > MDD, and link to MDD symptomatology. (A) Whole-brain seed-based functional connectivity (FC) of the salience network (SN) in healthy controls (HC; $p < 0.05$, FWE-corrected). (B) Group differences in the whole-brain seed-based FC of the SN, representing regions of decreased FC with the SN in MDD patients, when compared to HC (p cluster-level corrected < 0.05 , on underlying voxel-level correction of $p < 0.001$). (C) The overlap between (i) the regions of decreased FC with the SN in MDD patients and (ii) RSNs of which the SC values significantly correlate with the symptom severity scores. Modified figure and legend taken from Ries et al. (2018).

3.2.3 Correspondence of network dynamics across datasets

Both in Dataset 1 and Dataset 2, a significant grading (i.e., ordering) of SC values across RSNs was observed in healthy subjects. The correspondence between SC values of RSNs across the two datasets was subsequently examined. The SC values of RSNs from Dataset 1 (calculated from the power spectra which were restricted to 0.01–0.25 Hz) and the corresponding SC values of RSNs from healthy subjects in Dataset 2 yielded a significant positive correlation ($r = 0.58$, $p = 0.005$). The correlation is depicted in Figure 3.8. Due to the sample size, RSNs of Dataset 1 are characterized by smaller within-network variability in SC values, compared to RSNs of healthy controls from Dataset 2, which is reflected in the magnitude of the standard error of the mean (SEM).

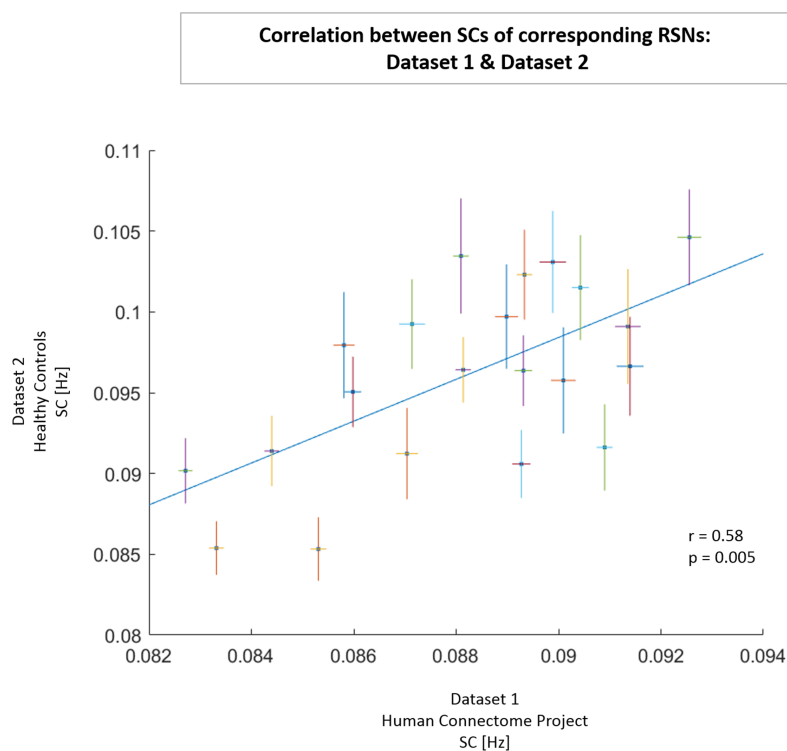


Fig. 3.8. | **Correspondence of RSN SC values across datasets.** Correlation between the spectral centroid (SC) values of 21 resting-state networks (RSNs) obtained from Dataset 1 (under consideration of FFT results restricted to 0.01–0.25 Hz; x-axis) and the corresponding RSNs obtained from healthy controls in Dataset 2 (y-axis). For each RSN, the horizontal line represents the standard error of the mean (SEM) in Dataset 1, and the vertical line represents the standard error of the mean (SEM) in Dataset 2. A least-squares fit line was added to the scatter plot. In the lower right corner, the correlation coefficient r and the p -value are depicted.

Project 2

4.1 Materials and methods

4.1.1 Participants & Data Acquisition

In Project 2, the same data was used as the one described under Dataset 2 in Project 1. Specifically, structural MRI and rs-fMRI images of twenty-five MDD patients and 25 age- and sex-matched HC were used. For detailed information on MDD patient characteristics as well as data acquisition protocols see section 3.1.2. In this project, however, the data underwent slightly different preprocessing procedures, which will be in detail described in the following section. Importantly, after the preprocessing procedure, one MDD patient and one HC subject had to be excluded due to spatial normalization problems which occurred during the correction for physiologic noise and motion. This resulted in a total of twenty-four MDD patients and 24 HC whose data were taken into further analysis. The updated demographic information of the 48 participants is presented in Table 4.1.

4.1.2 Data Preprocessing

Physiologic noise and motion correction

To begin with, rs-fMRI data was cleaned from physiological and motion artifacts using PESTICA (Beall and Lowe, 2007) and Slice-Oriented Motion Correction (SLO-MOCO)¹ software (Beall and Lowe, 2014), respectively. PESTICA was applied on the raw fMRI data to detect cardiac and respiratory cycles in the BOLD signal of each participant. Peak frequencies of cardiac and respiratory rate time courses obtained from PESTICA (with a temporal resolution of TR/slice number = 2 s/32) were calculated using FFT in Matlab. Precisely, a Gaussian fit in a search window was applied which corresponded to the expectation values for the physiological rhythms (cardiac 55–70 bpm; respiratory 10–24 bpm). For quality assurance, visual check of fit quality was performed. Differences in cardiac and respiratory rates between groups were tested with two-sample t-tests. These tests yielded no significant difference between the

¹<https://www.nitrc.org/projects/pestica>

Tab. 4.1. | Demographic and clinical characteristics of 48 subjects. Information about major depressive disorder patients and healthy controls.

Measure	MDD (n = 24)	HC (n = 24)	MDD vs. HC ^{a,b}
	Mean (SD)	Mean (SD)	p-value
Age [years]	48.25 (14.92)	43.62 (14.91)	>0.05 ^a
Gender (m/f)	11/13	10/14	>0.05 ^b
Duration of MDD [years]	16.92 (10.38)	NA	
Number of episodes	5.46 (2.47)	NA	
Duration of current episode [weeks]	16.38 (6.70)	NA	
GAF	50.17 (10.60)	99.50 (1.10)	<0.001 ^{a,*}
HAM-D	21.83 (7.06)	0	<0.001 ^{a,*}
BDI	23.58 (5.92)	0	<0.001 ^{a,*}

^a two-sample t-test

^b *chi*²-test

* significant for $p < 0.05$, Bonferroni-corrected for multiple comparisons.

groups regarding the cardiac rate ($p > 0.5$), as well as the respiratory rate ($p > 0.5$). Subsequently, the PESTICA monitored cardiac and respiration cycles were used for Retrospective Image Correction (RETROICOR) (Glover et al., 2000). RETROICOR is an image-based correction method, in which low-order Fourier series are fit to the image data, based on the time of each image acquisition relative to the phase of the cardiac and respiratory cycles. Via RETROICOR, physiological noise is removed from fMRI data in a voxel-wise fashion. Following the correction for physiologic noise, motion-induced artifacts were accounted for, using SLOMOCO. This method uses an algorithm to estimate the out-of-plane motion and to subsequently correct the data for the acquired estimates. This was done alternatively to the classical procedures of volume realignment in SPM12, as SLOMOCO has been shown to perform better than volumetric methods, and precisely detect motion of independent slices, correcting for almost all effects of motion corruption in BOLD data (Beall and Lowe, 2014). Differences in SLOMOCO estimates of head movement between groups were tested to further control for head motion effects across groups. The mean relative head displacement was calculated as the root mean squared volume-to-volume displacement (Power et al., 2014; Satterthwaite et al., 2013). The two-sample t-test revealed

no significant differences in the mean relative head motion between groups ($p > 0.05$).

Normalization

The data controlled for physiological and motion artifacts were subsequently normalized into the standard MNI space using SPM12.

Nuisance covariates regression

Further cleaning of the fMRI data from signals of non-neural sources included the regression of nuisance covariates, such as the WM and CSF time courses. The nuisance covariates regression was performed following the exact pipeline described previously in the context of Dataset 2 of Project 1 (see section 3.1.2). Subsequently, the fMRI data with regressed nuisance covariates was spatially smoothed in SPM12 using a 6-mm FWHM Gaussian kernel.

4.1.3 Data Analysis

Degree Centrality Maps

Degree centrality (DC) maps were computed for each participant using REST which implements an approach similar to that proposed by Buckner et al. (2009) and Zuo et al. (2012). The procedure for DC calculation is the following: for each voxel, a correlation coefficient between its own time course and the time course of every other voxel in the brain is calculated. This results in a connectivity map of the given voxel which, in the next step, is binarized at a selected threshold (here, $r = 0.2$). During binarization, all correlation coefficients below the given threshold are set to zero, while all correlation coefficients above the threshold are set to 1. In the last step, the sum of all non-zero connections for the given voxel is calculated. This procedure is repeated for all voxels, yielding a whole-brain DC map. The single-subject DC maps are then normalized by applying a z-transform (i.e., subtracting the mean, and dividing by the standard deviation of the degree across all voxels within the brain).

DC maps were calculated within the full frequency range of the rs-fMRI signal (i.e., 0.01–0.25 Hz), as well as within 10 frequency sub-bands (freq1: 0.01–0.025; freq2:

0.025–0.05; freq3: 0.05–0.075; freq4: 0.075–0.1; freq5: 0.1–0.125; freq6: 0.125–0.15; freq7: 0.15–0.175; freq8: 0.175–0.2; freq9: 0.2–0.225; freq10: 0.225–0.25 Hz). The BOLD signal was band-pass filtered into 10 frequency bands using REST toolbox which, by default, uses the ideal rectangle window. In REST, the ideal filter transforms the time series into the frequency domain via the discrete Fourier transform and adds zeros to extend the frequency coverage, then transforms back to the time domain by using the inverse discrete Fourier Transform (Song et al., 2011).

Construction of Gray Matter Volume Covariates

Gray matter atrophy can largely affect measures of FC. The variance of fMRI signal in a brain region characterized by decreased gray matter volume (GMV) would exhibit higher contribution of the cerebrospinal fluid (CSF) and thus, decreased signal-to-noise ratio (i.e., increased contributions of noise to the signal). Measures of FC, such as the correlation coefficient, are highly susceptible to noise (Birn et al., 2006; Chang et al., 2009; Dagli et al., 1999; Van Dijk et al., 2012; Power et al., 2012; Shmueli et al., 2007). Up to 25% of within-subject variance in DC was shown to be explained by the underlying structural properties of the brain, where lower DC was found in brain regions with higher contributions of non-GM tissues (Dukart and Bertolino, 2014). In conclusion, it is highly relevant to control for the impact of the differences in GMV on measures of FC, such as the DC.

Voxel-based morphometry (VBM) analysis was carried out using the SPM12-based Computational Anatomy Toolbox (CAT12)² to determine differences in brain volumetric measures between groups. The processing pipeline of CAT12 executes the following procedures: Structural T1 images are normalized to a template space and segmented into GM, WM, and CSF. Next, the total intracranial volume (TIV) and absolute as well as relative global GM, WM, and CSF volumes are estimated per participant. The resulting GM images are smoothed using an 8-mm FWHM Gaussian kernel.

In SPM12, voxel-wise two-sample t-tests were performed to investigate group differences in GMV (p cluster-level corrected < 0.05 , on underlying voxel-level correction of $p < 0.001$) while controlling for individual TIV values.

²<http://www.neuro.uni-jena.de/cat/>

Statistical Analysis

DC maps of individual subjects from the HC group were subjected to a one-sample t-test in SPM12 (p cluster-level corrected < 0.05 , on underlying voxel-level correction of $p < 0.001$, with voxels restricted to GM) to identify baseline, healthy DC patterns at each of the 10 frequency sub-bands, as well as at the full frequency range. Subsequently, potential differences in DC patterns between groups at each frequency sub-band were examined using a flexible factorial design with main factors group and frequency, and were tested with t-tests (p cluster-level corrected < 0.05 , on underlying voxel-level correction of $p < 0.001$, with voxels restricted to GM). Potential differences in DC patterns at the full frequency range, without division into specific sub-bands, were examined via a two-sample t-test (p cluster-level corrected < 0.05 , on underlying voxel-level correction of $p < 0.001$, with voxels restricted to GM).

To control for the impact of possible depression-related brain volumetric changes on the observed group differences in DC, a whole-brain voxel-wise regression between subjects' DC maps and their re-sliced GMV images was performed at each frequency band, using an in-house, Matlab-based script. Regression residuals from this procedure represented the new DC maps which were controlled for GMV. Next, and adequately to the statistical analysis carried out on the non-GMV-corrected DC maps, group differences in GMV-corrected DC maps were examined at each frequency band using a flexible factorial design with main factors group and frequency, and were tested with t-tests (p cluster-level corrected < 0.05 , on underlying voxel-level correction of $p < 0.001$, with voxels restricted to GM).

Degree Centrality and symptom severity

Clusters representing significant group differences in DC at specific frequency bands served as ROIs from which, at the subject level, averaged DC values were extracted. Pearson's correlation was calculated between the averaged DC values of each cluster at distinct frequency bands and the symptom severity scores (with Bonferroni-correction for multiple comparisons, $n = 9$ for only nine frequency bands significant alterations in patient DC were observed).

4.2 Results

4.2.1 Brain Volumetric Analysis

When compared to HC, MDD patients exhibited significant regional GM atrophy (see Figure 4.1). Decreased GMV was observed in the bilateral middle frontal gyrus (cluster 1 and 2); the right middle orbital gyrus (cluster 1); the left superior medial frontal gyrus and the left ACC (cluster 3); as well as in the left hippocampus and left superior temporal gyrus (cluster 4). Detailed information about cluster peaks, their coordinates, z-values, and attributed brain regions are summarized in Table 4.2.

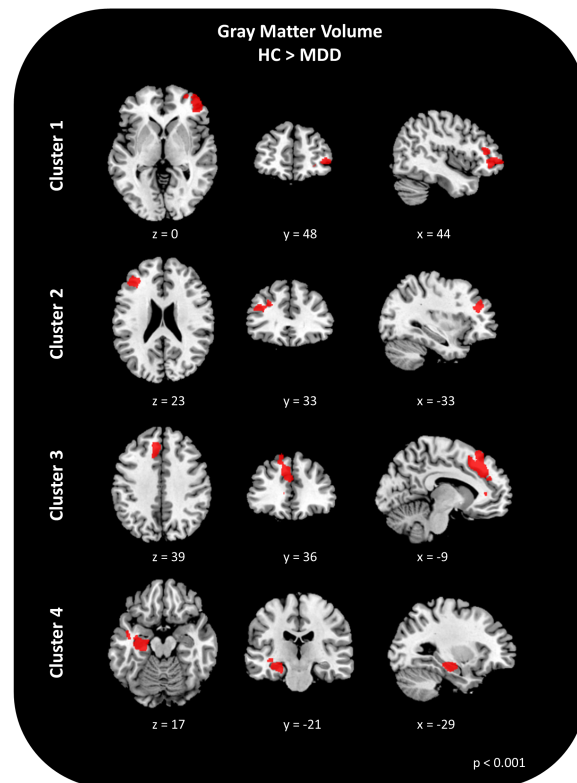


Fig. 4.1. | **MDD: Gray Matter Atrophy.** Regional differences in gray matter volume (GMV) between groups (p cluster-level corrected < 0.05 , on underlying voxel-level correction of $p < 0.001$, applying a cluster extent threshold of $k = 800$ voxels). The analysis of voxel-based morphometry yielded four clusters of significantly decreased GMV in MDD patients when compared to healthy controls (HC). Cluster 1: right middle frontal gyrus and right middle orbital gyrus; cluster 2: left middle frontal gyrus; cluster 3: left superior medial frontal gyrus and left anterior cingulate cortex (ACC); cluster 4: left hippocampus and left superior temporal gyrus.

Tab. 4.2. | **GMV: HC > MDD.** Results of the group comparison of voxel-based morphometry analysis. Significant decreases in gray matter volume (GMV) were observed in major depressive disorder (MDD) patients when compared to HC. Results presented in the table include the cluster size, z-value, MNI coordinates, side, and anatomical locations of the peak voxels. Reported are only the brain areas with p cluster-level corrected < 0.05, on underlying voxel-level correction of p < 0.001.

GMV: HC >MDD		MNI coordinates [mm]					
cluster size	z-value	x	y	z	side	location	
1032	4.44	44	48	0	R	Middle Frontal Gyrus	
	3.85	30	54	-3	R	Middle Orbital Gyrus	
872	4.11	-39	41	29	L	Middle Frontal Gyrus	
2000	4.37	-8	32	32	L	Superior Medial Frontal Gyrus	
	4.29	-3	36	29	L	ACC	
1473	4.07	-29	-21	-17	L	Hippocampus	
	4.05	-47	-5	-14	L	Superior Temporal Gyrus	

4.2.2 Healthy Controls: frequency-resolved Degree Centrality

DC maps of HC at each of the 10 frequency bands, as well as at the full frequency range (i.e., 0.01–0.25 Hz), are displayed in Figure 4.2. Figure 4.2.A depicts the frequency-specific organization of hubs—i.e., brain areas characterized by high DC. At low-frequency bands (freq1–3; 0.01–0.075 Hz) high DC voxels are observed in the cuneus, post- and precentral gyri, paracentral lobule, superior temporal gyrus, and midcingulate cortex (MCC). In addition, at freq1 (0.01–0.025 Hz) the insula constitutes a functional hub. At middle-frequency bands (freq4–7; 0.075–0.175 Hz) the middle occipital gyrus, cuneus, precuneus, MCC, angular gyrus, inferior parietal lobule (IPL), supramarginal gyrus, and the insula are characterized by high DC values. At high-frequency bands (freq8–10; 0.175–0.25 Hz), the cuneus, precuneus, angular gyrus, MCC, IPL, and ACC exhibit high DC values.

Athwart a wide range of frequency bands, the cuneus and MCC, as well as the precuneus, IPL, angular gyrus, and supramarginal gyrus appear as regions crucial for information integration—as defined by their high DC profile. Specifically, regions within the lateral parietal cortex (associated with the DMN) appear to be central to information integration at a wide range of frequency bands, i.e., freq3–10 (0.075–0.25 Hz), but most prominently at middle- to high-frequency bands 6–10 (0.125–0.25 Hz).

DC analysis of the rs-fMRI signal at the full frequency range (i.e., 0.01–0.25 Hz), without decomposition into frequency sub-bands, revealed the following hub regions: the cuneus, precuneus, MCC, paracentral lobule, post- and precentral gyri, middle temporal gyrus, superior temporal gyrus, middle occipital gyrus, angular gyrus, IPL, insula (see Figure 4.2.B).

A detailed list of hubs which occur in HC within the full frequency regime, as well as within the 10 individual frequency sub-bands, is presented in the Appendix Table B.1 and B.2, respectively.

4.2.3 MDD patients: alterations in frequency-resolved Degree Centrality

In MDD patients, significant frequency-specific decreases in regional DC were found in a broad range of frequency bands (see Figure 4.3.A). Importantly, no significant increases in DC in MDD patients were found when compared to HC. At low-frequency bands (freq1–2; 0.01–0.05 Hz), the insula (at freq1, 2) and the transverse temporal gyrus (at freq1) exhibited decreased DC. No significant difference in DC was observed at low-frequency band 3 (0.05–0.075 Hz). At the middle-frequency bands (freq4–7; 0.075–0.175 Hz), decreased DC was observed in the middle occipital gyrus, calcarine gyrus, superior temporal gyrus (at freq4), in the insula (at freq4, 5), the MCC and supramarginal gyrus (at freq5, 6), in the precuneus (at freq6, 7), and in the angular gyrus (at freq5, 7). At the high-frequency range (freq8–10; 0.175–0.25 Hz), DC reductions were observed in the ACC and the superior temporal gyrus (at freq8–10), in the insula, putamen, and hippocampus (at freq8), in the supramarginal gyrus and the IPL (at freq9). Notably, in MDD patients, the insula exhibited significantly decreased DC across several frequency bands (i.e., freq1, 2, 4, 5, 7 and 8). Upon closer inspection, it becomes visible that peak coordinates that represent voxels of decreased insular DC differ between frequency bands (see Figure 4.3.B). In summary, in MDD patients, largely distinct parts of the insula exhibit reduced DC at distinct frequency bands.

Next a two-sample t-test was carried out on the DC maps which were obtained from the rs-fMRI signal at the full frequency range (i.e., 0.1–0.25 Hz), without decomposition into specific sub-bands. This test, however, did not reveal any significant group differences at the given statistical threshold.

Subsequently, group differences in the GMV-corrected DC maps at each frequency sub-band were examined. The observed group differences are depicted in Figure 4.4 and resemble to a great extent the group differences observed from the non-GMV-corrected DC maps.

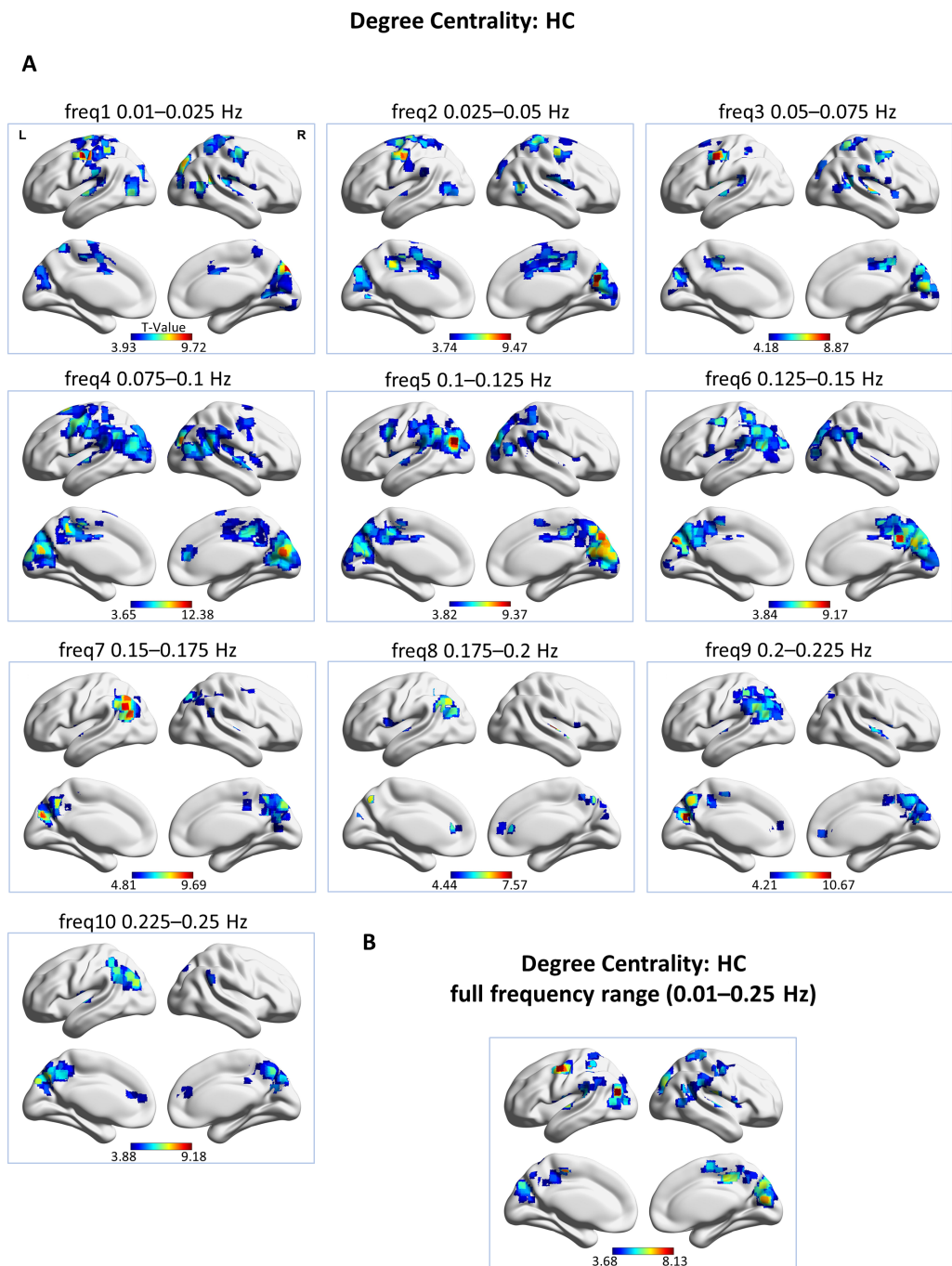


Fig. 4.2. | **DC: HC.** Group-level voxel-wise degree centrality (DC) maps for healthy controls (HC). DC maps were obtained by subjecting individual z-maps to a one-sample t-test (p cluster-level corrected < 0.05 , on underlying voxel-level correction of $p < 0.001$, with voxels restricted to gray matter). (A) DC maps at 10 different frequency bands, represented by t-values. (B) DC map at the full frequency range of 0.01–0.25 Hz, represented by t-values.

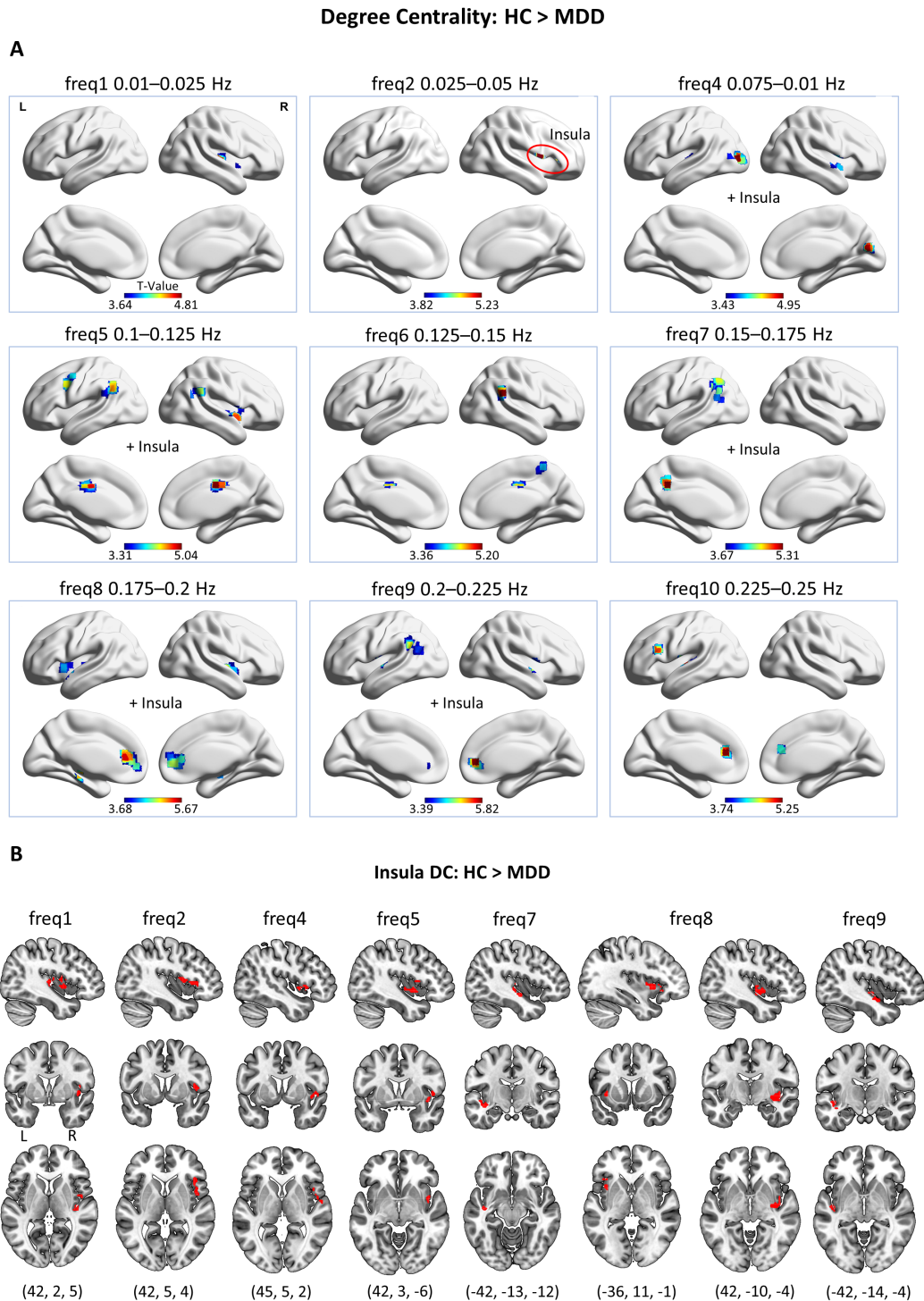


Fig. 4.3. | **DC: HC > MDD.** (A) Group differences in voxel-wise degree centrality (DC) across nine frequency bands (reported are only the frequency bands where significant differences were found, p cluster-level corrected < 0.05 , on underlying voxel-level correction of $p < 0.001$, with voxels restricted to gray matter). At freq2, the cluster is located exclusively in the insula. (B) Group differences in voxel-wise DC of the insula at different frequency bands. This figure encloses supplementary information to panel (A) for improved visibility. Abbreviations: HC, healthy controls; MDD, major depressive disorder; freq, frequency.

Degree Centrality: HC > MDD
corrected for gray matter volume

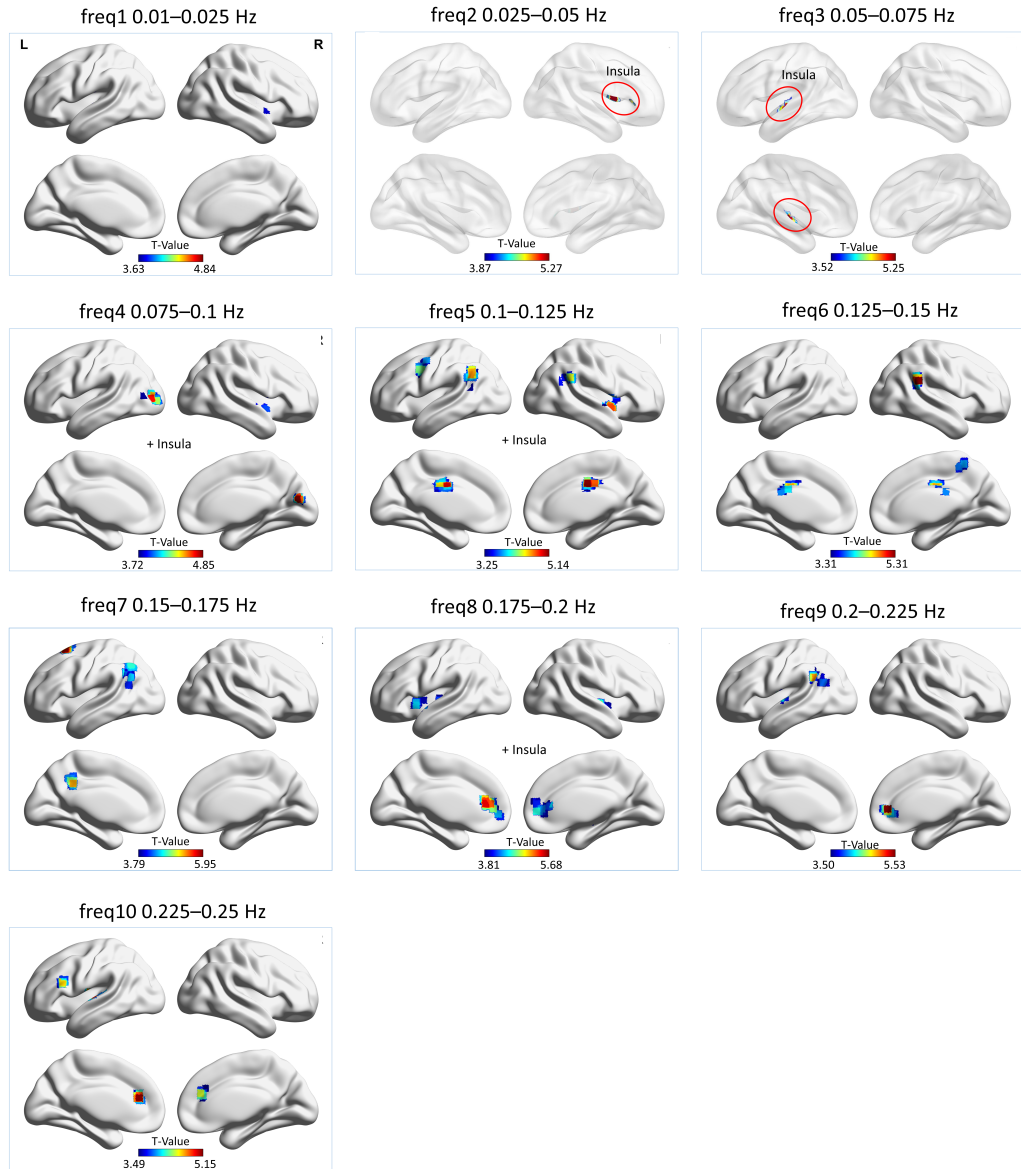


Fig. 4.4. | **DC: HC > MDD, corrected for GMV.** Group differences in voxel-wise degree centrality (DC) across 10 frequency bands, controlled for gray matter volume (GMV; p cluster-level corrected < 0.05, on underlying voxel-level correction of $p < 0.001$, with voxels restricted to gray matter). At freq2 and freq3, the clusters are located exclusively in the insula. Abbreviations: HC, healthy controls; MDD, major depressive disorder; freq, frequency.

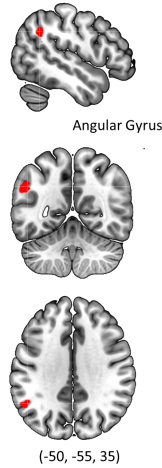
A detailed list of brain regions which exhibited significantly decreased DC in MDD patients compared to HC, derived from both the regular DC maps as well as the GMV-corrected DC maps is presented in the Appendix Table B.3 and B.4, respectively.

4.2.4 Degree Centrality and symptom severity

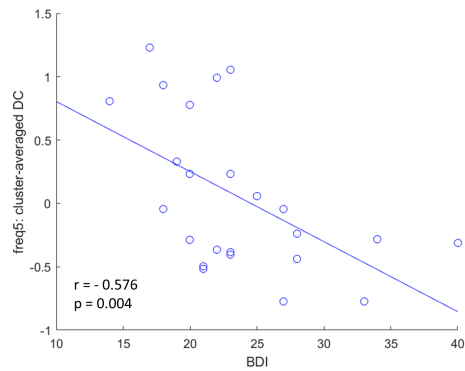
A significant correlation between decreases in regional DC at specific frequency bands and clinical characteristics of MDD was found. At frequency band 5 (0.1–0.125 Hz) a significant negative correlation was revealed between the BDI score and the averaged DC value within a cluster that spans the left angular and supramarginal gyri ($r = -0.576$, $p < 0.005$). At frequency band 9 (0.2–0.225 Hz) a significant negative correlation was found between the length of the current major depressive episode and the averaged DC value of the insula ($r = -0.586$, $p < 0.005$). The described two clusters of decreased DC in MDD as well as the correlation between the cluster-averaged DC values and symptom characteristics are displayed in Figure 4.5. These correlations were observed independently of the reductions in GMV, as they could be replicated in a subsequent correlation analysis based on averaged GMV-corrected DC values from those two clusters (freq5: DC x BDI, $r = -0.597$, $p < 0.005$; freq9: DC x length of current MD episode, $r = -0.539$, $p < 0.01$).

DC: HC > MDD

freq5
(0.1-0.125 Hz)



correlation with MDD symptoms



freq9
(0.2-0.225 Hz)

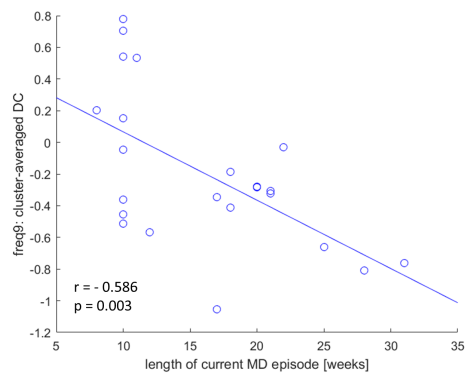
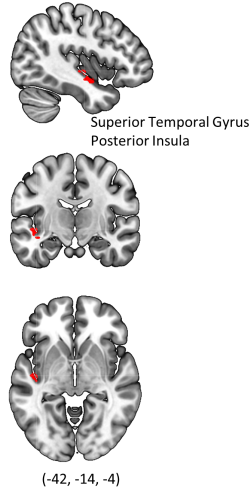


Fig. 4.5. | DC and MDD symptomatology. Correlation between the pathologically decreased degree centrality (DC) values of the angular gyrus at frequency 5 (0.1–0.125 Hz) and the BDI score (top panel); as well as between the decreased DC values of the insula at frequency 9 (0.2–0.225 Hz) and the length of current major depressive episode (in weeks; bottom panel). Abbreviations: HC, healthy controls; MDD, major depressive disorder; freq, frequency; BDI, Beck Depression Inventory.

Discussion

5.1 Project 1

In the first project, I performed a spectral analysis of BOLD network fluctuations using a high-quality, large sample dataset of the HCP. Results revealed a significant grading of spectral centroid values across RSNs. The grading of SC across RSNs refers to the observation that each RSN takes a distinct position in an ordering of all SC values. Thus, the grading of SC across RSNs implies that each RSN operates on a characteristic frequency regime. I successfully replicated this finding through an independent dataset of 25 healthy subjects. Network orderings in both datasets under investigation proved to be highly correlated. Thus, the grading of SC across RSNs proves to be highly reliable across two independent datasets.

Furthermore, the biological relevance of the SC as a meaningful representation of networks' spectral properties was validated via disorder effect. In the dataset of 25 MDD patients, I found that the grading of SC was significantly altered. Specifically, the SC of the salience network was significantly shifted towards higher frequencies. This shift was found to be due to decreased contributions of low frequencies and increased contributions of high frequencies to the BOLD signal of the SN in MDD.

Additionally, in the dataset of 25 healthy controls, I observed a grading of the percent signal change values across RSNs, which implicates significantly distinct levels of absolute BOLD activity within specific neural ensembles. The grading of PSC was also affected by MDD, where a significant increase in the PSC of a secondary visual-occipital network was found¹.

5.1.1 Grading of Spectral Centroid across RSNs

The first striking finding of my analysis is the occurrence of a highly organized grading of SC values derived from the power spectra of slow (i.e., < 1 Hz), broadband RSN BOLD fluctuations in healthy subjects. The SC was introduced as a novel measure describing the "center of gravity" of the full power spectrum of RSN BOLD

¹The argumentation presented in the discussion of Project 1 has been adapted from my first-author publication Ries et al. (2018)

fluctuations. Investigations performed on the dataset from the HCP revealed that different RSNs involve and operate on distinct broadband frequency patterns, via which information can selectively be exchanged between targeted systems. This ordering of RSNs according to their characteristic SC values is referred to as the "grading" of SC.

To validate the generalizability and replicability of the finding of the SC grading, I repeated the analysis on an independent dataset comprising 25 healthy controls, acquired at my research facility. In line with the findings from HCP data, the spectral analysis of the second dataset also revealed a significant grading of SC values of RSN BOLD network fluctuations. Correlation analysis between the SC values of individual RSNs from Dataset 1 and the corresponding RSNs from Dataset 2 endorse the reproducibility of SC as a network property—given the different acquisition sites and parameters, as well as different preprocessing pipelines. The findings derived from HC in Dataset 2 further highlight and support the meaningfulness of SC measure as a representative of underlying neural features of RSNs, by means of which a general organization—i.e., grading—of neural systems according to their spectral properties can be described.

Such grading is—in electrophysiology—believed to be characteristic for a highly interactive system of network oscillators (Buzsáki, 2006) and enables a degree of communication between oscillators, for only networks with overlapping oscillatory profiles are preferentially able to synchronize with each other and form FC. Respectively, any deviation from a network's healthy oscillation profile would result in a desynchronization between its own signal and the signal of networks it communicates to, and thus, in a breakdown of the brain's large-scale communication structure. Likewise, in the BOLD signal—which rather relates to fluctuations in broadband power of electrical oscillation—FC between any two brain areas can only arise with overlapping frequency spectra. Alterations of the spectra are therefore indicative of lack of communication.

Previous body of research suggests that resting-state BOLD fluctuations exhibit frequency-dependent, anatomically restricted spatial structure in the human brain (Baria et al., 2011; Kalcher et al., 2014; Salvador et al., 2008; Wu et al., 2008; Zuo et al., 2010). Salvador et al. (2008) investigated frequency-dependent FC profiles and found that limbic and temporal brain areas display the highest level of oscillation coherence at high (0.17–0.25 Hz) and middle (0.08–0.17 Hz) frequency bands, while at low frequencies (< 0.08 Hz) the strongest connectivity is present in frontal brain regions. Convergetly, Baria et al. (2011) provided evidence of whole-brain organization of BOLD fluctuations within the full spectrum of frequencies available from rs-fMRI. The power of BOLD fluctuations within the high-frequency band (0.15–0.20 Hz) was shown to be most dominant in the temporal and sub-cortical

regions as well as in the insula, whereas the power of BOLD fluctuations at the low-frequency band (0.01–0.05 Hz) was most accentuated in the prefrontal, occipital, and parietal lobes. Kalcher et al. (2014) showed that signals from cortical regions exhibit the highest contributions of frequencies below 0.25 Hz, while signals in subcortical regions, as well as the insula, are strongly influenced by high-frequency fluctuations (i.e., 0.25–1.4 Hz). More recently, a hierarchical organization of timescales of intrinsic dynamics has been suggested, highlighting the sensorimotor-to-transmodal temporal gradient (Cocchi et al., 2016; Gollo et al., 2015; Gollo et al., 2017; Honey et al., 2012; Stephens et al., 2013; for review see Huntenburg et al., 2018). According to this gradient, early sensory cortical areas such as the primary visual, somatomotor and auditory cortices, operate on faster intrinsic dynamics, while the frequency content becomes dominated by lower frequencies as the gradient shifts toward higher-order transmodal areas in the parietal, temporal and prefrontal cortex. Such an organization was also observed in the context of large-scale brain networks (Gollo et al., 2015; Gollo et al., 2017). Across networks, the early sensory RSNs showed faster dynamics when compared to the high-order RSNs. Within networks, the highly interconnected regions exhibited a slower dynamic regime when compared to the less interconnected peripheral regions.

In partial agreement with the aforementioned observations, the analysis on the HCP data yielded the following networks as showing the highest SC values (i.e., the strongest influence of high-frequency power on the network's fluctuations profile): the basal ganglia network (main hubs in the putamen, caudate nucleus, pallidum), the early sensorimotor networks (SM_R, SM_4, SM_L; main hubs in the precentral gyrus and paracentral lobule), the auditory network (main hubs in the superior temporal gyrus), and the anterior subsystem of the DMN (DMN_ant; main hubs in the middle and superior frontal gyri, and in the anterior cingulate cortex). On the other end of the power distribution, with relatively low SC values, the following networks were situated: the posterior-lateral DMN (DMN_postlat; main hubs in the posterior cingulate cortex, precuneus, cuneus, angular gyrus, IPL), the posterior DMN (DMN_post; main hubs in the PCC, precuneus, cuneus, IPL), and the bilateral attention networks (ATT_L, ATT_R; main hubs in the inferior and middle frontal gyri, IPL, angular gyrus). Two of the visual networks (VIS_4, VIS_6) and two of the sensorimotor networks (SM_1, SM_2) were also observed at the lower end of the spectrum. At first, the occurrence of the visual and sensorimotor networks at the lower end of the SC grading seems to be incongruent with the sensorimotor-to-transmodal organization. However, it is important to note that these networks represent—within their modality—higher order systems which fall toward the end of a modality's hierarchy of processing complexity.

When ordered accordingly to the decreasing SC magnitude, the spatial distribution of brain areas constituting individual visual networks exhibits a rather characteristic

pattern (see Figure 5.1). Networks encompassing predominantly early sensory areas in the striate cortex (i.e., primary visual area V1, calcarine sulcus) exhibit higher SC values (VIS_2, VIS_3), which indicates that their BOLD signal is strongly influenced by high frequencies. Networks that encompass higher-order cortical areas along the visual stream, i.e., the extrastriate cortex (i.e., visual areas V2, V3, V4, V5/MT) show comparably lower SC values (VIS_6, VIS_4), which indicates that the lower frequencies dominate their BOLD signal. However, with one exception: VIS_1 exhibits the highest SC among the visual networks, although it comprises the higher order visual area V5/MT in the middle temporal gyrus. This observation could be related to the findings of previous studies, which highlight extensive connections between area V5/MT and area V1 (Pascual-Leone and Walsh, 2001; Silvanto et al., 2005). The FC between these areas is likely to be facilitated through synchronous neural oscillations, which would be reflected in similar SC values between RSNs comprising these areas. Noteworthy, the observation that networks comprising the same V5/MT area are situated both at the higher and lower end of the SC gradient could relate to the multiple parallel processes being asynchronously undertaken by area V5/MT (for review see Zeki, 2015). To conclude, areas of the visual cortex are highly functionally specialized (Zeki et al., 1991). My findings further corroborate with this notion, as they reveal that distinct functional units within the visual system operate on distinct regimes of intrinsic BOLD dynamics—an organization which is congruent with the sensorimotor-to-transmodal gradient of timescales observed in the brain.

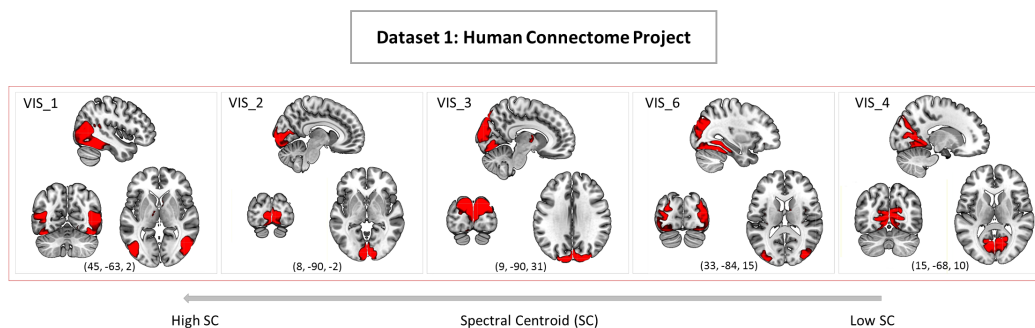


Fig. 5.1. | SC and the functional hierarchy within the visual system. Networks constituting the visual system ordered accordingly to their decreasing spectral centroid (SC) magnitude; displayed at the three most informative slices (MNI space). Figure taken from (Ries et al., 2018)

Interestingly, my observations show that the anterior and posterior subsystems of the DMN are situated at different ends with regards to the grading of SC. The anterior and anterior-medial DMNs show relatively higher SC values, while the posterior and posterior-lateral DMNs show relatively lower SC values. This is indicative of differential contributions of spectral power to different subsystems of the

DMN, possibly reflecting distinct processes facilitated via distinct frequencies. These observations are in line with previous reports which highlight the heterogeneous profile of the DMN functional architecture. Particularly, the DMN was shown to comprise of smaller anatomical-functional subsystems (Andrews-Hanna et al., 2010). Information integration across the subsystems of the DMN has been shown to be implicated in a number of neuropsychiatric disorders including Alzheimer's disease (Damoiseaux et al., 2012), schizophrenia (Du et al., 2016), OCD (Beucke et al., 2014) and MDD (Sambataro et al., 2014; Zhu et al., 2012; Zhu et al., 2017).

In summary, the grading of SC across RSNs points towards frequency-dependent functional specificity, which is indicative of differentiated information integration processes being executed at different frequency scales, in different brain regions. This is in accordance with the results of Neufang et al. (2014) and Cocchi et al. (2016) which hint towards the frequency-driven directionality of information flow in the brain.

5.1.2 Biological relevance of Spectral Centroid grading

Previous research viewing a number of neurological and psychiatric disorders revealed that these diseased states are associated with power shifts of ongoing BOLD network fluctuations across various frequency bands. Garrity et al. (2007) explored BOLD network fluctuations in schizophrenia, and found that this disorder was associated with a more rapidly fluctuating activity within the DMN. In this network, significantly decreased power of the low-frequency fluctuations (0.03 Hz) was detected, accompanied by significantly increased power at higher frequencies (0.08–0.24 Hz). Calhoun et al. (2011) investigated the spectral profile of RSNs in schizophrenia and bipolar disorder, and observed a consistent pattern of decreased low-frequency power along with increased high-frequency power across multiple RSNs, uniformly in both patient groups. In chronic pain, Malinen et al. (2010) detected increases in spectral power of activity within the insula and ACC at middle to higher frequency bands (0.12–0.25 Hz). Also in chronic pain, Baliki et al. (2011) found increases in power of high-frequency BOLD fluctuation (0.12–0.20 Hz) mainly in the mPFC and parts of the DMN. These studies all reveal significant shifts in spectral power of RSN time courses in several diseases, with the predominant common tendency of decreased power in low frequencies and increased power in high frequencies.

These observations are convergent with the results of my analysis. The grading of SC of BOLD network fluctuations in MDD patients significantly deviated from the grading observed in HC. Precisely, I found a shift of the SC of the SN towards higher frequencies, which could be attributed to a relatively attenuated power in low

frequencies (0.01–0.025 Hz) and amplified power in a broad range of higher frequencies (0.175–0.2 Hz) in MDD patients—implying increased activity with characteristic times corresponding to this frequency range within the salience system.

Since I postulate that the grading of the SC of BOLD network fluctuations is crucial to successful communication, I further investigated how shifts in BOLD fluctuations of the SN impact on the network's communication pattern. Through a subsequent whole-brain seed-based FC analysis of the SN, I gained insight into the consequences of the network's altered intrinsic dynamics and determined brain regions toward which SN showed aberrant communication in major depression. In MDD patients, I observed decreased FC of the SN toward the anterior DMN and one of the visual networks (VIS_4). Although I did not find a direct significant correlation between the SC of the SN and scores of depression severity, the SC values of the networks to which SN exhibited altered FC significantly correlated with BDI scores. Thus, I suspect an indirect influence that the shift in the power spectrum of the SN exerts on the severity of experienced symptoms. One possible mechanism underlying such a reaction chain could be that the decoupling of the SN from both the anterior DMN and the visual network forces these networks to regain the lost oscillation synchronicity, and that such compensatory attempts would be mirrored through depression severity. This interpretation is, however, only speculative and further investigations would be needed to support it.

Following up on this speculation, it would be highly interesting to examine the effects of non-invasive brain stimulation on the severity of symptoms experienced by MDD patients. Transcranial magnetic stimulation (TMS) is one of the techniques used for non-invasive brain stimulation. TMS utilizes short, rapidly changing magnetic field pulses to induce electrical currents in the underlying cortical tissue (for review see Hallett, 2007; Kobayashi and Pascual-Leone, 2003; Wagner et al., 2007). The application of repeated pulses TMS (rTMS) at low frequencies (e.g., 1 Hz) has been shown to result in the suppression of underlying cortical activity, while high-frequency stimulation (e.g., 20 Hz) results in excitatory changes. It has also been shown that the effects of rTMS on neural activity are not confined to the stimulation site, but can propagate beyond it—impacting a distributed network of brain regions (Ferreri et al., 2011; Fox et al., 2012b; Siebner et al., 2009). Thus, it would be interesting to examine whether rTMS applied to MDD patients—specifically targeting the SN, and aiming at bringing the SN dynamics closer to a healthy regime—results in reduced scores of symptom severity. If so, it would be interesting to further investigate whether the reductions in symptom severity relate to stimulation-induced changes in SC values of the anterior DMN and the VIS_4 network, since the SC values of these RSNs were shown to significantly correlate with symptom severity scores. Henceforth, the findings of this study pave the way for new, targeted investigations of the effects of brain stimulation on the symptomatic and pathophysiology of MDD.

5.1.3 Grading of BOLD activity levels across RSNs

The analysis of the absolute BOLD activity level—as quantified by PSC—revealed that distinct RSNs exhibit distinct levels of BOLD activity. In other words, the concept of a grading of RSNs according to their specific properties also holds true for the measure of PSC. Thus, one can speak of a grading of PSC across RSNs.

Previous studies in the human and macaque cortex revealed that widely distributed brain regions are characterized by distinct ratios of excitatory (glutamate) and inhibitory (GABA) receptor density (ExIn ratio) (van den Heuvel et al., 2016). Cortical areas with a relatively high ExIn ratio were shown to form stronger resting-state FC to other areas of the cortex. In humans, regions characterized by high ExIn ratios were situated across the precentral, superior frontal, orbitofrontal, supramarginal, superiotemporal and angular gyrus as well as the IPL, while regions with relatively low ExIn ratios were distributed across the parstriangularis, the inferior frontal gyrus, and the occipital lobe.

Such distribution is to a great extent consistent with the spatial variation in network PSC observed in the present study. Specifically, the posterior-lateral DMN (DMN_postlat; main hubs in superiotemporal, supramarginal and angular gyri) was found to exhibit by far the highest PSC. It was directly followed by the sensorimotor network (SM_1; main hubs in the precentral and superior temporal gyri, as well as in the IPL), the auditory network (main hubs in the superior and middle temporal gyri, as well as in the precentral gyrus), and the anterior-medial DMN (DMN_antmed; main hubs in the superior and middle frontal gyri, as well as in the ACC). The lowest PSC was observed in one of the visual networks (VIS_5; main hubs in the cuneus, as well as in the lingual, fusiform, and middle occipital gyri). Thus, I speculate that network PSC is a measure which largely relates to the excitation loading and magnitude of neural activity within an ensemble of brain regions, and that the activity profile of a network can be broadly influenced by the balanced impact of excitatory and inhibitory neurotransmitters and receptors. In parallel to the coupling between neural activity and changes in absolute BOLD signal, however, it is important to note that differences in BOLD PSC may also be driven by differences in cerebral vascular reactivity (CVR) (Bandettini and Wong, 1997; Handwerker et al., 2007; Thomason et al., 2007), baseline venous oxygenation (Lu et al., 2008), as well as baseline cerebral blood flow (CBF) (Liau and Liu, 2009).

5.1.4 Biological relevance of BOLD activity level grading

In addition to the observation of a grading of PSC across RSNs in healthy subjects, results of the current study reveal that MDD is associated with alterations in PSC

values of RSNs which span the occipital cortex. Precisely, MDD patients exhibited significantly increased PSC in one of the visual networks (VIS_2; main hubs in the lingual gyrus, cuneus, fusiform gyrus, and occipital gyrus) and a trend towards significance in another visual network (VIS_4). The observation of increased PSC of BOLD fluctuations within the visual network in MDD can be interpreted in the context of the study of Sanacora et al. (2004). In their study, Sanacora and colleagues found that, relative to healthy controls, MDD patients exhibited altered excitatory and inhibitory neurotransmitter levels in the occipital cortex. Specifically, MDD patients exhibited attenuated GABA and increased glutamate concentrations in the occipital cortex, along with decreased GABA/glutamate ratio which was particularly associated with- and discriminative of MDD subtypes characterized by melancholic and psychotic features.

MDD has previously been associated with GABA dysfunction (Brambilla et al., 2003; Sanacora et al., 2000; Tunnicliff and Malatynska, 2003) and converging findings reveal normalization of occipital cortex GABA concentrations following electroconvulsive therapy or selective serotonin reuptake inhibitors (SSRI) medication (Sanacora et al., 2003; Sanacora et al., 2002). Altogether, these findings support the notion that GABA function largely contributes to the pathophysiology and treatment of major depression.

Along these lines, I interpret that the increased PSC of the visual network observed in the current study could reflect the twofold mechanism underlying the overall changes in cortical excitability: (1) deficits in inhibitory processes governed by reduced GABA concentration, accompanied by (2) excessive excitatory stimulation due to increased glutamate concentration.

Moreover, studies of FC have established a link between the activity of the ventral tegmental area (VTA)—which is part of the SN—with occipital regions. Seed-based analysis shows an anti-correlated relation between VTA and the visual areas (Tomasi and Volkow, 2014; Zhang et al., 2016). Interpreted as an inhibitory influence of SN on visual areas, SN malfunctioning could relate to less inhibition exerted over these regions, which in turn could result in increased PSC of BOLD activity within occipital areas.

In accordance to the considerations on the effects of brain stimulation on RSN SC values, it would be highly interesting to additionally examine the effects of rTMS on the PSC values. More precisely, it would be interesting to investigate whether low-frequency rTMS (i.e., exerting an inhibitory effect) targeted to the occipital cortex (specifically, the VIS_2 network) results in a normalization of the pathologically increased activity within the VIS_2 network (which is reflected in increased PSC). Moreover it would be interesting to acquire Magnetic Resonance Spectroscopy (MRS)

data, concurrently to the rs-fMRI data acquired before, during, and after rTMS. MRS is used to measure the concentrations of various metabolites in cortical tissue (Stagg and Rothman, 2013), and thus could provide important information on the ratios between excitatory (glutamate) and inhibitory (GABA) receptor densities during the course of the brain stimulation procedures.

5.2 Project 2

In the second project, I examined frequency-resolved regional DC patterns determined from the full range of accessible frequencies (i.e., 0.01–0.25 Hz) of the rs-fMRI BOLD signal in HC and MDD patients. Main results indicate frequency-specific spatial configuration of functional hubs (i.e., highly connected regions) in HC, where the occurrence of dominant hubs gradually shifts from central to posterior regions and is lastly localized in the ACC and the posterior-occipital regions, with increasing frequency content. Moreover, the results highlight that regions of the DMN—a core resting-state system—retain the role of hubs over a wide range of frequencies. Noteworthy, the observation that the ACC constitutes a hub exclusively at high frequencies (i.e., 0.175–0.25 Hz) is striking and highlights how important it is to consider higher BOLD signal frequencies in connectivity analyses.

In MDD, regardless of regional gray matter atrophy, frequency-specific decreases in DC of distinct brain regions were observed. Regions of decreased DC included the occipital-, middle cingulate-, and sensorimotor cortices, as well as the lateral parietal cortex, precuneus, ACC, and the insula. The observed regions of decreased DC could be attributed to well-established RSNs such as the DMN and SN, as well as the visual, sensorimotor, and auditory networks.

5.2.1 Frequency-specific spatial distribution of hubs in healthy subjects

The DC is a measure of how well a given brain region is connected to the rest of the brain. Studies of structural (Hagmann et al., 2008; Sporns et al., 2007) and functional (Achard et al., 2006; Power et al., 2013) brain organization revealed a small number of cortical nodes that exhibit an outstandingly high number of connections to other regions. These are referred to as hubs and play an important role in global communication by (i) creating short and efficient paths of information flow, and by (ii) dynamically (Kabbara et al., 2017; de Pasquale et al., 2012; de Pasquale et al., 2016; de Pasquale et al., 2018) supporting information integration across remote brain systems (Bullmore and Sporns, 2012; Colizza et al., 2006).

Across studies, specific brain regions have consistently been reported as functional hubs (Buckner et al., 2009; Cole et al., 2010; Guye et al., 2010; van den Heuvel et al., 2008; Tomasi and Volkow, 2010; Tomasi and Volkow, 2011a; Tomasi and Volkow, 2011b; Zuo et al., 2012; for review see Kabbara et al., 2017; de Pasquale et al., 2018). These hub regions can be attributed to specific RSNs, and include: the medial prefrontal cortex (mPFC), inferior parietal lobule (IPL), angular gyrus, and ventral precuneus/posterior cingulate—associated with the DMN; the supplementary motor area, central sulcus and postcentral gyrus—associated with the sensorimotor network; the primary visual cortex and cuneus—associated with the visual network. On the structural level, brain regions with dense anatomical connections form structural hubs—which, in turn, facilitate FC. They include the precuneus/posterior cingulate, superior frontal cortex, medial orbitofrontal cortex, insula, dorsal anterior cingulate cortex (dACC), medial temporal cortex; and they overlap with all RSNs but can mostly be attributed to the SN and DMN (van den Heuvel and Sporns, 2013).

In the present study, I show that the spatial configuration of functional hubs is frequency-dependent, thus, information integration is governed in a frequency-specific manner over multiple timescales of neural activity. This is in line with previous work which revealed frequency-specific functional organization of the brain at rest (Gollo et al., 2017; Salvador et al., 2008; Sasai et al., 2014; Thompson and Fransson, 2015), as well as with reports of the dynamic processing regimes of hubs (Kabbara et al., 2017; de Pasquale et al., 2018). Combined, these results highlight the flexible and time-varying behavior of hubs, which facilitates information integration across multiple systems at multiple timescales.

In the group of HC, results of the current analysis revealed a graded shift in the occurrence of the most prominent functional hubs, with respect to the increasing frequency content. Precisely, brain regions constituting the visual system (i.e., the cuneus) and sensorimotor system (i.e., the post- and precentral gyri and the paracentral lobule) form functional hubs predominantly at lower frequencies (freq1–3; 0.01–0.075 Hz). Middle frequencies (freq4–6; 0.075–0.15 Hz) represent a somewhat intermediate state, where hubs occur widely spread across the brain but mostly within the visual system (i.e., the middle occipital gyrus, cuneus) and the DMN (i.e., the precuneus, angular gyrus, supramarginal gyrus, IPL). The ACC forms a functional hub exclusively at higher frequencies (freq8–10; 0.175–0.25 Hz). Alongside, the posterior subdivision of the DMN (i.e., the precuneus, angular gyrus, supramarginal gyrus, IPL) exhibits widespread connections at higher frequencies (freq7–10; 0.15–0.25 Hz). The insula (part of the SN) constitutes a functional hub across several low- and middle-frequency bands.

In the present study, functional hubs which were revealed both by the frequency-resolved DC analysis, as well as by the DC analysis at the full frequency range (i.e.,

without decomposition into distinct sub-bands), greatly correspond to hubs described in previous studies. Although most of the functional hubs which were revealed by the frequency-resolved DC analysis were also revealed by the full frequency range DC analysis, the unique hub profile of the ACC exclusively at higher frequencies was only captured by the frequency-resolved analysis. The ACC has been identified as a hub before (for review see Table 1 of Kabbara et al., 2017), however, to the best of my knowledge, no reports of ACC hubness unique to higher BOLD frequencies exist in the literature. With this finding, I stress the importance of frequency-resolved signal analysis under consideration of also higher frequencies of resting-state BOLD fluctuations (i.e., > 0.1 Hz)—as they hold unique information about functional integration in the brain.

Notably, a consistent hub character of regions within the DMN across a broad range of frequency bands (i.e., 0.05–0.25 Hz) was observed in this study. Previously, the DMN has been identified as a core system for information integration across remote networks. Most of the hubs determined within the whole brain can be attributed to the DMN (for review see de Pasquale et al., 2018) and hubs of the DMN are, in proportion to hubs of other networks, most widely integrated in the rich club—a strongly interlinked ensemble of highly central hubs (van den Heuvel and Sporns, 2011). Furthermore, the DMN co-forms the dynamic core network (de Pasquale et al., 2013; de Pasquale et al., 2016) whose hubs exhibit a pulsatile pattern of high-centrality states, facilitating a highly efficient topological regime for information integration across multiple brain networks in a flexible, time-varying manner (de Pasquale et al., 2018). Observations of the current study, regarding the consistent hub profile of the DMN across a wide range of frequency bands, further corroborate with the notion that the DMN is central to information integration across various functional systems at multiple timescales of neural activity.

5.2.2 Frequency-specific decreases in regional hubness in major depressive disorder

MDD has been associated with altered FC athwart multiple large-scale systems. Previous studies highlighted aberrant connectivity of the DMN, SN, and CEN as prominent features of MDD (Hamilton et al., 2013; Li et al., 2013; Manoliu et al., 2013; Menon, 2011; Sambataro et al., 2013; Sheline et al., 2009). Furthermore, disrupted FC of the visual, sensorimotor, and auditory networks has been reported (Veer et al., 2010; Zeng et al., 2012b). More recently, MDD-related alterations in resting-state activity have been examined in a frequency-resolved fashion. The results of Luo et al. (2015) yielded frequency-specific changes in nodal centrality in the DMN, CEN, and visual network at a frequency range of 0.03–0.06 Hz. Investigations of Xue et al. (2016) revealed altered regional homogeneity (ReHo) in the middle

occipital gyrus, ACC, inferior and superior frontal gyri, mPFC, and thalamus within the frequency bands of 0.01–0.027 Hz and 0.027–0.073 Hz. Within the same frequency bands, Wang et al. (2016) reported aberrant amplitude of low-frequency fluctuations (ALFF) in the ventromedial prefrontal cortex, inferior frontal gyrus, precentral gyrus, posterior cingulate, and precuneus.

In the current study, I examined frequency-resolved alterations in regional DC in MDD patients compared to HC. This analysis was carried out under the consideration of the full spectrum of accessible frequencies within the BOLD signal (i.e., 0.01–0.25 Hz). Moreover, the frequency-dependent spatial distribution of functional hubs was examined by dividing the BOLD signal into distinct frequency sub-bands at a fine-grained resolution (i.e., defining frequency intervals of 0.05 Hz). Subsequently, VBM analysis was carried out to control for the impact of altered brain structure on the measure of DC.

Results of the VBM analysis revealed regional decreases in GMV in MDD patients when compared to HC. Reduced GMV was found in the left dACC, in the left hippocampus, and in the bilateral middle frontal gyrus. These findings correspond to previous reports of GM abnormalities in MDD (Drevets et al., 2008; Grieve et al., 2013; Kempton et al., 2011; Koolschijn et al., 2009; Lai, 2013; Liu et al., 2010; Liu et al., 2017).

Independently of the regional gray matter atrophy in MDD patients, widespread, frequency-specific decreases in regional DC were observed in MDD patients. At the lowest frequency band (freq1: 0.01–0.025 Hz) decreased DC of the transverse temporal gyrus and the insula was observed. At the middle-frequency band 4 (0.075–0.1 Hz) the middle occipital gyrus and the calcarine gyrus exhibited decreased overall connectivity. At middle-frequency bands 5–7 (0.1–0.175 Hz) the supramarginal gyrus, precuneus, angular gyrus, and MCC were largely affected. At higher frequency bands 8–10 (0.175–0.25 Hz) the ventral and dorsal ACC was affected, as well as the IPL and supramarginal gyrus. Interestingly, distinct parts of the insula exhibited decreased DC at different frequency bands, including low-, middle-, and high-frequencies. Reduced DC of the left angular gyrus at frequency band 5 (0.1–0.125 Hz) was negatively correlated with depression severity, reflected in the BDI score. Reduced DC of the left superior temporal gyrus and the left posterior insula at frequency band 9 (0.2–0.225 Hz) was negatively correlated with the length of current major depressive episode. Altogether, brain regions which exhibited significantly reduced DC in MDD patients could be attributed to the DMN, SN as well as the visual, sensorimotor, and auditory networks—which is in line with previous findings reporting on functional changes in MDD.

Noteworthy, when compared to the full spectrum analysis, the frequency-resolved DC analysis proves to be a more sensitive method for the detection of significant alterations in regional hubness associated with MDD. The DC at the full frequency bandwidth did not reveal any significant changes at the given statistical threshold. Thus, it is important to consider the frequency content when analyzing resting-state FC patterns, and their alterations in MDD. Discrepant findings of altered FC in MDD across studies could occur due to the different frequency content of fMRI signal under investigation.

Notably, results of the current analysis only yielded pathological decreases in regional DC in MDD, but no increases. By the example of the dynamic core network, central hubness relates to dynamic integration from diverse sources and promotes flexible, time-varying topological states for highly efficient information transfer. Decreased hubness might result in loss of such flexibility and reduced variability in entering distinct connectivity states which, in turn, might translate to the pathophysiology of MDD. A recent model conceptualizes MDD as arising from an imbalanced state shift, in which patients are stuck in a state of negative mood (Holtzheimer and Mayberg, 2011). Respectively, recent rs-fMRI studies in MDD showed decreased variability in the FC of large-scale networks (Demirtaş et al., 2016), along with prolonged occurrence of certain dynamic FC states (Allen et al., 2014; Calhoun et al., 2014) which could be linked to ruminative behavior (Kaiser et al., 2016; Zhi et al., 2018).

In the following part, I will interpret the brain regions exhibiting decreased DC at the network level, and discuss the putative implications of decreased hubness in brain regions of the DMN, the SN, as well as the visual, sensorimotor and auditory networks on the pathophysiology and symptomatology of MDD.

Default-mode network The DMN is involved in self-referential and internally-oriented processes (Buckner et al., 2008). In the context of the pathophysiology and symptomatic of MDD, increased connectivity within the DMN has been linked to pathological ruminative behavior, where patients cannot disengage from internal mental processing of emotionally salient negative events (Berman et al., 2011; Zhu et al., 2012; Zhu et al., 2017). In this study, I observed decreased hubness of the DMN regions at a broad range of frequencies spanning the middle- to high-frequency bands. The ventral anterior cingulate cortex (vACC)—part of the anterior DMN—exhibited reduced hubness exclusively at high-frequencies. Loss of hubness in the vACC has been reported before by Wu et al. (2016). Furthermore, results of the current study yielded a significant correlation between decreased hubness of the angular and supramarginal gyri (regions of the DMN) at middle frequencies and the depressive symptoms. Decreased hubness of the DMN in MDD could reflect

increased intra-modular connectivity (i.e., FC within the DMN itself) at the expense of inter-modular connectivity (i.e., FC to other networks).

Saliency Network The SN is anchored in the bilateral anterior insula (AI) and the dorsal anterior cingulate cortex (dACC), but also includes three key subcortical structures: the amygdala, the ventral striatum, and the substantia nigra/VTA. The SN plays a key role in saliency detection and—through its extensive subcortical connections—in emotional control (Menon and Uddin, 2010; Uddin, 2014).

The insula is believed to be highly relevant to neuropsychiatric disorders, specifically the ones that entail deficits in higher order cognitive, emotional, and social processing. Studies propose a tripartite model of insula functional subdivisions, dividing it into dorsal-anterior, ventral-anterior, and posterior part (Chang et al., 2013; Deen et al., 2011; Kelly et al., 2012). Altogether, the insula constitutes a key hub for meta-awareness and affective processing (Craig, 2009b; Chang et al., 2013). The right anterior insula is a key node of the SN and initiates network switching between the DMN and CEN, thus, dynamically gates saliency allocation and behavioral response towards either internally or externally driven content (Goulden et al., 2014; Menon and Uddin, 2010; Sridharan et al., 2008). Due to its subjective and self-referential nature, however, the representation and perception of saliency can be vastly disrupted in psychopathology. And indeed, MDD patients exhibit:

- (i) altered insular structure (Liu et al., 2010; Peng et al., 2011; Takahashi et al., 2010),
- (ii) altered insular resting-state FC (Ambrosi et al., 2017; Avery et al., 2014; Iwabuchi et al., 2014; Liu et al., 2010; Manoliu et al., 2013; Peng et al., 2018),
- (iii) elevated insular reactivity to negatively-valenced stimuli (Lee et al., 2008),
- (iv) decreased insular reactivity to exteroceptive stimuli, leading to a predominance of interoceptive stimulus processing (Wiebking et al., 2010)—alongside with abnormal interoceptive representation (Avery et al., 2014).

These abnormalities can altogether lead to a bias toward negative thoughts and self-image (Northoff, 2017), and to the failure in the exertion of cognitive control over emotional processing. The insula also plays a key role in time perception (Craig, 2009a; Wittmann, 2009). Duration encoding is believed to represent the mental state of a person, and cognitive functions such as attention and memory, as well as drive states, mood, emotions, and personality traits have been shown to affect time perception (for an excellent review on time perception see Wittmann, 2009). Thus,

altered intrinsic activity of the insula could be putatively reflected in disturbed time perception in MDD patients, who often report a slowing down of the subjective flow of time (Bschor et al., 2004; Fuchs, 2013; Mahlberg et al., 2008; Stanghellini et al., 2017; Thönes and Oberfeld, 2015; Northoff, 2016).

The observation of decreased DC of the insula in MDD patients in this study, relates to the above reports. Moreover, the observation of frequency-specific alterations in distinct parts of the insula, corresponds to previous findings that distinct insular subdivisions are differentially affected in depression (Peng et al., 2018). It further supports the notion that distinct neural processes are being carried out at different frequencies of the neural signal (Draguhn and Buzsáki, 2004; Knyazev, 2007; Penttonen and Buzsáki, 2003).

Decreased DC of the dACC—observed exclusively at higher frequencies—could further contribute to impairments in saliency processing and deficits in attentional control over emotional stimuli. Moreover, the disrupted FC pattern of the dACC of SN at high-frequencies relates to the observations of Project 1—namely, to the altered SN power spectrum in MDD patients, which was partially driven by the elevated power at high-frequencies of BOLD fluctuations.

Visual Network In the current study, decreased overall connectivity of the occipital cortex at frequency band 4 (0.075–0.1 Hz) was observed. The visual system has been reported to be widely implicated in depression. Altered excitatory (glutamate) and inhibitory (GABA) neurotransmitter levels in the occipital cortex were observed in MDD (Sanacora et al., 2004)—implicating an overactive occipital system; efficient treatment was shown to bring GABA to presymptomatic levels along with reduced symptoms severity (Sanacora et al., 2003; Sanacora et al., 2002). Findings of Project 1 of this thesis, which reveal increased levels of absolute BOLD activity in one of the visual networks, further corroborate with the reports of a pathologically overactive visual system in MDD.

On the connectivity level, FC alterations within the visual system in MDD were reported before (Veer et al., 2010). A multivariate pattern analysis of rs-fMRI data showed that altered FC within and across regions of the visual cortex (including the lingual gyrus, fusiform gyrus, inferior occipital gyrus, and calcarine gyrus) was—concomitantly with aberrant FC of the DMN and affective (limbic) network—the most discriminative of major depression (Zeng et al., 2012b). Functional alterations of the fusiform gyrus, which plays a pivotal role in facial emotions perception (Kanwisher et al., 1997), may be linked to social avoidance in MDD patients (Liu et al., 2010; Yao et al., 2009). Alongside, FC abnormalities of other primary visual areas like the occipital cortex, calcarine gyrus, and lingual gyrus may

impact on impaired selective attention and working memory in MDD. A recent study of Le et al. (2017) supports this notion and shows that impairments in working memory updating—which relate to cognitive inflexibility in depression (manifested in rumination, perseveration of non-optimal problem-solving strategies, and inability to switch attention to new relevant information)—are linked to altered activity of the visual association areas and their FC to the prefrontal cortex.

Sensorimotor network In the current analysis, decreased DC of the left precentral gyrus—associated with the sensorimotor network—was observed at one of the middle-frequency bands (freq5; 0.1–0.125 Hz). Several reports of altered structure (Grieve et al., 2013; Peng et al., 2015; Taki et al., 2005; Zeng et al., 2012a) and function (Tsuji et al., 2017; Veer et al., 2010) of the precentral gyrus have been made in MDD. In depressive patients with a tendency for suicidal thoughts and records of committed suicide-attempts, altered structure and function of the precentral gyrus have been associated with malfunctioning impulsivity control, i.e., inhibitory control over exerted actions (Tsuji et al., 2017). Psychomotor functions are speculated to be strongly altered in depression; “the decreased environment-focus may also be manifest in lack of motivation and volition to act in the external environment which ultimately may result in psychomotor retardation and social withdrawal on the psychopathological side” (Northoff, 2016).

Auditory network At the lowest frequency band (freq1; 0.01–0.025 Hz), decreased DC of the right transverse temporal gyrus (also called the Heschl’s gyrus) within the primary auditory cortex was observed. Decreased resting-state FC of the Heschl’s gyrus has been reported in depression before (Veer et al., 2010). Reduced volume in the Heschl’s gyrus has been implicated in schizophrenia (Hirayasu et al., 2000), and was found to correlate with the severity of experienced hallucinations (Gaser et al., 2004). Altered connectivity of the primary auditory cortex might relate to psychotic symptoms that sometimes accompany severe depression. However, since the exclusion criteria for MDD patients in this study encompassed psychotic symptoms, schizophrenia, and schizoaffective disorder the aforementioned relation is rather of a general nature than one that directly relates to the observations in the study population.

5.3 Limitations

In this work, I applied the spectral centroid as an informative summary measure reflecting spectral properties of RSN BOLD fluctuations. However, it is important to note that the SC is an averaged representative of the center of gravity of a network's full power spectrum over time. Recent studies, however, show that the frequency content of BOLD network fluctuations varies over time (Yaesoubi et al., 2015; Yaesoubi et al., 2017). Throughout their time-courses, individual RSNs involve different “frequency modes” which capture characteristic spectral power distributions of network fluctuations. Occurrence rates of individual frequency modes as well as conditional co-occurrence of different modes (which is believed to reflect cross-frequency coupling in fMRI) were shown to differentiate between gender and age, possibly yielding a powerful characteristic measure in disease. Such transient states of coupling between and among remote brain systems at rest can underlie time- and frequency-dependent communication processes.

Moreover, it could be argued that different methods applied in the estimation of BOLD power spectra could yield different results. To this end, an additional analysis was performed where, instead of the Fast Fourier Transform, the modified periodogram method was applied (Welch's periodogram). Results of this analysis have been published (see Ries et al., 2018) and they highly resemble the results obtained via FFT. Thus, the properties of the observed grading of SC across RSNs occur independently of the power estimation method.

Another concern that could be expressed over my findings, is the undermined neural information content of high-frequency fMRI signal. It has been suggested that the higher band BOLD signal is primarily driven by confounding factors, such as physiological noise, and that information specific to RSNs is limited to the lower frequency range of 0.01–0.1 Hz (Cordes et al., 2001). However, as I have in detail explained in the introduction of this dissertation, convincing evidence exists highlighting that this assumption might be wrong, since meaningful neural content and stable resting-state connectivity patterns are observed in the BOLD signal at frequencies up to 0.25 Hz or even 0.75 Hz (Boubela et al., 2013; Lewis et al., 2016; Niazy et al., 2011). Higher frequencies of rs-fMRI BOLD fluctuations should be investigated, as they provide important information of the brain's functional organization. However, careful artifact removal methods need to be applied beforehand. In project 1, I operate on ICA-derived time courses which are likely to contain fewer artifacts than the raw fMRI time courses. In project 2, the motion and physiological artifacts were carefully removed using advanced signal estimation and regression methods.

On the other side, one should also consider the caveat that relates to potential non-neural effects in the low-frequency fMRI signal (< 0.15 Hz). Low frequencies can reflect effects of scanner drift, aliased high-frequency cardiac pulsations (Bhattacharyya and Lowe, 2004; Lowe et al., 1998) and slow physiological changes such as end-tidal CO₂ fluctuations (Wise et al., 2004). The effects of cardiac pulsations on observed group differences (i) in SC values were minimal since analysis on the pulsation rates did not reveal any significant differences in cardiac response between groups, and (ii) in DC were largely accounted for by regressing out the cardiac signal. However, CO₂ effects can be quite strong and are unlikely to be separated by ICA, as they constitute a global confound distributed across all independent components in the brain.

Lastly, a general concern could be expressed over the syndrome-based conceptualization and diagnosis of psychiatric disorders, including MDD. The medical model conceptualizes MDD as a group of related symptoms (DSM-V, American Psychiatric Association (2013)). Individuals are diagnosed with MDD based on the number of reported symptoms (i.e., experiencing at least five out of nine symptoms, including at least one of the two core symptoms), but are not further categorized into more specific subgroups based on a certain constellation of experienced symptoms. However, there are hundreds of possible combinations of symptoms leading to MDD diagnosis. Considering such a broad array of combinations, two individuals can be diagnosed with the same disorder while having very few symptoms in common. Thus, the syndrome-based approach may miss important information about the diversity of the psychological and biological substrates of distinct MDD phenotypes (Hasler et al., 2004). Instead, a more accurate diagnostic approach would incorporate the disaggregation of the complex and heterogeneous MDD phenotype into intermediate phenotypes or subtypes, based on differences in characteristic symptoms (e.g., melancholic, atypical, psychotic), depression onset (e.g., early vs. late, seasonal, post-partum), severity, and course of illness (e.g., single vs. recurrent, chronic) (Rush, 2007). MDD subtypes could also be characterized based on distinct neurobiological signatures obtained from neuroimaging data, in a data-driven way (Drysdale et al., 2017; Savitz and Drevets, 2009; Tokuda et al., 2018). Thus, it would be important to repeat the analyses, considering subgroups of MDD patients representing distinct depression subtypes, and investigate whether the organizational principles of resting-state BOLD activity differ between the distinct MDD subtypes. For such analysis, data from a larger population sample should be used to ensure sufficient statistical power in each of the subgroups. Still, the spectral centroid could be included as an informative measure in the investigations of spectral characteristics of RSN BOLD fluctuations across distinct MDD subtypes.

Conclusions and Outlook

The analysis of brain activity assessed via rs-fMRI has opened a window into viewing large-scale organizational principles of ongoing brain function in a non-invasive, in vivo manner. Insights from rs-fMRI studies have deepened our understanding of the brain's functional architecture at rest, as well as of the implications of such architecture to the healthy behavior and cognition. Alterations in rs-fMRI activity have been observed in a number of neurological and psychiatric disorders, including major depressive disorder. Insights from rs-fMRI data could complement current diagnostic procedures and guide a better, more precise treatment plan. Previous rs-fMRI studies in healthy subjects and MDD patients have substantially contributed to our understanding of the organizational principles of resting-state activity and, respectively, their breakdown. However, most of the previous studies were restricted in a twofold manner: (i) these studies mostly investigated the rs-fMRI BOLD signal in a limited frequency range (i.e., 0.01-0.1 Hz) and thus have ignored the higher frequencies of BOLD fluctuations; and (ii) these studies mostly viewed the rs-fMRI BOLD signal in a single frequency band, and did not divide it into distinct sub-bands. As such, the previous body of evidence in rs-fMRI studies may have ignored potentially important information carried within higher BOLD frequencies, and overlooked contributions of different frequency sub-bands to the functional brain architecture. In this work, I have addressed these limitations by two means, in two consecutive projects. I investigated what information is contained in selective frequencies of the rs-fMRI BOLD signal—under consideration of its broad frequency spectrum, also including the higher frequencies (i.e., > 0.1 Hz)—with regards to:

- (i) specialized, local processing—i.e., the spectral content of ongoing RSN BOLD fluctuations: Project 1,
- (ii) communication and information integration across brain areas—i.e., functional connectivity: Project 2.

Both projects focused on the organizational principles of resting-state BOLD activity in healthy subjects as well as the alterations in the brain's functional organization in major depressive disorder patients.

In the first project, I proposed an aggregate measure novel to the field of rs-fMRI analysis—the spectral centroid—which represents the “center of gravity” of the full power spectrum of individual RSN time courses. Based on a high-quality and large sample dataset of the Human Connectome Project, I showed that there is a highly organized grading of spectral centroid across RSNs. This indicates a characteristic balance between specific frequencies involved in the power spectrum of BOLD fluctuations in each of the RSN. I successfully replicated the finding of the occurrence of spectral centroid grading across RSNs in an independent dataset of 25 healthy subjects—which further supports the validity of the proposed approach. Moreover, I showed that the spectral centroid is a measure sensitive to power changes in BOLD network fluctuations in disease. In major depressive disorder, I observed a significantly increased spectral centroid of the salience network—a system well-known to be implicated in depression. Following the preliminary indication of altered spectral properties of salience network in depression, I selectively investigated the spectral power of salience network BOLD fluctuations within distinct frequency bands. Compared to healthy controls, increased contributions of high frequencies and reduced contributions of low frequencies to the BOLD signal of the salience network were revealed in depression. In summary, my work highlights the spectral centroid as a compact and reliable measure that allows the determination of the characteristics of the power distribution of BOLD network fluctuations and is highly sensitive in detecting changes in RSN spectral properties in major brain disease.

In the second project, I investigated frequency-resolved functional connectivity patterns—assessed via the measure of degree centrality—in healthy subjects and patients suffering from major depressive disorder. Results revealed a frequency-dependent spatial organization of functional hubs in the human brain. Major depressive disorder was found to be associated with frequency-specific alterations in regional hubness. More precisely, the overall connectivity of regions associated with the default-mode network, salience network, as well as sensorimotor, visual, and auditory networks was found to be decreased at specific frequency bands in depression. From the methodological perspective, the frequency-resolved signal analysis proved to be a more sensitive approach to detect disease-related alterations in regional hubness as compared to the full-band analysis via which no significant changes were detected. Importantly, results of the current analysis also stress the need for considering higher frequencies of the BOLD signal (i.e., > 0.1 Hz) in connectivity analyses, as they carry unique information about the functional organization of the brain at rest.

Altogether, my findings highlight the importance of frequency content when examining brain organizational properties—assessed via rs-fMRI—in health and their alterations in major depression. Specifically, I show that both the BOLD activity within large-scale functional brain systems (i.e., RSNs) as well as the overall BOLD FC

of highly central brain regions is governed in a frequency-specific manner. Crucially, in this work, I show that MDD is associated with both changes in spectral properties of the BOLD signal within selected RSNs as well as with frequency-specific alterations in the connectivity profiles of widespread brain regions. The consideration of frequency content of the BOLD signal in future rs-fMRI studies in MDD could possibly contribute to a better understanding of the underlying MDD pathophysiology, and drive more precise diagnostics and treatment procedures.

In a broader context, my results highlight the role of distinct frequency bands observed within the low-frequency BOLD fluctuations, which—comparable to the oscillation classes measured with EEG at higher frequencies—serve distinct functions, as mirrored in their differential role in information segregation and integration across the brain. As such, the observations of my study constitute an extension of the findings of distinct oscillatory classes derived from electrophysiological recordings at higher frequencies towards lower frequencies (i.e., < 1 Hz). The relationship between the characteristic spectral content of RSN BOLD fluctuations as well as the frequency-specific connectivity patterns and the underlying electrophysiological processes remains elusive. It would be of great importance to investigate which frequency classes of the EEG signal drive the BOLD activity at distinct frequencies. Deciphering these relationships would allow for the understanding of the brain's functional architecture in a mechanistic sense, on a deeper level. It would also contribute to a better understanding of the electrophysiological underpinnings of alterations in the brain's functional architecture at rest in major depression. Further work should involve concurrent resting-state EEG-fMRI recordings, and investigatory focus should be placed on the following aspects: (i) which frequency bands of the EEG signal correlate with distinct sub-bands of the rs-fMRI signal, and (ii) how does the power in distinct EEG bands relate to the FC metrics at distinct frequency sub-bands of the rs-fMRI signal.

All in all, the brain operates on distinct, fast and slow timescales of neural activity, which can be captured at different frequency levels via the use of different measurement techniques. Both the individual processes executed at fast and slow timescales and the interplay between them are of high relevance to healthy brain function. Alterations in brain processes executed at distinct timescales of neural activity significantly affect the intact brain function, as reflected in major depressive disorder. Just as alterations in the pace of the individual elements in a bird's life—the flights and the perchings (James, 1890)—would largely affect its healthy behavior.

Project 1

A

Tab. A.1. | Project 1: Correspondence between RSNs across study sites. Correspondence between established resting-state network (RSN) templates provided by Allen et al. (2011) and RSNs identified from the Human Connectome Project data (Dataset 1), as well as from the data of 25 HC & 25 MDD patients (Dataset 2). The table represents the independent component (IC) number from Allen et al. (2011), the corresponding RSN name, the abbreviated RSN name used for the purposes of this work, and an indication whether ICs from Dataset 1 and Dataset 2 could be attributed to the given RSN template. Abbreviations: DMN, default-mode network; CEN, central executive network.

RSN template from Allen et al. (2011)			IC attributed to RSN template?	
IC	RSN name	RSN name abbreviated	Dataset 1	Dataset 2
21	Basal Ganglia	BG	yes	yes
25	DMN anterior-medial	DMN_antmed	yes	yes
68	DMN anterior	DMN_ant	yes	yes
53	DMN posterior-lateral	DMN_postlat	yes	yes
50	DMN posterior	DMN_post	yes	yes
34	Attention left	ATT_L	yes	yes
60	Attention right	ATT_R	yes	yes
72	Attention	ATT	yes	yes
71	Attention Dorsal CEN	CEN	yes	yes
55	Saliience Network	SN	yes	yes
52	Attention left	-	no	no
17	Auditory	AUD	yes	yes
47	Frontal	FRONT_1	yes	yes
49	Frontal	FRONT_2	yes	yes
20	Frontal	FRONT_3	yes	no
42	Frontal	-	no	no
38	Sensorimotor	SM_1	yes	yes
7	Sensorimotor	SM_2	yes	yes
56	Sensorimotor	SM_3	no	yes
23	Sensorimotor left	SM_L	yes	yes
24	Sensorimotor right	SM_R	yes	yes
29	Sensorimotor	SM_4	yes	yes
39	Visual	VIS_1	yes	yes
46	Visual	VIS_2	yes	yes
59	Visual	VIS_3	yes	yes
64	Visual	VIS_4	yes	yes
67	Visual	VIS_5	no	yes
48	Visual	VIS_6	yes	no

Tab. A.2. | Project 1: Dataset 2: FC profile of RSNs. For each resting-state network (RSN) the set of brain regions constituting the network's positive functional connectivity (FC) are presented in the table.

Dataset 2: Healthy Controls & MDD patients	
RSN	Positive FC
BG	Parahippocampal Gyrus, Lentiform Nucleus, Subcallosal Gyrus, Lateral Ventricle, Inferior Frontal Gyrus, Claustrum, Caudate, Insula, Uncus, Medial Frontal Gyrus, Superior Temporal Gyrus
AUD	Superior Temporal Gyrus, Insula, Transverse Temporal Gyrus, Middle Temporal Gyrus, Precentral Gyrus, Postcentral Gyrus
SM_1	Transverse Temporal Gyrus, Postcentral Gyrus, Superior Temporal Gyrus, Inferior Parietal Lobule, Insula, Precentral Gyrus
SM_2	Precentral Gyrus, Postcentral Gyrus, Superior Temporal Gyrus, Inferior Frontal Gyrus, Transverse Temporal Gyrus, Insula, Middle Frontal Gyrus
SM_3	Medial Frontal Gyrus, Superior Frontal Gyrus, Cingulate Gyrus, Middle Frontal Gyrus, Paracentral Lobule, Precentral Gyrus
SM_L	Postcentral Gyrus, Inferior Parietal Lobule, Precentral Gyrus, Middle Frontal Gyrus, Superior Parietal Lobule
SM_R	Postcentral Gyrus, Precentral Gyrus, Middle Frontal Gyrus, Inferior Parietal Lobule, Insula, Paracentral Lobule, Medial Frontal Gyrus, Cingulate Gyrus, Transverse Temporal Gyrus
SM_4	Paracentral Lobule, Medial Frontal Gyrus, Precentral Gyrus, Postcentral Gyrus, Superior Frontal Gyrus, Precuneus, Superior Parietal Lobule
VIS_1	Fusiform Gyrus, Middle Occipital Gyrus, Inferior Temporal Gyrus, Inferior Occipital Gyrus, Middle Temporal Gyrus, Cuneus, Superior Occipital Gyrus, Precuneus, Lingual Gyrus, Cerebellum
VIS_2	Lingual Gyrus, Cuneus, Inferior Occipital Gyrus, Middle Occipital Gyrus, Fusiform Gyrus
VIS_3	Precuneus, Cuneus, Middle Occipital Gyrus, Posterior Cingulate
VIS_4	Lingual Gyrus, Cuneus, Posterior Cingulate, Precuneus, Cerebellum, Middle Occipital Gyrus
VIS_5	Cerebellum, Lingual Gyrus, Fusiform Gyrus, Parahippocampal Gyrus, Middle Occipital Gyrus, Cuneus, Posterior Cingulate
DMN_post	Cingulate Gyrus, Precuneus, Posterior Cingulate, Cuneus, Inferior Parietal Lobule, Supramarginal Gyrus
DMN_postlat	Cingulate Gyrus, Posterior Cingulate, Precuneus, Cuneus, Middle Temporal Gyrus, Superior Temporal Gyrus, Angular Gyrus, Supramarginal Gyrus
DMN_antmed	Medial Frontal Gyrus, Superior Frontal Gyrus, Anterior Cingulate, Middle Frontal Gyrus, Cerebellum
DMN_ant	Cingulate Gyrus, Superior Frontal Gyrus, Medial Frontal Gyrus, Anterior Cingulate, Middle Frontal Gyrus
ATT_L	Angular Gyrus, Inferior Parietal Lobule, Superior Temporal Gyrus, Middle Frontal Gyrus, Supramarginal Gyrus, Precuneus, Middle Temporal Gyrus, Precentral Gyrus, Superior Parietal Lobule, Inferior, Medial Frontal Gyrus, Superior Frontal Gyrus, Inferior Frontal Gyrus, Cerebellum
ATT_R	Inferior Parietal Lobule, Precuneus, Superior Parietal Lobule, Angular Gyrus, Supramarginal Gyrus, Middle Frontal Gyrus, Inferior Frontal Gyrus, Postcentral Gyrus, Superior Frontal Gyrus, Cerebellum
ATT	Precuneus, Superior Parietal Lobule, Postcentral Gyrus, Angular Gyrus, Superior Occipital Gyrus
CEN	Superior Temporal Gyrus, Middle Temporal Gyrus, Supramarginal Gyrus, Inferior Parietal Lobule, Precuneus, Inferior Temporal Gyrus
SN	Inferior Frontal Gyrus, Superior Temporal Gyrus, Insula, Cingulate Gyrus, Anterior Cingulate, Medial Frontal Gyrus
FRONT_1	Inferior Frontal Gyrus, Precentral Gyrus, Middle Frontal Gyrus, Inferior Parietal Lobule, Supramarginal Gyrus
FRONT_2	Middle Frontal Gyrus, Superior Frontal Gyrus, Inferior Frontal Gyrus

Project 2

B

Tab. B.1. | Project 2: DC HC: full frequency range. Results of the degree centrality (DC) analysis in healthy controls (HC) at the full frequency range. The table includes the cluster size, the z-value, the MNI coordinates, the side, and the anatomical locations of the peak voxels. Reported are only brain areas with p cluster-level corrected < 0.05, on underlying voxel-level correction of $p < 0.001$, with voxels restricted to gray matter.

DC HC; full frequency range		MNI coordinates [mm]				
cluster size	z-value	x	y	z	side	location
53	5.53	-45	-76	20	L	Middle Temporal Gyrus
	4.25	-36	-88	8	L	Middle Occipital Gyrus
41	5.49	-45	-4	50	L	Precentral Gyrus
34	5.38	-42	-43	56	L	Inferior Parietal Lobule
126	5.14	-3	-25	50	L	Paracentral Lobule
	4.73	9	-31	44	R	MCC
322	5.01	3	-79	17	L	Cuneus
	4.77	30	-79	29	R	Middle Occipital Gyrus
	4.72	12	-76	35	R	Cuneus
45	4.73	57	-19	17	R	Rolandic Operculum
	4.43	51	-16	8	R	Transverse Temporal Gyrus
46	3.54	66	-16	8	R	Superior Temporal gyrus
	4.71	48	11	-1	R	Insula lobe
	4.64	60	5	-1	R	Temporal Pole
	3.66	60	5	11	R	Rolandic Operculum
36	4.69	-60	-13	5	L	Superior Temporal Gyrus
	3.7	-48	-16	14	L	Rolandic Operculum
35	4.43	51	-13	50	R	Precentral Gyrus
	3.71	54	-22	50	R	Postcentral Gyrus
	3.42	45	-4	56	R	Middle Frontal Gyrus
33	4.3	-54	-34	20	L	Superior Temporal Gyrus
	3.8	-54	-46	26	L	SupraMarginal Gyrus
34	4.17	54	-55	26	R	Angular Gyrus
	3.68	57	-49	20	R	Superior Temporal Gyrus
	3.3	57	-43	29	R	SupraMarginal Gyrus
21	4.11	60	-37	32	R	SupraMarginal Gyrus
21	3.96	51	-61	8	R	Middle Temporal Gyrus
42	3.95	3	-55	41	R	Precuneus
	3.83	0	-67	47	L	Precuneus
20	3.81	-54	-52	32	L	Angular Gyrus
18	3.78	-27	-46	65	L	Superior Parietal Lobule
19	3.72	-30	-82	26	L	Middle Occipital Gyrus

Tab. B.2. | Project 2: DC HC: 10 frequency bands. Results of the degree centrality (DC) analysis in healthy controls (HC) at 10 frequency bands. The table includes the cluster size, the z-value, the MNI coordinates, the side, and the anatomical locations of the peak voxels. Reported are only brain areas with p cluster-level corrected < 0.05, on underlying voxel-level correction of p < 0.001, with voxels restricted to gray matter.

DC: HC		MNI coordinates [mm]					
frequency band	cluster size	z-value	x	y	z	side	location
freq1	240	5.14	-39	-40	56	L	Postcentral Gyrus
	400	5.91	15	-85	38	R	Cuneus
		5.46	21	-79	38	R	Superior Occipital Gyrus
	118	5.57	12	-28	65	R	Paracentral Lobule
		4.51	24	-49	65	R	Superior Parietal Lobule
	21	5.36	51	-46	20	R	Superior Temporal Gyrus
	190	5.11	-18	-16	71	L	Precentral Gyrus
		4.52	-3	-25	50	L	Paracentral Lobule
	121	5.11	-63	-13	5	L	Superior Temporal Gyrus
		4.63	-60	-25	26	L	SupraMarginal Gyrus
	87	4.96	-45	-70	2	L	Middle Occipital Gyrus
		4.13	-42	-64	20	L	Middle Temporal Gyrus
	69	4.94	48	-61	8	R	Middle Temporal Gyrus
		62	4.86	42	-13	53	R
	4.38		54	-22	50	R	Postcentral Gyrus
	45	4.8	-24	-79	26	L	Superior Occipital Gyrus
		4.29	-33	-88	23	L	Middle Occipital Gyrus
	60	3.4	-21	-88	26	L	Superior Occipital Gyrus
		4.69	54	-19	17	R	Rolandic Operculum
	24	4.68	54	-16	8	R	Superior Temporal Gyrus
		4.59	42	-31	14	R	Superior Temporal Gyrus
	40	4.32	48	8	-1	R	Insula Lobe
		4.3	60	2	5	R	Superior Temporal Gyrus
	38	4.11	21	-82	-10	R	Lingual Gyrus
		3.71	6	-94	-4	R	Calcarine Gyrus
	378	5.99	12	-73	26	R	Cuneus
		4.83	-3	-64	8	L	Calcarine Gyrus
	68	5.27	-45	-4	53	L	Precentral Gyrus
		3.66	-60	-19	32	L	Postcentral Gyrus
	85	4.95	-18	-19	71	L	Precentral Gyrus
		4.85	-24	-7	65	L	Superior Frontal Gyrus
	349	5.21	-12	-37	44	L	MCC
		4.91	3	8	44	R	MCC
	45	4.89	-3	-25	50	L	Paracentral Lobule
		5.12	42	-13	53	R	Precentral Gyrus
	38	4.18	45	-1	53	R	Middle Frontal Gyrus
		4.97	48	-58	8	R	Middle Temporal Gyrus
	102	4.95	24	-40	62	R	Postcentral Gyrus
		3.87	24	-28	71	R	Precentral Gyrus
	121	4.51	57	-22	17	R	Superior Temporal Gyrus
		4.5	57	8	2	R	Rolandic Operculum
	24	4.45	54	-7	5	R	Transverse Temporal Gyrus
		4.34	-57	-4	2	L	Superior Temporal Gyrus
	40	4.31	-51	-67	5	L	Middle Temporal Gyrus
		4.14	-45	-76	2	L	Middle Occipital Gyrus
	33	3.27	-60	-31	23	L	Superior Temporal Gyrus
		3.98	-24	-46	65	L	Superior Parietal Lobule

		3.8	-24	-55	59	L	Superior Parietal Lobule	
		3.46	-15	-52	65	L	Precuneus	
	25	3.74	12	-4	68	R	Posterior-Medial-Frontal	
		3.55	24	-1	65	R	Superior Frontal Gyrus	
		3.45	15	8	68	R	Posterior-Medial-Frontal	
freq3	146	5.79	60	-16	11	R	Superior Temporal Gyrus	
		5.23	51	-19	8	R	Heschls Gyrus	
		4.47	63	-31	32	R	SupraMarginal Gyrus	
	60	5.71	-48	-4	47	L	Precentral Gyrus	
		4.96	-51	-13	47	L	Postcentral Gyrus	
		3.85	-39	2	50	L	Middle Frontal Gyrus	
	325	5.08	3	-82	17	L	Cuneus	
	58	5.08	42	2	56	R	Middle Frontal Gyrus	
		4.66	45	-7	44	R	Precentral Gyrus	
	170	4.95	3	-40	47	R	MCC	
		4.82	-3	-28	50	L	Paracentral Lobule	
	31	4.91	-45	-46	53	L	Inferior Parietal Lobule	
		3.8	-39	-46	59	L	Superior Parietal Lobule	
	31	4.89	-57	-13	11	L	Superior Temporal Gyrus	
		4.66	-54	-1	5	L	Rolandic Operculum	
	59	4.86	30	-49	62	R	Superior Temporal Lobule	
		4.12	24	-34	68	R	Postcentral Gyrus	
	35	4.59	54	-46	14	R	Superior Temporal Gyrus	
	26	4.51	-42	-19	-1	L	Superior Temporal Gyrus	
	27	4.34	-57	-34	17	L	Superior Temporal Gyrus	
		4.13	-48	-34	20	L	Superior Temporal Gyrus	
	24	4.11	54	5	-1	R	Temporal Pole	
		3.65	42	11	5	R	IFG (p. Opercularis)	
	29	4.14	-15	8	65	L	Superior Frontal Gyrus	
		3.57	-24	-1	68	L	Superior Frontal Gyrus	
	27	4.04	51	-55	8	R	Middle Temporal Gyrus	
	1214	6.78	0	-76	20	L	Cuneus	
		5.76	6	-85	23	R	Cuneus	
	101	6.21	27	-82	26	R	Superior Occipital Gyrus	
		5.03	30	-73	29	R	Middle Occipital Gyrus	
	411	5.95	-3	-43	50	L	MCC	
		5.94	0	-49	35	L	Precuneus	
	82	5.77	-15	11	65	L	Superior Frontal Gyrus	
		3.86	-27	-4	56	L	Precentral Gyrus	
	171	5.65	39	-16	-4	R	Insula Lobe	
		5.48	51	-16	5	R	Transverse Temporal Gyrus	
		4.86	57	5	2	R	Rolandic Operculum	
	freq4	21	5.56	-57	2	2	L	Rolandic Operculum
		284	5.52	57	-49	23	R	Superior Temporal Gyrus
			5.24	51	-73	17	R	Middle Temporal Gyrus
		280	5.48	-51	-43	50	L	Inferior Parietal Lobule
			5.46	-45	-1	50	L	Precentral Gyrus
			5.3	-51	-16	47	L	Postcentral Gyrus
		62	5.36	-63	-13	5	L	Superior Temporal Gyrus
			3.78	-54	-16	14	L	Postcentral Gyrus
		23	4.83	6	41	14	R	ACC
		30	4.51	42	-25	17	R	Rolandic Operculum
57		4.43	42	-10	41	R	Precentral Gyrus	
20		3.23	57	-1	41	R	Precentral Gyrus	
1953		5.96	-42	-76	26	L	Middle Occipital Gyrus	
		5.65	0	-82	32	L	Cuneus	
		5.62	12	-79	38	R	Cuneus	
103		4.68	-45	5	38	L	Precentral Gyrus	
		4.3	-48	8	29	L	IFG (p. Opercularis)	

freq5	91	4.53	-51	-10	5	L	Superior Temporal Gyrus
	34	4.5	48	-73	17	R	Middle Temporal Gyrus
		3.32	51	-61	14	R	Middle Temporal Gyrus
	55	4.42	48	11	-1	R	Insula Lobe
		4	57	5	2	R	Rolandic Operculum
		3.77	63	-4	2	R	Superior Temporal Gyrus
	78	4.34	63	-31	32	R	SupraMarginal Gyrus
		3.97	54	-49	26	R	Angular Gyrus
	59	4.18	36	-43	53	R	Inferior Parietal Lobule
		4.08	33	-46	44	R	Postcentral Gyrus
freq6	1194	5.89	3	-43	44	R	Precuneus
		5.74	-6	-82	35	L	Cuneus
		5.63	6	-52	35	R	MCC
	531	5.28	-48	-43	53	L	Inferior Parietal Lobule
		5.25	-45	-58	20	L	Middle Temporal Gyrus
	29	4.75	-45	-7	50	L	Precentral Gyrus
		4.17	-45	2	53	L	Precentral Gyrus
	112	4.68	57	-46	32	R	SupraMarginal Gyrus
		4.25	54	-58	32	R	Angular Gyrus
	54	4.63	-27	-82	23	L	Middle Occipital Gyrus
	26	4.3	33	-88	11	R	Middle Occipital Gyrus
	38	4.08	51	-10	2	R	Superior Temporal Gyrus
		3.39	51	5	-7	R	Temporal Pole
	freq7	963	6.06	3	-40	47	R
		5.77	-6	-76	29	L	Cuneus
		5.49	0	-58	44	L	Precuneus
415		5.88	-51	-61	32	L	Angular Gyrus
		5.76	-45	-67	23	L	Middle Temporal Gyrus
		5.71	-45	-64	44	L	Angular Gyrus
228		4.9	36	-67	44	R	Angular Gyrus
		4.5	57	-49	26	R	SupraMarginal Gyrus
		4.24	45	-52	44	R	Inferior Parietal Lobule
21		4.76	51	-16	8	R	Transverse Temporal Gyrus
54		4.68	-57	-1	2	L	Rolandic Operculum
		4	-48	-16	11	L	Transverse Temporal Gyrus
35		4.25	42	2	53	R	Middle Frontal Gyrus
		4.05	45	-7	56	R	Precentral Gyrus
freq8	91	5.31	54	-19	8	R	Superior Temporal Gyrus
		4.69	57	2	-1	R	Superior Temporal Gyrus
	169	4.81	-3	-70	47	L	Precuneus
		4.27	0	-73	26	L	Cuneus
	170	4.77	-45	-67	38	L	Angular Gyrus
		4.57	-42	-73	26	L	Middle Occipital Gyrus
	81	4.54	-3	38	14	L	ACC
		3.94	6	47	14	R	ACC
	75	4.43	-51	-10	5	L	Superior Temporal Gyrus
		4.03	-54	8	11	L	IFG (p. Opercularis)
freq9	591	6.35	-12	-70	26	L	Cuneus
		5.77	3	-40	47	R	MCC
		5.62	-3	-64	47	L	Precuneus
	517	5.32	-54	-52	32	L	Angular Gyrus
		5.24	-42	-40	50	L	Inferior Parietal Lobule
		5.22	-45	-64	23	L	Middle Temporal Gyrus
	110	5.1	57	2	-1	R	Superior Temporal Gyrus
		4.49	42	-13	-1	R	Insula Lobe
	76	4.85	-51	-10	8	L	Transverse Temporal Gyrus
		4.13	-42	-16	-4	L	Superior Temporal Gyrus
		3.59	-54	5	2	L	Rolandic Operculum
	49	4.35	9	47	5	R	ACC

		3.98	0	41	14	L	ACC
	400	5.9	0	-40	44	L	MCC
		5.36	0	-67	47	L	Precuneus
	253	5.11	-45	-43	50	L	Inferior Parietal Lobule
		5	-42	-76	26	L	Middle Occipital Gyrus
		4.89	-45	-70	35	L	Angular Gyrus
freq10	41	4.56	-54	-13	5	L	Superior Temporal Gyrus
		3.37	-54	-1	5	L	Rolandic Operculum
	20	4.11	60	-49	29	R	SupraMarginal Gyrus
		3.53	57	-52	38	R	Inferior Parietal Lobule
	53	3.89	-3	35	17	L	ACC

Tab. B.3. | Project 2: DC HC > MDD: 10 frequency bands. Results of the degree centrality (DC) group comparison analysis at 10 frequency bands. The table includes the cluster size, the z-value, the MNI coordinates, the side, and the anatomical locations of the peak voxels. Reported are only brain areas with p cluster-level corrected < 0.05, on underlying voxel-level correction of $p < 0.001$, with voxels restricted to gray matter. Significant group differences in DC were found only in the HC > MDD contrast.

DC: HC > MDD		MNI coordinates [mm]						
frequency band	cluster size	z-value	x	y	z	side	location	
freq1	23	4.74	42	-19	5	R	Transverse Temporal Gyrus	
	38	4.05	45	5	-4	R	Insula Lobe	
		3.6	45	8	8	R	IFG (p. Opercularis)	
freq2	50	5.14	42	5	8	R	Insula Lobe	
freq4	31	4.87	-36	-85	5	L	Middle Occipital Gyrus	
	26	4.78	3	-76	17	L	Calcarine Gyrus	
	27	4.31	-45	-16	-4	L	Superior Temporal Gyrus	
	30	3.97	51	2	2	R	Rolandic Operculum	
		3.88	42	5	-7	R	Insula Lobe	
freq5	57	4.96	3	-10	35	R	MCC	
		3.81	-6	-16	38	L	MCC	
	43	4.65	42	2	-7	R	Insula Lobe	
		4.35	42	8	8	R	IFG (p. Opercularis)	
		4.15	54	-4	2	R	Superior Temporal Gyrus	
	44	4.52	-51	-52	32	L	Angular Gyrus	
		3.42	-57	-43	26	L	SupraMarginal Gyrus	
		3.29	-57	-52	17	L	Middle Temporal Gyrus	
		32	4.31	-45	8	38	L	Precentral Gyrus
		24	4.21	63	-46	29	R	SupraMarginal Gyrus
freq6		3.79	57	-52	26	R	Angular Gyrus	
	30	5.12	60	-43	26	R	SupraMarginal Gyrus	
	30	4.52	0	-13	38	L	MCC	
freq7	22	3.89	6	-46	59	R	Precuneus	
	34	5.22	-9	-43	35	L	MCC	
		4.21	-12	-43	44	L	Precuneus	
	31	4.47	-42	-22	-1	L	Insula Lobe	
		3.64	-48	-13	-4	L	Superior Temporal Gyrus	
	89	4.58	-45	-61	44	L	Angular Gyrus	
		4.53	-45	-52	53	L	Inferior Parietal Lobule	
	57	5.56	36	-13	-7	R	Putamen	
157		4.52	42	-10	-1	R	Insula Lobe	
		5.4	-3	35	11	L	ACC	
		4.7	9	47	2	R	ACC	

freq8	40	4.29	-48	-16	5	L	Superior Temporal Gyrus
	23	4.96	-24	-25	-13	L	Hippocampus
	26	4.3	-57	2	-4	L	Superior Temporal Gyrus
		3.86	-45	14	-16	L	Temporal Pole
	32	4.23	-36	11	-1	L	Insula Lobe
		3.64	-48	20	-4	L	IFG (p. Opercularis)
freq9	43	5.82	6	44	5	R	ACC
		3.49	-3	41	-1	L	ACC
	31	5.1	-51	-13	5	L	Superior Temporal Gyrus
		3.49	-57	-1	2	L	Rolandic Operculum
	25	4.87	54	2	-1	R	Superior Temporal Gyrus
		3.81	57	-1	8	R	Rolandic Operculum
	54	4.81	-54	-49	29	L	SupraMarginal Gyrus
		3.79	-51	-61	23	L	Middle Temporal Gyrus
		3.39	-57	-52	38	L	Inferior Parietal Lobule
	freq10	57	5.25	-6	35	17	L
4.32			9	35	20	R	ACC
27		4.96	-54	-16	8	L	Transverse Temporal Gyrus
		3.87	-54	-28	11	L	Superior Temporal Gyrus

Tab. B.4. | Project 2: DC HC > MDD: 10 frequency bands, controlled for GMV. Results of the degree centrality (DC) group comparison analysis at 10 frequency bands, corrected for gray matter volume (GMV). The table includes the cluster size, the z-value, the MNI coordinates, the side, and the anatomical locations of the peak voxels. Reported are only brain areas with p cluster-level corrected < 0.05, on underlying voxel-level correction of p < 0.001, with voxels restricted to gray matter. Significant group differences in DC were found only in the HC > MDD contrast.

DC: HC >MDD, GMV corrected		MNI coordinates [mm]					
frequency band	cluster size	Z value	x	y	z	side	location
freq1	21	4.77	-45	-16	-1	L	Superior Temporal Gyrus
	37	4.13	45	5	-4	R	Insula Lobe
		3.6	45	8	8	R	IFG (p.Opercularis)
freq2	54	5.18	42	5	8	R	Insula Lobe
freq3	25	5.16	-42	-19	-1	L	Superior Temporal Gyrus
		3.89	-45	-19	8	L	Transverse Temporal Gyrus
freq4	27	4.78	3	-76	17	L	Calcarine Gyrus
	35	4.63	-36	-85	5	L	Middle Occipital Gyrus
	32	3.93	45	2	-1	R	Insula Lobe
		3.82	54	-4	2	R	Superior Temporal Gyrus
freq5	59	5.06	3	-10	35	R	MCC
	38	4.71	42	2	-7	R	Insula Lobe
		4.36	42	8	8	R	IFG (p.Opercularis)
	39	4.57	-51	-52	32	L	Angular Gyrus
		3.35	-57	-52	17	L	Middle Temporal Gyrus
	24	4.32	63	-46	29	R	SupraMarginal Gyrus
		3.72	57	-52	26	R	Angular Gyrus
31	4.14	-45	5	38	L	Precentral Gyrus	
freq6	33	5.22	60	-43	26	R	SupraMarginal Gyrus
	42	4.66	0	-13	38	L	MCC
	21	3.84	6	-46	59	R	Precuneus
		3.77	12	-40	56	R	Paracentral Lobule
31	5.82	-18	17	62	L	Superior Frontal gyrus	

freq7		3.76	-9	11	68	L	Posterior-Medial Frontal
	37	5.22	-9	-43	35	L	MCC
	83	4.64	-45	-61	44	L	Angular Gyrus
		4.45	-45	-55	53	L	Inferior Parietal Lobule
	35	3.78	-45	-16	5	L	Transverse Temporal Gyrus
freq8	50	5.57	36	-13	-7	R	Putamen
		4.48	42	-10	-1	R	Insula Lobe
	137	5.4	-3	35	11	L	ACC
		4.51	9	50	2	R	Superior Medial Gyrus
	57	4.56	-48	-16	5	L	Superior Temporal Gyrus
	30	4.39	-36	11	-4	L	Insula Lobe
		3.82	-42	23	-1	L	IFG (p.Triangularis)
	23	4.32	-54	5	2	L	Rolandic Operculum
		3.87	-45	14	-16	L	Temporal Pole
	freq9	30	5.43	6	44	5	R
24		5.18	-51	-13	5	L	Superior Temporal Gyrus
46		4.9	-54	-49	29	L	SupraMarginal Gyrus
		3.93	-51	-61	23	L	Middle Temporal Gyrus
		3.48	-57	-55	38	L	Inferior Parietal Lobule
21		4.39	-45	-13	-4	L	Superior Temporal Gyrus
freq10	42	5.07	-6	35	17	L	ACC
		4.4	6	38	23	R	ACC
	31	4.93	-54	-16	8	L	Transverse Temporal Gyrus
		3.96	-54	-28	11	L	Superior Temporal Gyrus

References

- Abou-Elseoud, A, T Starck, J Remes, J Nikkinen, O Tervonen, and V Kiviniemi (2009). „The effect of model order selection in group PICA“. In: *Human Brain Mapping* 31.8, pp. 1207–16.
- Achard, S, R Salvador, B Whitcher, J Suckling, and E Bullmore (2006). „A resilient, low-frequency, small-world human brain functional network with highly connected association cortical hubs.“ In: *The Journal of neuroscience: the official journal of the Society for Neuroscience* 26.1, pp. 63–72.
- Aguirre, G K, E Zarahn, and M D’Esposito (1998). „The Variability of Human, BOLD Hemodynamic Responses“. In: *NeuroImage* 8.4, pp. 360–369.
- Alexander-Bloch, A F, D S Bassett, and D A Ross (2018). „Missed Connections: A Network Approach to Understanding Psychiatric Illness“. In: *Biological Psychiatry* 84.2, e9–e11.
- Allen, E A, E B Erhardt, E Damaraju, et al. (2011). „A baseline for the multivariate comparison of resting-state networks.“ In: *Frontiers in systems neuroscience* 5, p. 2.
- Allen, E A, E Damaraju, S M Plis, E B Erhardt, T Eichele, and V D Calhoun (2014). „Tracking Whole-Brain Connectivity Dynamics in the Resting State“. In: *Cerebral Cortex* 24.3, pp. 663–676.
- Alonso, J, M C Angermeyer, S Bernert, et al. (2004). „Disability and quality of life impact of mental disorders in Europe: results from the European Study of the Epidemiology of Mental Disorders (ESEMeD) project“. In: *Acta Psychiatrica Scandinavica* 109.s420, pp. 38–46.
- Ambrosi, E, D B Arciniegas, A Madan, et al. (2017). „Insula and amygdala resting-state functional connectivity differentiate bipolar from unipolar depression“. In: *Acta Psychiatrica Scandinavica* 136.1, pp. 129–139.
- American Psychiatric Association (2013). *Diagnostic and Statistical Manual of Mental Disorders*. American Psychiatric Association.
- Ames, A (2000). „CNS energy metabolism as related to function.“ In: *Brain research. Brain research reviews* 34.1-2, pp. 42–68.
- Andrews-Hanna, J R, J S Reidler, J Sepulcre, R Poulin, and R L Buckner (2010). „Functional-anatomic fractionation of the brain’s default network.“ In: *Neuron* 65.4, pp. 550–62.
- Attwell, D and S B Laughlin (2001). „An Energy Budget for Signaling in the Grey Matter of the Brain“. In: *Journal of Cerebral Blood Flow & Metabolism* 21.10, pp. 1133–1145.

- Avery, J A, W C Drevets, S E Moseman, J Bodurka, J C Barcalow, and W K Simmons (2014). „Major depressive disorder is associated with abnormal interoceptive activity and functional connectivity in the insula.“ In: *Biological psychiatry* 76.3, pp. 258–66.
- Badhwar, AP, A Tam, C Dansereau, P Orban, F Hoffstaedter, and P Bellec (2017). „Resting-state network dysfunction in Alzheimer’s disease: A systematic review and meta-analysis“. In: *Alzheimer’s & Dementia: Diagnosis, Assessment & Disease Monitoring* 8, pp. 73–85.
- Baldassano, C, J Chen, A Zadbood, J W Pillow, U Hasson, and K A Norman (2017). „Discovering Event Structure in Continuous Narrative Perception and Memory“. In: *Neuron* 95.3, pp. 709–721.
- Baliki, M N, A T Baria, and A V Apkarian (2011). „The cortical rhythms of chronic back pain.“ In: *The Journal of neuroscience: the official journal of the Society for Neuroscience* 31.39, pp. 13981–90.
- Bandettini, P A and E C Wong (1997). „A hypercapnia-based normalization method for improved spatial localization of human brain activation with fMRI“. In: *NMR in Biomedicine* 10.4-5, pp. 197–203.
- Barabási, A-L (2009). „Scale-free networks: a decade and beyond.“ In: *Science (New York, N.Y.)* 325.5939, pp. 412–3.
- Barabási, A-L and R Albert (1999). „Emergence of scaling in random networks“. In: *Science (New York, N.Y.)* 286.5439, pp. 509–12.
- Barabási, A-L and E Bonabeau (2003). „Scale-free networks.“ In: *Scientific American* 288.5, pp. 60–9.
- Baria, A T, M N Baliki, T Parrish, and A V Apkarian (2011). „Anatomical and functional assemblies of brain BOLD oscillations.“ In: *The Journal of neuroscience: the official journal of the Society for Neuroscience* 31.21, pp. 7910–9.
- Bassett, Danielle Smith and Ed Bullmore (2006). „Small-World Brain Networks“. In: *The Neuroscientist* 12.6, pp. 512–523.
- Başar, E, M Schürmann, C Başar-Eroglu, and S Karakaş (1997). „Alpha oscillations in brain functioning: an integrative theory.“ In: *International journal of psychophysiology: official journal of the International Organization of Psychophysiology* 26.1-3, pp. 5–29.
- Başar, E, C Başar-Eroglu, S Karakaş, and M Schürmann (2001). „Gamma, alpha, delta, and theta oscillations govern cognitive processes.“ In: *International journal of psychophysiology: official journal of the International Organization of Psychophysiology* 39.2-3, pp. 241–8.
- Beall, E B and M J Lowe (2007). „Isolating physiologic noise sources with independently determined spatial measures“. In: *NeuroImage* 37.4, pp. 1286–1300.
- Beall, E B and M J Lowe (2014). „SimPACE: Generating simulated motion corrupted BOLD data with synthetic-navigated acquisition for the development and evaluation of SLO-MOCO: A new, highly effective slice-wise motion correction“. In: *NeuroImage* 101, pp. 21–34.
- Beck, A T, C H Ward, M Mendelson, J Mock, and J Erbaugh (1961). „An inventory for measuring depression.“ In: *Archives of general psychiatry* 4, pp. 561–71.
- Beckmann, C F, M DeLuca, J T Devlin, and S M Smith (2005). „Investigations into resting-state connectivity using independent component analysis.“ In: *Philosophical transactions of the Royal Society of London. Series B, Biological sciences* 360.1457, pp. 1001–13.

- Belleau, E L, L E Taubitz, and C L Larson (2015). „Imbalance of default mode and regulatory networks during externally focused processing in depression.“ In: *Social cognitive and affective neuroscience* 10.5, pp. 744–51.
- Belujon, P and A A Grace (2017). „Dopamine System Dysregulation in Major Depressive Disorders.“ In: *The international journal of neuropsychopharmacology* 20.12, pp. 1036–1046.
- Berman, M G, S Peltier, D E Nee, E Kross, P J Deldin, and J Jonides (2011). „Depression, rumination and the default network.“ In: *Social cognitive and affective neuroscience* 6.5, pp. 548–55.
- Berman, M G, B Misic, M Buschkuehl, et al. (2014). „Does resting-state connectivity reflect depressive rumination? A tale of two analyses.“ In: *NeuroImage* 103, pp. 267–279.
- Beucke, J C, J Sepulcre, M C Eldaief, M Sebold, N Kathmann, and C Kaufmann (2014). „Default mode network subsystem alterations in obsessive–compulsive disorder“. In: *British Journal of Psychiatry* 205.05, pp. 376–382.
- Bhattacharyya, P K and M J Lowe (2004). „Cardiac-induced physiologic noise in tissue is a direct observation of cardiac-induced fluctuations“. In: *Magnetic Resonance Imaging* 22.1, pp. 9–13.
- Bianciardi, M, M Fukunaga, P van Gelderen, S G Horovitz, J A de Zwart, and J H Duyn (2009). „Modulation of spontaneous fMRI activity in human visual cortex by behavioral state.“ In: *NeuroImage* 45.1, pp. 160–8.
- Birn, R M, J B Diamond, M A Smith, and P A Bandettini (2006). „Separating respiratory-variation-related fluctuations from neuronal-activity-related fluctuations in fMRI“. In: *NeuroImage* 31.4, pp. 1536–1548.
- Biswal, B, F Z Yetkin, V M Haughton, and J S Hyde (1995). „Functional connectivity in the motor cortex of resting human brain using echo-planar mri“. In: *Magnetic Resonance in Medicine* 34.4, pp. 537–541.
- Bora, E, A Fornito, C Pantelis, and M Yücel (2012). „Gray matter abnormalities in Major Depressive Disorder: A meta-analysis of voxel based morphometry studies“. In: *Journal of Affective Disorders* 138.1-2, pp. 9–18.
- Boubela, R N, K Kalcher, C Nasel, and E Moser (2014). „Scanning fast and slow: current limitations of 3 Tesla functional MRI and future potential.“ In: *Frontiers in physics* 2, p. 00001.
- Boubela, Roland N, Klaudius Kalcher, Wolfgang Huf, Claudia Kronnerwetter, Peter Filzmoser, and Ewald Moser (2013). „Beyond Noise: Using Temporal ICA to Extract Meaningful Information from High-Frequency fMRI Signal Fluctuations during Rest.“ In: *Frontiers in human neuroscience* 7, p. 168.
- Boveroux, P, A Vanhaudenhuyse, M-A Bruno, et al. (2010). „Breakdown of within- and between-network resting state functional magnetic resonance imaging connectivity during propofol-induced loss of consciousness.“ In: *Anesthesiology* 113.5, pp. 1038–53.
- Boyacioglu Rand Beckmann, C F and M Barth (2013). „An Investigation of RSN Frequency Spectra Using Ultra-Fast Generalized Inverse Imaging.“ In: *Frontiers in human neuroscience* 7, p. 156.

- Brambilla, P, J Perez, F Barale, G Schettini, and J C Soares (2003). „GABAergic dysfunction in mood disorders“. In: *Molecular Psychiatry* 8.8, pp. 721–737.
- Bschor, T, M Ising, M Bauer, et al. (2004). „Time experience and time judgment in major depression, mania and healthy subjects. A controlled study of 93 subjects“. In: *Acta Psychiatrica Scandinavica* 109.3, pp. 222–229.
- Buckholtz, J W and A Meyer-Lindenberg (2012). „Psychopathology and the Human Connectome: Toward a Transdiagnostic Model of Risk For Mental Illness“. In: *Neuron* 74.6, pp. 990–1004.
- Buckner, R L, P A Bandettini, K M O’Craven, et al. (1996). „Detection of cortical activation during averaged single trials of a cognitive task using functional magnetic resonance imaging.“ In: *Proceedings of the National Academy of Sciences of the United States of America* 93.25, pp. 14878–83.
- Buckner, R L, J R Andrews-Hanna, and D L Schacter (2008). „The Brain’s Default Network“. In: *Annals of the New York Academy of Sciences* 1124.1, pp. 1–38.
- Buckner, R L, J Sepulcre, T Talukdar, et al. (2009). „Cortical hubs revealed by intrinsic functional connectivity: mapping, assessment of stability, and relation to Alzheimer’s disease.“ In: *The Journal of neuroscience: the official journal of the Society for Neuroscience* 29.6, pp. 1860–73.
- Bullmore, E and O Sporns (2009). „Complex brain networks: graph theoretical analysis of structural and functional systems.“ In: *Nature reviews. Neuroscience* 10.3, pp. 186–98.
- Bullmore, E and O Sporns (2012). „The economy of brain network organization“. In: *Nature Reviews Neuroscience* 13.5, pp. 336–349.
- Buxton, R B (2012). „Dynamic models of BOLD contrast“. In: *NeuroImage* 62.2, pp. 953–961.
- Buxton, R B, K Uludağ, D J Dubowitz, and T T Liu (2004). „Modeling the hemodynamic response to brain activation“. In: *NeuroImage* 23, S220–33.
- Buzsáki, G (2006). *Rhythms of the brain*. Oxford University Press, p. 448.
- Buzsáki, G and E I Moser (2013). „Memory, navigation and theta rhythm in the hippocampal-entorhinal system.“ In: *Nature neuroscience* 16.2, pp. 130–8.
- Calhoun, V D, T Adali, G D Pearlson, and J J Pekar (2001). „Spatial and temporal independent component analysis of functional MRI data containing a pair of task-related waveforms.“ In: *Human brain mapping* 13.1, pp. 43–53.
- Calhoun, V D, J Liu, and T Adali (2009). „A review of group ICA for fMRI data and ICA for joint inference of imaging, genetic, and ERP data.“ In: *NeuroImage* 45.1 Suppl, pp. 163–72.
- Calhoun, V D, J Sui, K Kiehl, J Turner, E A Allen, and G Pearlson (2011). „Exploring the psychosis functional connectome: aberrant intrinsic networks in schizophrenia and bipolar disorder.“ In: *Frontiers in psychiatry* 2, p. 75.
- Calhoun, V D, R Miller, G Pearlson, and T Adali (2014). „The chronnectome: time-varying connectivity networks as the next frontier in fMRI data discovery.“ In: *Neuron* 84.2, pp. 262–74.
- Carr, M F, M P Karlsson, and L M Frank (2012). „Transient Slow Gamma Synchrony Underlies Hippocampal Memory Replay“. In: *Neuron* 75.4, pp. 700–713.

- Cauda, F, K Sacco, S Duca, F Cocito Dand D'Agata, G C Geminiani, and S Canavero (2009). „Altered Resting State in Diabetic Neuropathic Pain“. In: *PLoS ONE* 4.2. Ed. by Eshel Ben-Jacob, e4542.
- Chang, C, J P Cunningham, and G H Glover (2009). „Influence of heart rate on the BOLD signal: the cardiac response function.“ In: *NeuroImage* 44.3, pp. 857–69.
- Chang, L J, T Yarkoni, M W Khaw, and A G Sanfey (2013). „Decoding the role of the insula in human cognition: functional parcellation and large-scale reverse inference.“ In: *Cerebral cortex (New York, N.Y. : 1991)* 23.3, pp. 739–49.
- Chaudhuri, R, K Knoblauch, M-A Gariel, H Kennedy, and X-J Wang (2015). „A Large-Scale Circuit Mechanism for Hierarchical Dynamical Processing in the Primate Cortex“. In: *Neuron* 88.2, pp. 419–431.
- Chen, J E and G H Glover (2015). „BOLD fractional contribution to resting-state functional connectivity above 0.1 Hz.“ In: *NeuroImage* 107, pp. 207–218.
- Chen, Y-C, W Xia, B Luo, et al. (2015). „Frequency-specific alternations in the amplitude of low-frequency fluctuations in chronic tinnitus.“ In: *Frontiers in neural circuits* 9, p. 67.
- Cocchi, L, M V Sale, L Gollo, et al. (2016). „A hierarchy of timescales explains distinct effects of local inhibition of primary visual cortex and frontal eye fields.“ In: *eLife* 5.
- Cole, M W, S Pathak, and W Schneider (2010). „Identifying the brain's most globally connected regions“. In: *NeuroImage* 49.4, pp. 3132–3148.
- Cole, M W, J R Reynolds, J D Power, G Repovš, A Anticevic, and T S Braver (2013). „Multi-task connectivity reveals flexible hubs for adaptive task control“. In: *Nature Neuroscience* 16.9, pp. 1348–1355.
- Cole, M W, G Repovš, and A Anticevic (2014). „The Frontoparietal Control System“. In: *The Neuroscientist* 20.6, pp. 652–664.
- Colgin, L L (2013). „Mechanisms and Functions of Theta Rhythms“. In: *Annual Review of Neuroscience* 36.1, pp. 295–312.
- Colgin, L L, T Denninger, M Fyhn, et al. (2009). „Frequency of gamma oscillations routes flow of information in the hippocampus“. In: *Nature* 462.7271, pp. 353–357.
- Colizza, V, A Flammini, M A Serrano, and A Vespignani (2006). „Detecting rich-club ordering in complex networks“. In: *Nature Physics* 2.2, pp. 110–115.
- Cooney, R E, J Joormann, F Eugène, E L Dennis, and I H Gotlib (2010). „Neural correlates of rumination in depression.“ In: *Cognitive, affective & behavioral neuroscience* 10.4, pp. 470–8.
- Cordes, D, V M Haughton, K Arfanakis, et al. (2000). „Mapping functionally related regions of brain with functional connectivity MR imaging.“ In: *AJNR. American journal of neuroradiology* 21.9, pp. 1636–44.
- Cordes, D, V M Haughton, K Arfanakis, et al. (2001). „Frequencies Contributing to Functional Connectivity in the Cerebral Cortex in “Resting-state” Data“. In: *American Journal of Neuroradiology* 22.7.
- Cordes, D, V Haughton, J D Carew, K Arfanakis, and K Maravilla (2002). „Hierarchical clustering to measure connectivity in fMRI resting-state data.“ In: *Magnetic resonance imaging* 20.4, pp. 305–17.

- Craig, A D (2009a). „Emotional moments across time: a possible neural basis for time perception in the anterior insula.“ In: *Philosophical transactions of the Royal Society of London. Series B, Biological sciences* 364.1525, pp. 1933–42.
- Craig, A D (2009b). „How do you feel — now? The anterior insula and human awareness“. In: *Nature Reviews Neuroscience* 10.1, pp. 59–70.
- Crossley, N A, A Mechelli, J Scott, et al. (2014). „The hubs of the human connectome are generally implicated in the anatomy of brain disorders“. In: *Brain* 137.8, pp. 2382–2395.
- Dagli, M S, J E Ingeholm, and J V Haxby (1999). „Localization of Cardiac-Induced Signal Change in fMRI“. In: *NeuroImage* 9.4, pp. 407–415.
- Damoiseaux, J S, S A Rombouts, F Barkhof, et al. (2006). „Consistent resting-state networks across healthy subjects.“ In: *Proceedings of the National Academy of Sciences of the United States of America* 103.37, pp. 13848–53.
- Damoiseaux, J S, K E Prater, B L Miller, and M D Greicius (2012). „Functional connectivity tracks clinical deterioration in Alzheimer’s disease.“ In: *Neurobiology of aging* 33.4, pp. 19–30.
- De Domenico, M, S Sasai, and A Arenas (2016). „Mapping Multiplex Hubs in Human Functional Brain Networks.“ In: *Frontiers in neuroscience* 10, p. 326.
- De Luca, M, C F Beckmann, N De Stefano, P M Matthews, and S M Smith (2006). „fMRI resting state networks define distinct modes of long-distance interactions in the human brain“. In: *NeuroImage* 29.4, pp. 1359–1367.
- de Pasquale, F, Stefania Della Penna, Abraham Z Snyder, et al. (2012). „A cortical core for dynamic integration of functional networks in the resting human brain.“ In: *Neuron* 74.4, pp. 753–64.
- de Pasquale, F, U Sabatini, S Della Penna, et al. (2013). „The connectivity of functional cores reveals different degrees of segregation and integration in the brain at rest“. In: *NeuroImage* 69, pp. 51–61.
- de Pasquale, F, S Della Penna, O Sporns, G L Romani, and M Corbetta (2016). „A Dynamic Core Network and Global Efficiency in the Resting Human Brain.“ In: *Cerebral cortex (New York, N.Y. : 1991)* 26.10, pp. 4015–33.
- de Pasquale, F, M Corbetta, V Betti, and S Della Penna (2018). „Cortical cores in network dynamics“. In: *NeuroImage* 180, pp. 370–382.
- Deco, G, V K Jirsa, and A R McIntosh (2011). „Emerging concepts for the dynamical organization of resting-state activity in the brain“. In: *Nature Reviews Neuroscience* 12.1, pp. 43–56.
- Deco, G, M L Kringelbach, V K Jirsa, and P Ritter (2017). „The dynamics of resting fluctuations in the brain: metastability and its dynamical cortical core.“ In: *Scientific reports* 7.1, p. 3095.
- Deen, B, N B Pitskel, and K A Pelphrey (2011). „Three systems of insular functional connectivity identified with cluster analysis.“ In: *Cerebral cortex (New York, N.Y. : 1991)* 21.7, pp. 1498–506.
- Dehaene, S and J-P Changeux (2011). „Experimental and Theoretical Approaches to Conscious Processing“. In: *Neuron* 70.2, pp. 200–227.

- Demirtaş, M, C Tornador, C Falcón, et al. (2016). „Dynamic functional connectivity reveals altered variability in functional connectivity among patients with major depressive disorder.“ In: *Human brain mapping* 37.8, pp. 2918–30.
- Dichter, G S, D Gibbs, and M J Smoski (2015). „A systematic review of relations between resting-state functional-MRI and treatment response in major depressive disorder.“ In: *Journal of affective disorders* 172, pp. 8–17.
- Diener, C, C Kuehner, W Brusniak, Ubl, M Wessa, and H Flor (2012). „A meta-analysis of neurofunctional imaging studies of emotion and cognition in major depression“. In: *NeuroImage* 61.3, pp. 677–685.
- Ding, N, L Melloni, H Zhang, X Tian, and D Poeppel (2016). „Cortical tracking of hierarchical linguistic structures in connected speech“. In: *Nature Neuroscience* 19.1, pp. 158–164.
- Dong, D, Y Wang, X Chang, C Luo, and D Yao (2018). „Dysfunction of Large-Scale Brain Networks in Schizophrenia: A Meta-analysis of Resting-State Functional Connectivity“. In: *Schizophrenia Bulletin* 44.1, pp. 168–181.
- Draguhn, A and G Buzsáki (2004). „Neuronal oscillations in cortical networks“. In: *Science* 304.5679, pp. 1926–9.
- Drevets, Wayne C, Joseph L Price, and Maura L Furey (2008). „Brain structural and functional abnormalities in mood disorders: implications for neurocircuitry models of depression“. In: *Brain Struct Funct* 213.1-2, pp. 93–118.
- Drysdale, A T, L Grosenick, J Downar, et al. (2017). „Resting-state connectivity biomarkers define neurophysiological subtypes of depression“. In: *Nature Medicine* 23.1, pp. 28–38.
- Du, Y, G D Pearlson, Q Yu, et al. (2016). „Interaction among subsystems within default mode network diminished in schizophrenia patients: A dynamic connectivity approach.“ In: *Schizophrenia research* 170.1, pp. 55–65.
- Dubois, J, P Galdi, L K Han Yand Paul, and R Adolphs (2018). „Resting-State Functional Brain Connectivity Best Predicts the Personality Dimension of Openness to Experience“. In: *Personality Neuroscience* 1, e6.
- Dukart, J and A Bertolino (2014). „When structure affects function—the need for partial volume effect correction in functional and resting state magnetic resonance imaging studies.“ In: *PloS one* 9.12, e114227.
- Dunlop, B W and C B Nemeroff (2007). „The Role of Dopamine in the Pathophysiology of Depression“. In: *Archives of General Psychiatry* 64.3, p. 327.
- Dutta, Arpan, Shane McKie, and J.F. William Deakin (2014). „Resting state networks in major depressive disorder“. In: *Psychiatry Research: Neuroimaging* 224.3, pp. 139–151.
- Eckert, M A, N V Kamdar, C E Chang, C F Beckmann, M D Greicius, and V Menon (2008). „A cross-modal system linking primary auditory and visual cortices: Evidence from intrinsic fMRI connectivity analysis“. In: *Human Brain Mapping* 29.7, pp. 848–857.
- Eguíluz, V M, D R Chialvo, G A Cecchi, M Baliki, and A V Apkarian (2005). „Scale-Free Brain Functional Networks“. In: *Physical Review Letters* 94.1, p. 018102.
- Feinberg, D A and E Yacoub (2012). „The rapid development of high speed, resolution and precision in fMRI.“ In: *NeuroImage* 62.2, pp. 720–5.

- Feinberg, D A, S Moeller, S M Smith, et al. (2010). „Multiplexed echo planar imaging for sub-second whole brain fMRI and fast diffusion imaging.“ In: *PloS one* 5.12, e15710.
- Ferreri, F, P Pasqualetti, S Määttä, et al. (2011). „Human brain connectivity during single and paired pulse transcranial magnetic stimulation“. In: *NeuroImage* 54.1, pp. 90–102.
- Finn, E S, X Shen, D Scheinost, et al. (2015). „Functional connectome fingerprinting: identifying individuals using patterns of brain connectivity“. In: *Nature Neuroscience* 18.11, pp. 1664–1671.
- First, M B, R L Spitzer, M Gibbon, and J B W Williams (1996). *Structured Clinical Interview for DSM-IV Axis I Disorders, Clinician Version (SCDIV-CV)*. Washington, D.C.: American Psychiatric Press, Inc.
- Fischer, A S, C J Keller, and A Etkin (2016). „The Clinical Applicability of Functional Connectivity in Depression: Pathways Toward More Targeted Intervention“. In: *Biological Psychiatry: Cognitive Neuroscience and Neuroimaging* 1.3, pp. 262–270.
- Fitzgerald, P J and B O Watson (2018). „Gamma oscillations as a biomarker for major depression: an emerging topic“. In: *Translational Psychiatry* 8.1, p. 177.
- Fox, M D and M D Greicius (2010). „Clinical applications of resting state functional connectivity.“ In: *Frontiers in systems neuroscience* 4, p. 19.
- Fox, M D and M E Raichle (2007). „Spontaneous fluctuations in brain activity observed with functional magnetic resonance imaging“. In: *Nature Reviews Neuroscience* 8.9, pp. 700–711.
- Fox, M D, A Z Snyder, J L Vincent, M Corbetta, D C Van Essen, and M E Raichle (2005). „The human brain is intrinsically organized into dynamic, anticorrelated functional networks.“ In: *Proceedings of the National Academy of Sciences of the United States of America* 102.27, pp. 9673–8.
- Fox, M D, M Corbetta, A Z Snyder, J L Vincent, and M E Raichle (2006). „Spontaneous neuronal activity distinguishes human dorsal and ventral attention systems.“ In: *Proceedings of the National Academy of Sciences of the United States of America* 103.26, pp. 10046–51.
- Fox, M D, A Z Snyder, J L Vincent, and M E Raichle (2007). „Intrinsic Fluctuations within Cortical Systems Account for Intertrial Variability in Human Behavior“. In: *Neuron* 56.1, pp. 171–184.
- Fox, M D, R L Buckner, M P White, M D Greicius, and A Pascual-Leone (2012a). „Efficacy of transcranial magnetic stimulation targets for depression is related to intrinsic functional connectivity with the subgenual cingulate.“ In: *Biological psychiatry* 72.7, pp. 595–603.
- Fox, M D, M A Halko, M C Eldaief, and A Pascual-Leone (2012b). „Measuring and manipulating brain connectivity with resting state functional connectivity magnetic resonance imaging (fcMRI) and transcranial magnetic stimulation (TMS).“ In: *NeuroImage* 62.4, pp. 2232–43.
- Fransson, P and G Marrelec (2008). „The precuneus/posterior cingulate cortex plays a pivotal role in the default mode network: Evidence from a partial correlation network analysis“. In: *NeuroImage* 42.3, pp. 1178–1184.
- Fransson, P, B Skiold, S Horsch, et al. (2007). „Resting-state networks in the infant brain“. In: *Proceedings of the National Academy of Sciences* 104.39, pp. 15531–15536.

- Fries, P (2005). „A mechanism for cognitive dynamics: neuronal communication through neuronal coherence“. In: *Trends in Cognitive Sciences* 9.10, pp. 474–480.
- Fries, P (2009). „Neuronal Gamma-Band Synchronization as a Fundamental Process in Cortical Computation“. In: *Annual Review of Neuroscience* 32.1, pp. 209–224.
- Fries, P (2015). „Rhythms for Cognition: Communication through Coherence“. In: *Neuron* 88.1, pp. 220–235.
- Fries, P, J H Reynolds, A E Rorie, and R Desimone (2001). „Modulation of oscillatory neuronal synchronization by selective visual attention.“ In: *Science (New York, N.Y.)* 291.5508, pp. 1560–3.
- Friston, K J (1994). „Functional and effective connectivity in neuroimaging: A synthesis“. In: *Human Brain Mapping* 2.1-2, pp. 56–78.
- Friston, K J, C D Frith, P Fletcher, P F Liddle, and R S J Frackowiak (1996). „Functional Topography: Multidimensional Scaling and Functional Connectivity in the Brain“. In: *Cerebral Cortex* 6.2, pp. 156–164.
- Friston, K J (2011). „Functional and Effective Connectivity: A Review“. In: *Brain Connectivity* 1.1, pp. 13–36.
- Fuchs, T (2013). „Temporality and psychopathology“. In: *Phenomenology and the Cognitive Sciences* 12.1, pp. 75–104.
- Garrity, A G, G D Pearlson, K McKiernan, D Lloyd, K A Kiehl, and V D Calhoun (2007). „Aberrant “Default Mode” Functional Connectivity in Schizophrenia“. In: *American Journal of Psychiatry* 164.3, pp. 450–457.
- Gaser, C, I Nenadic, H-P Volz, C Büchel, and H Sauer (2004). „Neuroanatomy of “hearing voices”: a frontotemporal brain structural abnormality associated with auditory hallucinations in schizophrenia.“ In: *Cerebral cortex (New York, N.Y. : 1991)* 14.1, pp. 91–6.
- Gläscher, J (2009). „Visualization of Group Inference Data in Functional Neuroimaging“. In: *Neuroinformatics* 7.1, pp. 73–82.
- Glasser, M F, S N Sotiropoulos, J A Wilson, et al. (2013). „The minimal preprocessing pipelines for the Human Connectome Project“. In: *NeuroImage* 80, pp. 105–124.
- Glover, G H, T Q Li, and D Ress (2000). „Image-based method for retrospective correction of physiological motion effects in fMRI: RETROICOR.“ In: *Magnetic resonance in medicine* 44.1, pp. 162–7.
- Goense, J B M and N K Logothetis (2008). „Neurophysiology of the BOLD fMRI Signal in Awake Monkeys“. In: *Current Biology* 18.9, pp. 631–640.
- Gohel, S R and B B Biswal (2015). „Functional integration between brain regions at rest occurs in multiple-frequency bands.“ In: *Brain connectivity* 5.1, pp. 23–34.
- Goldman, R I, J M Stern, J Engel, and M S Cohen (2002). „Simultaneous EEG and fMRI of the alpha rhythm.“ In: *Neuroreport* 13.18, pp. 2487–92.
- Gollo, L, J A Roberts, and L Cocchi (2017). „Mapping how local perturbations influence systems-level brain dynamics“. In: *NeuroImage* 160, pp. 97–112.
- Gollo, L L, A Zalesky, R M Hutchison, M van den Heuvel, and M Breakspear (2015). „Dwelling quietly in the rich club: brain network determinants of slow cortical fluctuations“. In: *Phil. Trans. R. Soc. B* 370.1668, p. 20140165.

- Goodkind, M, S B Eickhoff, D J Oathes, et al. (2015). „Identification of a Common Neurobiological Substrate for Mental Illness“. In: *JAMA Psychiatry* 72.4, p. 305.
- Goulden, N, A Khusnulina, N J Davis, et al. (2014). „The salience network is responsible for switching between the default mode network and the central executive network: Replication from DCM“. In: *NeuroImage* 99, pp. 180–190.
- Gregoriou, G G, S J Gotts, H Zhou, and R Desimone (2009). „High-Frequency, Long-Range Coupling Between Prefrontal and Visual Cortex During Attention“. In: *Science* 324.5931, pp. 1207–1210.
- Greicius, M D, B Krasnow, A L Reiss, and V Menon (2003). „Functional connectivity in the resting brain: A network analysis of the default mode hypothesis“. In: *Proceedings of the National Academy of Sciences* 100.1, pp. 253–258.
- Greicius, M D, G Srivastava, A L Reiss, and V Menon (2004). „Default-mode network activity distinguishes Alzheimer’s disease from healthy aging: evidence from functional MRI.“ In: *Proceedings of the National Academy of Sciences of the United States of America* 101.13, pp. 4637–42.
- Greicius, M D, B H Flores, V Menon, et al. (2007). „Resting-state functional connectivity in major depression: abnormally increased contributions from subgenual cingulate cortex and thalamus.“ In: *Biological psychiatry* 62.5, pp. 429–37.
- Greicius, M D, V Kiviniemi, O Tervonen, et al. (2008). „Persistent default-mode network connectivity during light sedation“. In: *Human Brain Mapping* 29.7, pp. 839–847.
- Grieve, S M, M S Korgaonkar, S H Koslow, E Gordon, and L M Williams (2013). „Widespread reductions in gray matter volume in depression.“ In: *NeuroImage. Clinical* 3, pp. 332–9.
- Griffanti, Ludovica, Gholamreza Salimi-Khorshidi, Christian F. Beckmann, et al. (2014). „ICA-based artefact removal and accelerated fMRI acquisition for improved resting state network imaging“. In: *NeuroImage* 95, pp. 232–247.
- Gürsel, D A, M Avram, C Sorg, F Brandl, and K Koch (2018). „Frontoparietal areas link impairments of large-scale intrinsic brain networks with aberrant fronto-striatal interactions in OCD: a meta-analysis of resting-state functional connectivity“. In: *Neuroscience & Biobehavioral Reviews* 87, pp. 151–160.
- Guye, M, G Bettus, F Bartolomei, and P J Cozzone (2010). „Graph theoretical analysis of structural and functional connectivity MRI in normal and pathological brain networks“. In: *Magnetic Resonance Materials in Physics, Biology and Medicine* 23.5-6, pp. 409–421.
- Haan, W de, K Mott, E C W van Straaten, P Scheltens, and C J Stam (2012). „Activity dependent degeneration explains hub vulnerability in Alzheimer’s disease.“ In: *PLoS computational biology* 8.8, e1002582.
- Hagmann, P, L Cammoun, X Gigandet, et al. (2008). „Mapping the structural core of human cerebral cortex.“ In: *PLoS biology* 6.7, e159.
- Hallett, M (2007). „Transcranial Magnetic Stimulation: A Primer“. In: *Neuron* 55.2, pp. 187–199.
- Hamilton, J P, M Siemer, and I H Gotlib (2008). „Amygdala volume in major depressive disorder: a meta-analysis of magnetic resonance imaging studies“. In: *Molecular Psychiatry* 13.11, pp. 993–1000.

- Hamilton, J P, D J Furman, C Chang, M E Thomason, E Dennis, and I H Gotlib (2011). „Default-mode and task-positive network activity in major depressive disorder: implications for adaptive and maladaptive rumination.“ In: *Biological psychiatry* 70.4, pp. 327–33.
- Hamilton, J P, A Etkin, D J Furman, M G Lemus, R F Johnson, and I H Gotlib (2012). „Functional Neuroimaging of Major Depressive Disorder: A Meta-Analysis and New Integration of Baseline Activation and Neural Response Data“. In: *American Journal of Psychiatry* 169.7, pp. 693–703.
- Hamilton, J Paul, Michael C Chen, and Ian H Gotlib (2013). „Neural systems approaches to understanding major depressive disorder: an intrinsic functional organization perspective.“ In: *Neurobiology of disease* 52, pp. 4–11.
- Hamilton, M (1960). „A rating scale for depression.“ In: *Journal of neurology, neurosurgery, and psychiatry* 23, pp. 56–62.
- Hampson, M, N R Driesen, P Skudlarski, J C Gore, and R T Constable (2006). „Brain connectivity related to working memory performance.“ In: *The Journal of neuroscience: the official journal of the Society for Neuroscience* 26.51, pp. 13338–43.
- Handwerker, D A, A Gazzaley, B A Inglis, and M D’Esposito (2007). „Reducing vascular variability of fMRI data across aging populations using a breathholding task“. In: *Human Brain Mapping* 28.9, pp. 846–859.
- Harris, Julia J., Clare Reynell, and David Attwell (2011). „The physiology of developmental changes in BOLD functional imaging signals“. In: *Developmental Cognitive Neuroscience* 1.3, pp. 199–216.
- Hasler, G, W C Drevets, H K Manji, and D S Charney (2004). „Discovering Endophenotypes for Major Depression“. In: *Neuropsychopharmacology* 29.10, pp. 1765–1781.
- Hasson, U, E Yang, I Vallines, D J Heeger, and N Rubin (2008). „A hierarchy of temporal receptive windows in human cortex.“ In: *The Journal of neuroscience: the official journal of the Society for Neuroscience* 28.10, pp. 2539–50.
- Hasson, U, J Chen, and C J Honey (2015). „Hierarchical process memory: memory as an integral component of information processing.“ In: *Trends in cognitive sciences* 19.6, pp. 304–13.
- He, B J (2011). „Scale-free properties of the functional magnetic resonance imaging signal during rest and task.“ In: *The Journal of neuroscience: the official journal of the Society for Neuroscience* 31.39, pp. 13786–95.
- He, B J and M E Raichle (2009). „The fMRI signal, slow cortical potential and consciousness.“ In: *Trends in cognitive sciences* 13.7, pp. 302–9.
- He, B J, A Z Snyder, J L Vincent, A Epstein, G L Shulman, and M Corbetta (2007). „Breakdown of Functional Connectivity in Frontoparietal Networks Underlies Behavioral Deficits in Spatial Neglect“. In: *Neuron* 53.6, pp. 905–918.
- He, B J, A Z Snyder, J M Zempel, M D Smyth, and M E Raichle (2008). „Electrophysiological correlates of the brain’s intrinsic large-scale functional architecture.“ In: *Proceedings of the National Academy of Sciences of the United States of America* 105.41, pp. 16039–44.
- Hiltunen, T, J Kantola, A Abou Elseoud, et al. (2014). „Infra-slow EEG fluctuations are correlated with resting-state network dynamics in fMRI.“ In: *The Journal of neuroscience: the official journal of the Society for Neuroscience* 34.2, pp. 356–62.

- Hirayasu, Y, R W McCarley, D F Salisbury, et al. (2000). „Planum temporale and Heschl gyrus volume reduction in schizophrenia: a magnetic resonance imaging study of first-episode patients.“ In: *Archives of general psychiatry* 57.7, pp. 692–9.
- Hoff, G E A-J, M P van den Heuvel, M J N L Benders, K J Kersbergen, and L S De Vries (2013). „On development of functional brain connectivity in the young brain.“ In: *Frontiers in human neuroscience* 7, p. 650.
- Holtzheimer, P E and H S Mayberg (2011). „Stuck in a rut: rethinking depression and its treatment.“ In: *Trends in neurosciences* 34.1, pp. 1–9.
- Honey, C J, T Thesen, T H Donner, et al. (2012). „Slow cortical dynamics and the accumulation of information over long timescales.“ In: *Neuron* 76.2, pp. 423–34.
- Hong, J-Y, L A Kilpatrick, J Labus, et al. (2013). „Patients with chronic visceral pain show sex-related alterations in intrinsic oscillations of the resting brain.“ In: *The Journal of neuroscience: the official journal of the Society for Neuroscience* 33.29, pp. 11994–2002.
- Huang, Z, X Liu, G A Mashour, and A G Hudetz (2018). „Timescales of Intrinsic BOLD Signal Dynamics and Functional Connectivity in Pharmacologic and Neuropathologic States of Unconsciousness.“ In: *The Journal of neuroscience: the official journal of the Society for Neuroscience* 38.9, pp. 2304–2317.
- Huntenburg, Julia M, Pierre-Louis Bazin, and Daniel S Margulies (2018). „Large-Scale Gradients in Human Cortical Organization.“ In: *Trends in cognitive sciences* 22.1, pp. 21–31.
- Hutchison, R M, T Womelsdorf, E A Allen, et al. (2013a). „Dynamic functional connectivity: promise, issues, and interpretations.“ In: *NeuroImage* 80, pp. 360–78.
- Hutchison, R M, T Womelsdorf, J S Gati, S Everling, and R S Menon (2013b). „Resting-state networks show dynamic functional connectivity in awake humans and anesthetized macaques.“ In: *Human Brain Mapping* 34.9, pp. 2154–2177.
- Iraji, A, T DeRamus, N Lewis, et al. (2018). „The spatial chronnectome reveals a dynamic interplay between functional segregation and integration“. In: *bioRxiv*, p. 427450.
- Iwabuchi, S J, D Peng, Y Fang, et al. (2014). „Alterations in effective connectivity anchored on the insula in major depressive disorder“. In: *European Neuropsychopharmacology* 24.11, pp. 1784–1792.
- Jacobs, R H, L M Jenkins, L B Gabriel, et al. (2014). „Increased coupling of intrinsic networks in remitted depressed youth predicts rumination and cognitive control.“ In: *PloS one* 9.8, e104366.
- James, W (1890). *The principles of psychology*. New York, NY: Henry Holt and Company.
- Jann, K, M Kottlow, T Dierks, C Boesch, and T Koenig (2010). „Topographic Electrophysiological Signatures of fMRI Resting State Networks“. In: *PLoS ONE* 5.9. Ed. by Björn Brembs, e12945.
- Jensen, O and L L Colgin (2007). „Cross-frequency coupling between neuronal oscillations“. In: *Trends in Cognitive Sciences* 11.7, pp. 267–269.
- Jonckers, E, J Van Audekerke, G De Visscher, A Van der Linden, and M Verhoye (2011). „Functional connectivity fMRI of the rodent brain: comparison of functional connectivity networks in rat and mouse.“ In: *PloS one* 6.4, e18876.

- Jun, C, Y Choi, S M Lim, et al. (2014). „Disturbance of the glutamatergic system in mood disorders.“ In: *Experimental neurobiology* 23.1, pp. 28–35.
- Kabbara, A, W EL Falou, M Khalil, F Wendling, and M Hassan (2017). „The dynamic functional core network of the human brain at rest“. In: *Scientific Reports* 7.1, p. 2936.
- Kaiser, R H, J R Andrews-Hanna, T D Wager, and D A Pizzagalli (2015). „Large-Scale Network Dysfunction in Major Depressive Disorder: A Meta-analysis of Resting-State Functional Connectivity.“ In: *JAMA psychiatry* 72.6, pp. 603–11.
- Kaiser, R H, S Whitfield-Gabrieli, D G Dillon, et al. (2016). „Dynamic Resting-State Functional Connectivity in Major Depression.“ In: *Neuropsychopharmacology: official publication of the American College of Neuropsychopharmacology* 41.7, pp. 1822–30.
- Kalcher, K, R N Boubela, W Huf, et al. (2014). „The spectral diversity of resting-state fluctuations in the human brain.“ In: *PloS one* 9.4, e93375.
- Kanwisher, N, J McDermott, and M M Chun (1997). „The fusiform face area: a module in human extrastriate cortex specialized for face perception.“ In: *The Journal of neuroscience: the official journal of the Society for Neuroscience* 17.11, pp. 4302–11.
- Kasagi, M, Z Huang, K Narita, et al. (2017). „Association between Scale-Free Brain Dynamics and Behavioral Performance: Functional MRI Study in Resting State and Face Processing Task“. In: *Behavioural Neurology* 2017, pp. 1–9.
- Kelly, C, R Toro, A Di Martino, et al. (2012). „A convergent functional architecture of the insula emerges across imaging modalities.“ In: *NeuroImage* 61.4, pp. 1129–42.
- Kempton, M J, Z Salvador, M R Munafò, et al. (2011). „Structural Neuroimaging Studies in Major Depressive Disorder“. In: *Archives of General Psychiatry* 68.7, p. 675.
- Kerestes, R, C G Davey, K Stephanou, S Whittle, and B J Harrison (2014). „Functional brain imaging studies of youth depression: a systematic review.“ In: *NeuroImage. Clinical* 4, pp. 209–31.
- Kessler, R C (2012). „The costs of depression.“ In: *The Psychiatric clinics of North America* 35.1, pp. 1–14.
- Khader, P, T Schicke, B Röder, and F Rösler (2008). „On the relationship between slow cortical potentials and BOLD signal changes in humans“. In: *International Journal of Psychophysiology* 67.3, pp. 252–261.
- Kiviniemi, V, J-H Kantola, J Jauhiainen, A Hyvärinen, and O Tervonen (2003). „Independent component analysis of nondeterministic fMRI signal sources.“ In: *NeuroImage* 19.2 Pt 1, pp. 253–60.
- Kiviniemi, V, T Starck, J Remes, et al. (2009). „Functional segmentation of the brain cortex using high model order group PICA“. In: *Human Brain Mapping* 30.12, pp. 3865–3886.
- Klaassens, B L, H C van Gersel, N Khalili-Mahani, et al. (2015). „Single-dose serotonergic stimulation shows widespread effects on functional brain connectivity“. In: *NeuroImage* 122, pp. 440–450.
- Klimesch, W (1996). „Memory processes, brain oscillations and EEG synchronization.“ In: *International journal of psychophysiology: official journal of the International Organization of Psychophysiology* 24.1-2, pp. 61–100.

- Klimesch, W, M Doppelmayr, T Pachinger, and B Ripper (1997a). „Brain oscillations and human memory: EEG correlates in the upper alpha and theta band.“ In: *Neuroscience letters* 238.1-2, pp. 9–12.
- Klimesch, W, M Doppelmayr, H Schimke, and B Ripper (1997b). „Theta synchronization and alpha desynchronization in a memory task.“ In: *Psychophysiology* 34.2, pp. 169–76.
- Klimesch, W, M Doppelmayr, W Stadler, D Pöllhuber, P Sauseng, and D Röhms (2001). „Episodic retrieval is reflected by a process specific increase in human electroencephalographic theta activity.“ In: *Neuroscience letters* 302.1, pp. 49–52.
- Knyazev, G G (2007). „Motivation, emotion, and their inhibitory control mirrored in brain oscillations“. In: *Neuroscience & Biobehavioral Reviews* 31.3, pp. 377–395.
- Kobayashi, M and A Pascual-Leone (2003). „Transcranial magnetic stimulation in neurology.“ In: *The Lancet. Neurology* 2.3, pp. 145–56.
- Koolschijn, P C, N E van Haren, G J Lensvelt-Mulders, H E Hulshoff Pol, and R S. Kahn (2009). „Brain volume abnormalities in major depressive disorder: A meta-analysis of magnetic resonance imaging studies“. In: *Human Brain Mapping* 30.11, pp. 3719–3735.
- Kyathanahally, S P, Y Wang, V Calhoun, and G Deshpande (2017). „Investigation of True High Frequency Electrical Substrates of fMRI-Based Resting State Networks Using Parallel Independent Component Analysis of Simultaneous EEG/fMRI Data“. In: *Frontiers in Neuroinformatics* 11, p. 74.
- Lai, C-H (2013). „Gray matter volume in major depressive disorder: A meta-analysis of voxel-based morphometry studies“. In: *Psychiatry Research: Neuroimaging* 211.1, pp. 37–46.
- Lakatos, P, G Karmos, A D Mehta, I Ulbert, and C E Schroeder (2008). „Entrainment of Neuronal Oscillations as a Mechanism of Attentional Selection“. In: *Science* 320.5872, pp. 110–113.
- Latora, V and M Marchiori (2001). „Efficient Behavior of Small-World Networks“. In: *Physical Review Letters* 87.19, p. 198701.
- Le, T M, J A Borghi, A J Kujawa, D N Klein, and H-C Leung (2017). „Alterations in visual cortical activation and connectivity with prefrontal cortex during working memory updating in major depressive disorder.“ In: *NeuroImage. Clinical* 14, pp. 43–53.
- Lee, B-T, J-H Seok, B-C Lee, et al. (2008). „Neural correlates of affective processing in response to sad and angry facial stimuli in patients with major depressive disorder“. In: *Progress in Neuro-Psychopharmacology and Biological Psychiatry* 32.3, pp. 778–785.
- Lee, H-L, B Zahneisen, T Hugger, P LeVan, and J Hennig (2013). „Tracking dynamic resting-state networks at higher frequencies using MR-encephalography“. In: *NeuroImage* 65, pp. 216–222.
- Lee, J-H, R Durand, V Gradinaru, et al. (2010). „Global and local fMRI signals driven by neurons defined optogenetically by type and wiring.“ In: *Nature* 465.7299, pp. 788–92.
- Lennie, P (2003). „The cost of cortical computation.“ In: *Current biology: CB* 13.6, pp. 493–7.
- Leopold, D A, Y Murayama, and N K Logothetis (2003). „Very Slow Activity Fluctuations in Monkey Visual Cortex: Implications for Functional Brain Imaging“. In: *Cerebral Cortex* 13.4, pp. 422–433.

- Lerner, Y, C J Honey, L J Silbert, and U Hasson (2011). „Topographic mapping of a hierarchy of temporal receptive windows using a narrated story.“ In: *The Journal of neuroscience: the official journal of the Society for Neuroscience* 31.8, pp. 2906–15.
- Lewis, C M, A Baldassarre, G Committeri, G L Romani, and M Corbetta (2009). „Learning sculpts the spontaneous activity of the resting human brain.“ In: *Proceedings of the National Academy of Sciences of the United States of America* 106.41, pp. 17558–63.
- Lewis, L D, K Setsompop, B R Rosen, and J R Polimeni (2016). „Fast fMRI can detect oscillatory neural activity in humans“. In: *Proceedings of the National Academy of Sciences* 113.43, e6679–85.
- Li, B, L Liu, K J Friston, et al. (2013). „A Treatment-Resistant Default Mode Subnetwork in Major Depression“. In: *Biological Psychiatry* 74.1, pp. 48–54.
- Liao, X-H, M-R Xia, T Xu, et al. (2013). „Functional brain hubs and their test–retest reliability: A multiband resting-state functional MRI study“. In: *NeuroImage* 83, pp. 969–982.
- Liau, J and T T Liu (2009). „Inter-subject variability in hypercapnic normalization of the BOLD fMRI response“. In: *NeuroImage* 45.2, pp. 420–430.
- Liu, J, X Xu, Q Luo, et al. (2017). „Brain grey matter volume alterations associated with antidepressant response in major depressive disorder.“ In: *Scientific reports* 7.1, p. 10464.
- Liu, T T (2016). „Noise contributions to the fMRI signal: An overview“. In: *NeuroImage* 143, pp. 141–151.
- Liu, W-C, J F Flax, K G Guise, V Sukul, and A A Benasich (2008). „Functional connectivity of the sensorimotor area in naturally sleeping infants“. In: *Brain Research* 1223, pp. 42–49.
- Liu, Z, C Xu, Y Xu, et al. (2010). „Decreased regional homogeneity in insula and cerebellum: a resting-state fMRI study in patients with major depression and subjects at high risk for major depression.“ In: *Psychiatry research* 182.3, pp. 211–5.
- Logothetis, N K (2008). „What we can do and what we cannot do with fMRI“. In: *Nature* 453.7197, pp. 869–878.
- Logothetis, N K, Pauls, M Augath, T Trinath, and A Oeltermann (2001). „Neurophysiological investigation of the basis of the fMRI signal.“ In: *Nature* 412.6843, pp. 150–157.
- Lopes da Silva, F (2013). „EEG and MEG: relevance to neuroscience.“ In: *Neuron* 80.5, pp. 1112–28.
- Lowe, M J (2012). „The emergence of doing “nothing” as a viable paradigm design“. In: *NeuroImage* 62.2, pp. 1146–1151.
- Lowe, M J, B J Mock, and J A Sorenson (1998). „Functional Connectivity in Single and Multislice Echoplanar Imaging Using Resting-State Fluctuations“. In: *NeuroImage* 7.2, pp. 119–132.
- Lu, H, C Zhao, Y Ge, and K Lewis-Amezcu (2008). „Baseline blood oxygenation modulates response amplitude: Physiologic basis for intersubject variations in functional MRI signals“. In: *Magnetic Resonance in Medicine* 60.2, pp. 364–372.
- Lu, H, Q Zou, H Gu, M E Raichle, E A Stein, and Y Yang (2012). „Rat brains also have a default mode network.“ In: *Proceedings of the National Academy of Sciences of the United States of America* 109.10, pp. 3979–84.

- Luo, Q, Z Deng, J Qin, et al. (2015). „Frequency Dependant Topological Alterations of Intrinsic Functional Connectome in Major Depressive Disorder“. In: *Scientific Reports* 5.1, p. 9710.
- Luscher, B, Q Shen, and N Sahir (2011). „The GABAergic deficit hypothesis of major depressive disorder.“ In: *Molecular psychiatry* 16.4, pp. 383–406.
- Mahlberg, R, T Kienast, T Bschor, and M Adli (2008). „Evaluation of time memory in acutely depressed patients, manic patients, and healthy controls using a time reproduction task.“ In: *European psychiatry: the journal of the Association of European Psychiatrists* 23.6, pp. 430–3.
- Malinen, S, N Vartiainen, Y Hlushchuk, et al. (2010). „Aberrant temporal and spatial brain activity during rest in patients with chronic pain.“ In: *Proceedings of the National Academy of Sciences of the United States of America* 107.14, pp. 6493–7.
- Manoliu, Ai, C Meng, F Brandl, et al. (2013). „Insular dysfunction within the salience network is associated with severity of symptoms and aberrant inter-network connectivity in major depressive disorder.“ In: *Frontiers in human neuroscience* 7, p. 930.
- Mantini, D, M G Perrucci, C Del Gratta, G L Romani, and M Corbetta (2007). „Electrophysiological signatures of resting state networks in the human brain.“ In: *Proceedings of the National Academy of Sciences of the United States of America* 104.32, pp. 13170–5.
- Mathews, D C, I D Henter, and C A Zarate (2012). „Targeting the glutamatergic system to treat major depressive disorder: rationale and progress to date.“ In: *Drugs* 72.10, pp. 1313–33.
- Mathias, N and V Gopal (2001). „Small worlds: How and why“. In: *Physical Review E* 63.2, p. 021117.
- Meda, S A, Z Wang, E I Ivleva, et al. (2015). „Frequency-Specific Neural Signatures of Spontaneous Low-Frequency Resting State Fluctuations in Psychosis: Evidence From Bipolar-Schizophrenia Network on Intermediate Phenotypes (B-SNIP) Consortium“. In: *Schizophrenia Bulletin* 41.6, pp. 1336–1348.
- Melloni, L, C Molina, M Pena, D Torres, W Singer, and E Rodriguez (2007). „Synchronization of Neural Activity across Cortical Areas Correlates with Conscious Perception“. In: *Journal of Neuroscience* 27.11, pp. 2858–2865.
- Meng, C, F Brandl, M Tahmasian, et al. (2014). „Aberrant topology of striatum’s connectivity is associated with the number of episodes in depression.“ In: *Brain: a journal of neurology* 137.Pt 2, pp. 598–609.
- Menon, V (2011). „Large-scale brain networks and psychopathology: a unifying triple network model.“ In: *Trends in cognitive sciences* 15.10, pp. 483–506.
- Menon, V and L Q Uddin (2010). „Saliency, switching, attention and control: a network model of insula function.“ In: *Brain structure & function* 214.5-6, pp. 655–67.
- Moeller, S, E Yacoub, C A Olman, et al. (2010). „Multiband multislice GE-EPI at 7 tesla, with 16-fold acceleration using partial parallel imaging with application to high spatial and temporal whole-brain fMRI“. In: *Magnetic Resonance in Medicine* 63.5, pp. 1144–1153.
- Mukamel, R, H Gelbard, A Arieli, U Hasson, I Fried, and R Malach (2005). „Coupling Between Neuronal Firing, Field Potentials, and fMRI in Human Auditory Cortex“. In: *Science* 309.5736, pp. 951–954.

- Mulders, P C, P F van Eijndhoven, A H Schene, C F Beckmann, and I Tendolkar (2015). „Resting-state functional connectivity in major depressive disorder: A review“. In: *Neuroscience & Biobehavioral Reviews* 56, pp. 330–344.
- Murphy, K, J Bodurka, and P A Bandettini (2007). „How long to scan? The relationship between fMRI temporal signal to noise ratio and necessary scan duration“. In: *NeuroImage* 34.2, pp. 565–574.
- Murphy, K, R M Birn, and P A Bandettini (2013). „Resting-state fMRI confounds and cleanup“. In: *NeuroImage* 80, pp. 349–59.
- Murray, C J L, T Vos, R Lozano, et al. (2012). „Disability-adjusted life years (DALYs) for 291 diseases and injuries in 21 regions, 1990–2010: a systematic analysis for the Global Burden of Disease Study 2010“. In: *The Lancet* 380.9859, pp. 2197–2223.
- Murray, J D, A Bernacchia, D J Freedman, et al. (2014). „A hierarchy of intrinsic timescales across primate cortex.“ In: *Nature neuroscience* 17.12, pp. 1661–3.
- Neufang, S, A Akhrif, V Riedl, et al. (2014). „Predicting effective connectivity from resting-state networks in healthy elderly and patients with prodromal Alzheimer’s disease“. In: *Human Brain Mapping* 35.3, pp. 954–963.
- Niazy, R K, J Xie, K Miller, C F Beckmann, and S M Smith (2011). „Chapter 17 – Spectral characteristics of resting state networks“. In: *Progress in Brain Research*. Vol. 193, pp. 259–276.
- Nijhuis, E H, A-M van Cappellen van Walsum, and D G Norris (2013). „Topographic hub maps of the human structural neocortical network.“ In: *PloS one* 8.6, e65511.
- Nordentoft, M, P B Mortensen, and C B Pedersen (2011). „Absolute Risk of Suicide After First Hospital Contact in Mental Disorder“. In: *Archives of General Psychiatry* 68.10, p. 1058.
- Northoff, G (2016). „Spatiotemporal psychopathology I: No rest for the brain’s resting state activity in depression? Spatiotemporal psychopathology of depressive symptoms“. In: *Journal of Affective Disorders* 190, pp. 854–866.
- Northoff, G (2017). „Spatiotemporal Psychopathology II: How does a psychopathology of the brain’s resting state look like? Spatiotemporal approach and the history of psychopathology“. In: *Journal of Affective Disorders* 190, pp. 867–879.
- Northoff, G and Z Huang (2017). „How do the brain’s time and space mediate consciousness and its different dimensions? Temporo-spatial theory of consciousness (TTC)“. In: *Neuroscience & Biobehavioral Reviews* 80, pp. 630–645.
- Northoff, G, C Wiebking, T Feinberg, and J Panksepp (2011). „The ‘resting-state hypothesis’ of major depressive disorder—A translational subcortical–cortical framework for a system disorder“. In: *Neuroscience & Biobehavioral Reviews* 35.9, pp. 1929–1945.
- Nostro, A D, V I Müller, D P Varikuti, et al. (2018). „Predicting personality from network-based resting-state functional connectivity“. In: *Brain Structure and Function* 223.6, pp. 2699–2719.
- Ogawa, S, T M Lee, A R Kay, and D W Tank (1990). „Brain magnetic resonance imaging with contrast dependent on blood oxygenation.“ In: *Proceedings of the National Academy of Sciences of the United States of America* 87.24, pp. 9868–72.

- Ogawa, S, D W Tank, R Menon, et al. (1992). „Intrinsic signal changes accompanying sensory stimulation: functional brain mapping with magnetic resonance imaging.“ In: *Proceedings of the National Academy of Sciences of the United States of America* 89.13, pp. 5951–5.
- Otti, A, H Guendel, A Wohlschläger, C Zimmer, and M Noll-Hussong (2013). „Frequency shifts in the anterior default mode network and the salience network in chronic pain disorder“. In: *BMC Psychiatry* 13.1, p. 84.
- Pandya, M, M Altinay, D A Malone, and A Anand (2012). „Where in the brain is depression?“ In: *Current psychiatry reports* 14.6, pp. 634–42.
- Pascual-Leone, A and V Walsh (2001). „Fast Backprojections from the Motion to the Primary Visual Area Necessary for Visual Awareness“. In: *Science* 292.5516, pp. 510–512.
- Pauling, L and C D Coryell (1936). „The Magnetic Properties and Structure of Hemoglobin, Oxyhemoglobin and Carbonmonoxyhemoglobin.“ In: *Proceedings of the National Academy of Sciences of the United States of America* 22.4, pp. 210–6.
- Peng, D, F Shi, G Li, et al. (2015). „Surface Vulnerability of Cerebral Cortex to Major Depressive Disorder“. In: *PLOS ONE* 10.3. Ed. by Yong He, e0120704.
- Peng, J, J Liu, B Nie, et al. (2011). „Cerebral and cerebellar gray matter reduction in first-episode patients with major depressive disorder: a voxel-based morphometry study.“ In: *European journal of radiology* 80.2, pp. 395–9.
- Peng, X, P Lin, X Wu, R Gong, R Yang, and J Wang (2018). „Insular subdivisions functional connectivity dysfunction within major depressive disorder“. In: *Journal of Affective Disorders* 227, pp. 280–288.
- Penttonen, M and G Buzsáki (2003). „Natural logarithmic relationship between brain oscillators“. In: *Thalamus and Related Systems* 2.02, p. 145.
- Pfurtscheller, G, A Stancák, and C Neuper (1996). „Post-movement beta synchronization. A correlate of an idling motor area?“ In: *Electroencephalography and clinical neurophysiology* 98.4, pp. 281–93.
- Pizzagalli, D A (2011). „Frontocingulate dysfunction in depression: toward biomarkers of treatment response.“ In: *Neuropsychopharmacology: official publication of the American College of Neuropsychopharmacology* 36.1, pp. 183–206.
- Power, J D, A L Cohen, S M Nelson, et al. (2011). „Functional network organization of the human brain.“ In: *Neuron* 72.4, pp. 665–78.
- Power, J D, K A Barnes, A Z Snyder, B L Schlaggar, and S E Petersen (2012). „Spurious but systematic correlations in functional connectivity MRI networks arise from subject motion.“ In: *NeuroImage* 59.3, pp. 2142–54.
- Power, J D, B L Schlaggar, C N Lessov-Schlaggar, and S E Petersen (2013). „Evidence for hubs in human functional brain networks.“ In: *Neuron* 79.4, pp. 798–813.
- Power, J D, A Mitra, T O Laumann, A Z Snyder, B L Schlaggar, and S E Petersen (2014). „Methods to detect, characterize, and remove motion artifact in resting state fMRI.“ In: *NeuroImage* 84, pp. 320–41.
- Qian, L, Y Zhang, L Zheng, et al. (2017). „Frequency specific brain networks in Parkinson’s disease and comorbid depression“. In: *Brain Imaging and Behavior* 11.1, pp. 224–239.
- Raichle, M E (2011). „The Restless Brain“. In: *Brain Connectivity* 1.1, pp. 3–12.

- Raichle, M E (2015). „The restless brain: how intrinsic activity organizes brain function.“ In: *Philosophical transactions of the Royal Society of London. Series B, Biological sciences* 370.1668.
- Raichle, M E, A M MacLeod, A Z Snyder, W J Powers, D A Gusnard, and G L Shulman (2001). „A default mode of brain function.“ In: *Proceedings of the National Academy of Sciences of the United States of America* 98.2, pp. 676–82.
- Ray, K L, D R McKay, P M Fox, et al. (2013). „ICA model order selection of task co-activation networks“. In: *Frontiers in Neuroscience* 7, p. 237.
- Ries, A, C Chang, S Glim, C Meng, C Sorg, and A Wohlschlaeger (2018). „Grading of frequency spectral centroid across resting-state networks“. In: *Frontiers in Human Neuroscience* 12, p. 436.
- Robinson, S, G Basso, N Soldati, et al. (2009). „A resting state network in the motor control circuit of the basal ganglia“. In: *BMC Neuroscience* 10.1, p. 137.
- Rodriguez, E, N George, J-P Lachaux, J Martinerie, B Renault, and F J Varela (1999). „Perception’s shadow: long-distance synchronization of human brain activity“. In: *Nature* 397.6718, pp. 430–433.
- Rush, A J (2007). „The varied clinical presentations of major depressive disorder.“ In: *The Journal of clinical psychiatry* 68 Suppl 8, pp. 4–10.
- Sadaghiani, S, R Scheeringa, K Lehongre, B Morillon, A-L Giraud, and A Kleinschmidt (2010). „Intrinsic connectivity networks, alpha oscillations, and tonic alertness: a simultaneous electroencephalography/functional magnetic resonance imaging study.“ In: *The Journal of neuroscience: the official journal of the Society for Neuroscience* 30.30, pp. 10243–50.
- Sala-Llonch, R, D Bartrés-Faz, and C Junqué (2015). „Reorganization of brain networks in aging: a review of functional connectivity studies.“ In: *Frontiers in psychology* 6, p. 663.
- Salimi-Khorshidi, G, G Douaud, C F Beckmann, M F Glasser, L Griffanti, and S M Smith (2014). „Automatic denoising of functional MRI data: Combining independent component analysis and hierarchical fusion of classifiers“. In: *NeuroImage* 90, pp. 449–468.
- Salvador, R, J Suckling, C Schwarzbauer, and E Bullmore (2005). „Undirected graphs of frequency-dependent functional connectivity in whole brain networks.“ In: *Philosophical transactions of the Royal Society of London. Series B, Biological sciences* 360.1457, pp. 937–46.
- Salvador, R, A Martínez, E Pomarol-Clotet, et al. (2008). „A simple view of the brain through a frequency-specific functional connectivity measure“. In: *NeuroImage* 39.1, pp. 279–289.
- Sambataro, F, N D Wolf, P Giusti, N Vasic, and R C Wolf (2013). „Default mode network in depression: a pathway to impaired affective cognition?“ In: *Clinical Neuropsychiatry* 10.5, pp. 212–216.
- Sambataro, F, N D Wolf, M Pennuto, N Vasic, and R C Wolf (2014). „Revisiting default mode network function in major depression: evidence for disrupted subsystem connectivity“. In: *Psychological Medicine* 44.10, pp. 2041–2051.
- Sanacora, G, G F Mason, and J H Krystal (2000). „Impairment of GABAergic transmission in depression: new insights from neuroimaging studies.“ In: *Critical reviews in neurobiology* 14.1, pp. 23–45.

- Sanacora, G, G F Mason, D L Rothman, and J H Krystal (2002). „Increased Occipital Cortex GABA Concentrations in Depressed Patients After Therapy With Selective Serotonin Reuptake Inhibitors“. In: *American Journal of Psychiatry* 159.4, pp. 663–665.
- Sanacora, G, G F Mason, D L Rothman, et al. (2003). „Increased Cortical GABA Concentrations in Depressed Patients Receiving ECT“. In: *American Journal of Psychiatry* 160.3, pp. 577–579.
- Sanacora, G, R Gueorguieva, C N Epperson, et al. (2004). „Subtype-Specific Alterations of γ -Aminobutyric Acid and Glutamate in Patients With Major Depression“. In: *Archives of General Psychiatry* 61.7, p. 705.
- Sanacora, G, G Treccani, and M Popoli (2012). „Towards a glutamate hypothesis of depression: an emerging frontier of neuropsychopharmacology for mood disorders.“ In: *Neuropharmacology* 62.1, pp. 63–77.
- Sasai, S, F Homae, H Watanabe, et al. (2014). „Frequency-specific network topologies in the resting human brain“. In: *Frontiers in Human Neuroscience* 8, p. 1022.
- Satterthwaite, T D, M A Elliott, R T Gerraty, et al. (2013). „An improved framework for confound regression and filtering for control of motion artifact in the preprocessing of resting-state functional connectivity data.“ In: *NeuroImage* 64, pp. 240–56.
- Sauseng, P, W Klimesch, W Gruber, M Doppelmayr, W Stadler, and M Schabus (2002). „The interplay between theta and alpha oscillations in the human electroencephalogram reflects the transfer of information between memory systems“. In: *Neuroscience Letters* 324.2, pp. 121–124.
- Sauseng, P, B Griesmayr, R Freunberger, and W Klimesch (2010). „Control mechanisms in working memory: A possible function of EEG theta oscillations“. In: *Neuroscience & Biobehavioral Reviews* 34.7, pp. 1015–1022.
- Savitz, J B and W C Drevets (2009). „Imaging phenotypes of major depressive disorder: genetic correlates.“ In: *Neuroscience* 164.1, pp. 300–30.
- Savitz, J B and W C Drevets (2013). „Neuroreceptor imaging in depression“. In: *Neurobiology of Disease* 52, pp. 49–65.
- Schölvinck, M L, A Maier, F Q Ye, J H Duyn, and D A Leopold (2010). „Neural basis of global resting-state fMRI activity.“ In: *Proceedings of the National Academy of Sciences of the United States of America* 107.22, pp. 10238–43.
- Schultz, D H and M W Cole (2016). „Higher Intelligence Is Associated with Less Task-Related Brain Network Reconfiguration.“ In: *The Journal of neuroscience: the official journal of the Society for Neuroscience* 36.33, pp. 8551–61.
- Schürmann, M, C Başar-Eroglu, V Kolev, and E Başar (2001). „Delta responses and cognitive processing: single-trial evaluations of human visual P300.“ In: *International journal of psychophysiology: official journal of the International Organization of Psychophysiology* 39.2-3, pp. 229–39.
- Seeley, W W, V Menon, A F Schatzberg, et al. (2007). „Dissociable intrinsic connectivity networks for salience processing and executive control.“ In: *The Journal of neuroscience: the official journal of the Society for Neuroscience* 27.9, pp. 2349–56.

- Sheline, Y I, D M Barch, J L Price, et al. (2009). „The default mode network and self-referential processes in depression.“ In: *Proceedings of the National Academy of Sciences of the United States of America* 106.6, pp. 1942–7.
- Shmuel, A and D A Leopold (2008). „Neuronal correlates of spontaneous fluctuations in fMRI signals in monkey visual cortex: Implications for functional connectivity at rest“. In: *Human Brain Mapping* 29.7, pp. 751–761.
- Shmueli, K, P van Gelderen, J A de Zwart, et al. (2007). „Low-frequency fluctuations in the cardiac rate as a source of variance in the resting-state fMRI BOLD signal.“ In: *NeuroImage* 38.2, pp. 306–20.
- Shulman, R G, D L Rothman, K L Behar, and F Hyder (2004). „Energetic basis of brain activity: implications for neuroimaging“. In: *Trends in Neurosciences* 27.8, pp. 489–495.
- Siebner, H R, T O Bergmann, S Bestmann, et al. (2009). „Consensus paper: Combining transcranial stimulation with neuroimaging“. In: *Brain Stimulation* 2.2, pp. 58–80.
- Silvanto, J, A Cowey, N Lavie, and V Walsh (2005). „Striate cortex (V1) activity gates awareness of motion“. In: *Nature Neuroscience* 8.2, pp. 143–144.
- Singer, W (1999). „Neuronal synchrony: a versatile code for the definition of relations?“ In: *Neuron* 24.1, pp. 49–65, 111–25.
- Singer, W and C M Gray (1995). „Visual Feature Integration and the Temporal Correlation Hypothesis“. In: *Annual Review of Neuroscience* 18.1, pp. 555–586.
- Smith, S M, P T Fox, K L Miller, et al. (2009). „Correspondence of the brain’s functional architecture during activation and rest.“ In: *Proceedings of the National Academy of Sciences of the United States of America* 106.31, pp. 13040–5.
- Smith, S M, C F Beckmann, J Andersson, et al. (2013). „Resting-state fMRI in the Human Connectome Project“. In: *NeuroImage* 80, pp. 144–168.
- Song, X-W, Z-Y Dong, X-Y Long, et al. (2011). „REST: a toolkit for resting-state functional magnetic resonance imaging data processing.“ In: *PloS one* 6.9, e25031.
- Sperling, R A, P S Laviolette, K O’Keefe, et al. (2009). „Amyloid deposition is associated with impaired default network function in older persons without dementia.“ In: *Neuron* 63.2, pp. 178–88.
- Spitzer, R L, J B Williams, M Gibbon, and M B First (1992). „The Structured Clinical Interview for DSM-III-R (SCID). I: History, rationale, and description.“ In: *Archives of general psychiatry* 49.8, pp. 624–9.
- Sporns, O, G Tononi, and G M Edelman (2000). „Theoretical neuroanatomy: relating anatomical and functional connectivity in graphs and cortical connection matrices.“ In: *Cerebral cortex (New York, N.Y. : 1991)* 10.2, pp. 127–41.
- Sporns, O, D Chialvo, M Kaiser, and C Hilgetag (2004). „Organization, development and function of complex brain networks“. In: *Trends in Cognitive Sciences* 8.9, pp. 418–425.
- Sporns, O, C J Honey, R Kötter, P A Valdes-Hernandez, and E Martinez-Montes (2007). „Identification and Classification of Hubs in Brain Networks“. In: *PLoS ONE* 2.10. Ed. by Marcus Kaiser, e1049.

- Sridharan, D, D J Levitin, and V Menon (2008). „A critical role for the right fronto-insular cortex in switching between central-executive and default-mode networks.“ In: *Proceedings of the National Academy of Sciences of the United States of America* 105.34, pp. 12569–74.
- Stagg, C and D L Rothman (2013). *Magnetic resonance spectroscopy: tools for neuroscience research and emerging clinical applications*. Academic Press, p. 500.
- Stanghellini, G, M Ballerini, S Presentza, M Mancini, G Northoff, and J Cutting (2017). „Abnormal Time Experiences in Major Depression: An Empirical Qualitative Study“. In: *Psychopathology* 50.2, pp. 125–140.
- Stephens, G J, C J Honey, and U Hasson (2013). „A place for time: the spatiotemporal structure of neural dynamics during natural audition“. In: *Journal of Neurophysiology* 110.9, pp. 2019–2026.
- Steriade, M, I Timofeev, and F Grenier (2001). „Natural Waking and Sleep States: A View From Inside Neocortical Neurons“. In: *Journal of Neurophysiology* 85.5, pp. 1969–1985.
- Tagliazucchi, E, L Roseman, M Kaelen, et al. (2016). „Increased Global Functional Connectivity Correlates with LSD-Induced Ego Dissolution“. In: *Current Biology* 26.8, pp. 1043–1050.
- Takahashi, T, M Yücel, V Lorenzetti, et al. (2010). „Volumetric MRI study of the insular cortex in individuals with current and past major depression.“ In: *Journal of affective disorders* 121.3, pp. 231–8.
- Takeuchi, H, Y Taki, R Nouchi, et al. (2015). „Degree centrality and fractional amplitude of low-frequency oscillations associated with Stroop interference“. In: *NeuroImage* 119, pp. 197–209.
- Taki, Y, S Kinomura, S Awata, et al. (2005). „Male elderly subthreshold depression patients have smaller volume of medial part of prefrontal cortex and precentral gyrus compared with age-matched normal subjects: a voxel-based morphometry.“ In: *Journal of affective disorders* 88.3, pp. 313–20.
- Tallon-Baudry, C (2009). „The roles of gamma-band oscillatory synchrony in human visual cognition.“ In: *Frontiers in bioscience (Landmark edition)* 14, pp. 321–32.
- Thomason, M E, L C Foland, and G H Glover (2007). „Calibration of BOLD fMRI using breath holding reduces group variance during a cognitive task“. In: *Human Brain Mapping* 28.1, pp. 59–68.
- Thompson, W H and P Fransson (2015). „The frequency dimension of fMRI dynamic connectivity: Network connectivity, functional hubs and integration in the resting brain“. In: *NeuroImage* 121, pp. 227–242.
- Thönes, S and D Oberfeld (2015). „Time perception in depression: a meta-analysis.“ In: *Journal of affective disorders* 175, pp. 359–72.
- Tokuda, T, J Yoshimoto, Y Shimizu, et al. (2018). „Identification of depression subtypes and relevant brain regions using a data-driven approach“. In: *Scientific Reports* 8.1, p. 14082.
- Tomasi, D and N D Volkow (2010). „Functional connectivity density mapping.“ In: *Proceedings of the National Academy of Sciences of the United States of America* 107.21, pp. 9885–90.
- Tomasi, D and N D Volkow (2011a). „Association between functional connectivity hubs and brain networks“. In: *Cerebral Cortex* 21.9, pp. 2003–2013.

- Tomasi, D and N D Volkow (2011b). „Functional connectivity hubs in the human brain“. In: *NeuroImage* 57.3, pp. 908–917.
- Tomasi, D and N D Volkow (2014). „Functional Connectivity of Substantia Nigra and Ventral Tegmental Area: Maturation During Adolescence and Effects of ADHD“. In: *Cerebral Cortex* 24.4, pp. 935–944.
- Treadway, M T and D A Pizzagalli (2014). „Imaging the pathophysiology of major depressive disorder - from localist models to circuit-based analysis.“ In: *Biology of mood & anxiety disorders* 4.1, p. 5.
- Tsujii, N, W Mikawa, E Tsujimoto, et al. (2017). „Reduced left precentral regional responses in patients with major depressive disorder and history of suicide attempts.“ In: *PloS one* 12.4, e0175249.
- Tunnicliff, G and E Malatynska (2003). „Central GABAergic Systems and Depressive Illness“. In: *Neurochemical Research* 28.6, pp. 965–976.
- Uddin, L Q (2014). „Salience processing and insular cortical function and dysfunction“. In: *Nature Reviews Neuroscience* 16.1, pp. 55–61.
- Uğurbil, K, J Xu, E J Auerbach, et al. (2013). „Pushing spatial and temporal resolution for functional and diffusion MRI in the Human Connectome Project“. In: *NeuroImage* 80, pp. 80–104.
- Uhlhaas, P J, G Pipa, B Lima, et al. (2009). „Neural synchrony in cortical networks: history, concept and current status.“ In: *Frontiers in integrative neuroscience* 3, p. 17.
- van den Heuvel, M P and O Sporns (2011). „Rich-club organization of the human connectome.“ In: *The Journal of neuroscience: the official journal of the Society for Neuroscience* 31.44, pp. 15775–86.
- van den Heuvel, M P and Olaf Sporns (2013). „Network hubs in the human brain“. In: *Trends in Cognitive Sciences* 17.12, pp. 683–696.
- van den Heuvel, M P, C J Stam, M Boersma, and H E Hulshoff Pol (2008). „Small-world and scale-free organization of voxel-based resting-state functional connectivity in the human brain“. In: *NeuroImage* 43.3, pp. 528–539.
- van den Heuvel, M P, L H Scholtens, E Turk, D Mantini, W Vanduffel, and L Feldman Barrett (2016). „Multimodal analysis of cortical chemoarchitecture and macroscale fMRI resting-state functional connectivity“. In: *Human Brain Mapping* 37.9, pp. 3103–3113.
- Van Dijk, K R A, M R Sabuncu, and R L Buckner (2012). „The influence of head motion on intrinsic functional connectivity MRI.“ In: *NeuroImage* 59.1, pp. 431–8.
- Van Essen, D C, S M Smith, D M Barch, et al. (2013). „The WU-Minn Human Connectome Project: an overview.“ In: *NeuroImage* 80, pp. 62–79.
- van Oort, E, D Norris, S M Smith, and C Beckmann (2012). „Resting state networks are characterized by high frequency BOLD fluctuations“. In: *OHBM, Minneapolis: Abstract Number 739*.
- Vanhatalo, S, J M Palva, M D Holmes, J W Miller, J Voipio, and K Kaila (2004). „Infraslow oscillations modulate excitability and interictal epileptic activity in the human cortex during sleep.“ In: *Proceedings of the National Academy of Sciences of the United States of America* 101.14, pp. 5053–7.

- Vanhatalo, S, J Voipio, and K Kaila (2005). „Full-band EEG (FbEEG): an emerging standard in electroencephalography.“ In: *Clinical neurophysiology: official journal of the International Federation of Clinical Neurophysiology* 116.1, pp. 1–8.
- Veer, I M, C F Beckmann, M-J van Tol, et al. (2010). „Whole brain resting-state analysis reveals decreased functional connectivity in major depression.“ In: *Frontiers in systems neuroscience* 4.
- Vincent, J L, G H Patel, M D Fox, et al. (2007). „Intrinsic functional architecture in the anaesthetized monkey brain“. In: *Nature* 447.7140, pp. 83–86.
- Vincent, J L, I Kahn, A Z Snyder, M E Raichle, and R L Buckner (2008). „Evidence for a Frontoparietal Control System Revealed by Intrinsic Functional Connectivity“. In: *Journal of Neurophysiology* 100.6, pp. 3328–3342.
- Voytek, B and R T Knight (2015). „Dynamic network communication as a unifying neural basis for cognition, development, aging, and disease.“ In: *Biological psychiatry* 77.12, pp. 1089–97.
- Wagner, T, A Valero-Cabre, and A Pascual-Leone (2007). „Noninvasive Human Brain Stimulation“. In: *Annual Review of Biomedical Engineering* 9.1, pp. 527–565.
- Wang, J, Z Zhang, G-J Ji, et al. (2015). „Frequency-Specific Alterations of Local Synchronization in Idiopathic Generalized Epilepsy“. In: *Medicine* 94.32, e1374.
- Wang, L, D F Hermens, I B Hickie, and J Lagopoulos (2012). „A systematic review of resting-state functional-MRI studies in major depression“. In: *Journal of Affective Disorders* 142.1-3, pp. 6–12.
- Wang, Li, Qingmei Kong, Ke Li, et al. (2016). „Frequency-dependent changes in amplitude of low-frequency oscillations in depression: A resting-state fMRI study“. In: *Neuroscience Letters* 614.June, pp. 105–111.
- Wang, X, Y Zhang, Z Long, et al. (2017). „Frequency-specific alteration of functional connectivity density in antipsychotic-naïve adolescents with early-onset schizophrenia“. In: *Journal of Psychiatric Research* 95, pp. 68–75.
- Wang, X-J (2010). „Neurophysiological and computational principles of cortical rhythms in cognition.“ In: *Physiological reviews* 90.3, pp. 1195–268.
- Watts, D J and S H Strogatz (1998). „Collective dynamics of ‘small-world’ networks“. In: *Nature* 393.6684, pp. 440–442.
- Wei, M, J Qin, R Yan, H Li, Z Yao, and Q Lu (2013). „Identifying major depressive disorder using Hurst exponent of resting-state brain networks“. In: *Psychiatry Research: Neuroimaging* 214.3, pp. 306–312.
- Wiebking, C, A Bauer, M de GRECK, N W Duncan, C Tempelmann, and G Northoff (2010). „Abnormal body perception and neural activity in the insula in depression: An fMRI study of the depressed “material me”“. In: *The World Journal of Biological Psychiatry* 11.3, pp. 538–549.
- Wise, R G, K Ide, M J Poulin, and I Tracey (2004). „Resting fluctuations in arterial carbon dioxide induce significant low frequency variations in BOLD signal“. In: *NeuroImage* 21.4, pp. 1652–1664.
- Wittmann, M (2009). „The inner experience of time.“ In: *Philosophical transactions of the Royal Society of London. Series B, Biological sciences* 364.1525, pp. 1955–67.

- Womelsdorf, T, J-M Schoffelen, R Oostenveld, et al. (2007). „Modulation of Neuronal Interactions Through Neuronal Synchronization“. In: *Science* 316.5831, pp. 1609–1612.
- Wu, C W, H Gu, H Lu, E A Stein, J-H Chen, and Y Yang (2008). „Frequency specificity of functional connectivity in brain networks“. In: *NeuroImage* 42.3, pp. 1047–1055.
- Wu, C W, C-L Chen, P-Y Liu, Y-P Chao, B B Biswal, and C-P Lin (2011a). „Empirical Evaluations of Slice-Timing, Smoothing, and Normalization Effects in Seed-Based, Resting-State Functional Magnetic Resonance Imaging Analyses“. In: *Brain Connectivity* 1.5, pp. 401–410.
- Wu, H, H Sun, J Xu, et al. (2016). „Changed Hub and Corresponding Functional Connectivity of Subgenual Anterior Cingulate Cortex in Major Depressive Disorder“. In: *Front. Neuroanat* 10, p. 120.
- Wu, M, C Andreescu, M A Butters, R Tamburo, C F Reynolds, and H Aizenstein (2011b). „Default-mode network connectivity and white matter burden in late-life depression.“ In: *Psychiatry research* 194.1, pp. 39–46.
- Xu, T, K R Cullen, B Mueller, et al. (2016). „Network analysis of functional brain connectivity in borderline personality disorder using resting-state fMRI“. In: *NeuroImage: Clinical* 11, pp. 302–315.
- Xue, S, X Wang, W Wang, J Liu, and J Qiu (2016). „Frequency-dependent alterations in regional homogeneity in major depression“. In: *Behavioural Brain Research* 306, pp. 13–19.
- Yaesoubi, M, E A Allen, R L Miller, and V D Calhoun (2015). „Dynamic coherence analysis of resting fMRI data to jointly capture state-based phase, frequency, and time-domain information“. In: *NeuroImage* 120, pp. 133–142.
- Yaesoubi, M, R L Miller, V D Calhoun, M S Cetin, R Miller, and G D Pearlson (2017). „Time-varying spectral power of resting-state fMRI networks reveal cross-frequency dependence in dynamic connectivity“. In: *PLOS ONE* 12.2, e0171647.
- Yao, Z, L Wang, Q Lu, H Liu, and G Teng (2009). „Regional homogeneity in depression and its relationship with separate depressive symptom clusters: A resting-state fMRI study“. In: *Journal of Affective Disorders* 115.3, pp. 430–438.
- Yeo, B T, F M Krienen, J Sepulcre, et al. (2011). „The organization of the human cerebral cortex estimated by intrinsic functional connectivity.“ In: *Journal of neurophysiology* 106.3, pp. 1125–65.
- Ystad, M, T Eichele, A J Lundervold, and A Lundervold (2010). „Subcortical functional connectivity and verbal episodic memory in healthy elderly—A resting state fMRI study“. In: *NeuroImage* 52.1, pp. 379–388.
- Zeki, S (2015). „Area V5-a microcosm of the visual brain.“ In: *Frontiers in integrative neuroscience* 9, p. 21.
- Zeki, S, J D Watson, C J Lueck, K J Friston, C Kennard, and R S Frackowiak (1991). „A direct demonstration of functional specialization in human visual cortex.“ In: *The Journal of neuroscience: the official journal of the Society for Neuroscience* 11.3, pp. 641–9.
- Zeng, L-L, L Liu, Y Liu, H Shen, Y Li, and D Hu (2012a). „Antidepressant treatment normalizes white matter volume in patients with major depression.“ In: *PloS one* 7.8, e44248.
- Zeng, L-L, H Shen, L Liu, et al. (2012b). „Identifying major depression using whole-brain functional connectivity: a multivariate pattern analysis“. In: *Brain* 135.5, pp. 1498–1507.

- Zhang, D and M E Raichle (2010). „Disease and the brain’s dark energy.“ In: *Nature reviews. Neurology* 6.1, pp. 15–28.
- Zhang, S, S Hu, H H Chao, and C-S Li (2016). „Resting-State Functional Connectivity of the Locus Coeruleus in Humans: In Comparison with the Ventral Tegmental Area/Substantia Nigra Pars Compacta and the Effects of Age“. In: *Cerebral Cortex* 26.8, pp. 3413–3427.
- Zhang, Y, C Zhu, H Chen, et al. (2015). „Frequency-dependent alterations in the amplitude of low-frequency fluctuations in social anxiety disorder“. In: *Journal of Affective Disorders* 174, pp. 329–335.
- Zhang, Z, M Liao, Z Yao, et al. (2017). „Frequency-Specific Functional Connectivity Density as an Effective Biomarker for Adolescent Generalized Anxiety Disorder“. In: *Frontiers in Human Neuroscience* 11, p. 549.
- Zhi, D, V D Calhoun, L Lv, et al. (2018). „Aberrant Dynamic Functional Network Connectivity and Graph Properties in Major Depressive Disorder“. In: *Frontiers in Psychiatry* 9, p. 339.
- Zhong, X, W Pu, and S Yao (2016). „Functional alterations of fronto-limbic circuit and default mode network systems in first-episode, drug-naïve patients with major depressive disorder: A meta-analysis of resting-state fMRI data“. In: *Journal of Affective Disorders* 206, pp. 280–286.
- Zhu, X, X Wang, J Xiao, et al. (2012). „Evidence of a Dissociation Pattern in Resting-State Default Mode Network Connectivity in First-Episode, Treatment-Naïve Major Depression Patients“. In: *Biological Psychiatry* 71.7, pp. 611–617.
- Zhu, X, Q Zhu, H Shen, W Liao, and F Yuan (2017). „Rumination and Default Mode Network Subsystems Connectivity in First-episode, Drug-Naïve Young Patients with Major Depressive Disorder“. In: *Scientific Reports* 7, p. 43105.
- Zuo, X N, A Di Martino, C Kelly, et al. (2010). „The oscillating brain: Complex and reliable“. In: *NeuroImage* 49.2, pp. 1432–1445.
- Zuo, X N, R Ehmke, M Mennes, et al. (2012). „Network Centrality in the Human Functional Connectome“. In: *Cerebral Cortex* 22.8, pp. 1862–1875.

List of Figures

1.1	Rhythms of the brain	5
1.2	Example RSNs and their power spectra	10
1.3	BOLD power spectra under different pharmacologic and neuropathologic conditions	16
1.4	SC: calculation workflow	23
3.1	Schematic analysis workflow for Dataset 2	40
3.2	Dataset 1: RSNs	44
3.3	Dataset 1: Results of the SC analysis	46
3.4	Dataset 2: RSNs	48
3.5	Dataset 2: Results of SC and PSC analyses	50
3.6	Dataset 2: Power spectra of the salience network in HC and MDD	52
3.7	Dataset 2: Seed-based FC of the SN in HC > MDD, and link to MDD symptomatology	54
3.8	Correspondence of RSN SC values across datasets	55
4.1	MDD: Gray Matter Atrophy	62
4.2	DC: HC	65
4.3	DC: HC > MDD	66
4.4	DC: HC > MDD, corrected for GMV	67
4.5	DC and MDD symptomatology	69
5.1	SC and the functional hierarchy within the visual system	74

List of Tables

3.1	Demographic and clinical characteristics	34
3.2	Dataset 1: RSN FC profiles and results of SC analysis	45
3.3	Dataset 2: Results of SC and PSC analyses	51
4.1	Demographic and clinical characteristics of 48 subjects	58
4.2	GMV: HC > MDD	63
A.1	Project 1: Correspondence between RSNs across study sites	94
A.2	Project 1: Dataset 2: FC profile of RSNs	95
B.1	Project 2: DC HC: full frequency range	98
B.2	Project 2: DC HC: 10 frequency bands	99
B.3	Project 2: DC HC > MDD: 10 frequency bands	102
B.4	Project 2: DC HC > MDD: 10 frequency bands, controlled for GMV . .	103

Acronyms

ACC anterior cingulate cortex.

ALFF amplitude of low-frequency fluctuations.

ANOVA analysis of variance.

BDI Beck Depression Inventory.

BOLD blood oxygen level dependent.

bpm beats per minute.

CAT12 Computational Anatomy Toolbox.

CBF cerebral blood flow.

CEN central executive network.

CSF cerebrospinal fluid.

CVR cerebral vascular reactivity.

dACC dorsal anterior cingulate cortex.

DC degree centrality.

dIPFC dorsolateral prefrontal cortex.

DMN default-mode network.

DSM–IV Diagnostic and Statistical Manual of Mental Disorders–IV.

ECoG electrocorticography.

EEG electroencephalography.

EPI Echo-Planar Imaging.

FC functional connectivity.

FFT Fast Fourier Transform.

FHWM full width at half maximum.

FIX FMRIB’s ICA-based Xnoiseifier.

fMRI functional magnetic resonance imaging.

FSL FMRIB Software Library.

FWE familywise error.

GABA gamma-Aminobutyric acid.

GAD generalized anxiety disorder.

GAF Global Assessment of Functioning.

GIFT Group ICA of fMRI Toolbox.

GLM general linear model.

GM gray matter.

GMV gray matter volume.

HAM–D Hamilton Rating Scale for Depression.

HC healthy controls.

HCP Human Connectome Project.

IC independent component.

ICA independent component analysis.

IPL inferior parietal lobule.

LFP local field potential.

LTMS long-term memory system.

MCC midcingulate cortex.

MDD major depressive disorder.

MEG magnetoencephalography.

MELODIC Multivariate Exploratory Linear Optimized Decomposition into Independent Components.

MNI Montreal Neurological Institute.

mPFC medial prefrontal cortex.

MPP minimal preprocessing pipelines.

MPRAGE Magnetization-Prepared Rapid Gradient-Echo.

MRI magnetic resonance imaging.

MRS Magnetic Resonance Spectroscopy.

OCD obsessive-compulsive disorder.

OFC orbitofrontal cortex.

PCA principal component analysis.

PCC posterior cingulate cortex.

PESTICA Physiologic Estimation by Temporal ICA.

PSC percent signal change.

ReHo regional homogeneity.

REST Resting-State fMRI Data Analysis Toolkit.

RETROICOR Retrospective Image Correction.

ROI region of interest.

rs-fMRI resting-state functional magnetic resonance imaging.

RSN resting-state network.

rTMS repeated pulses transcranial magnetic stimulation.

SC spectral centroid.

SCcorr corrected spectral centroid.

SCID Structured Clinical Interview.

SEM standard error of the mean.

SLOMOCO Slice-Oriented Motion Correction.

SN salience network.

SPM12 statistical parametric mapping.

SSRI selective serotonin reuptake inhibitors.

TE echo time.

TIV total intracranial volume.

TMS transcranial magnetic stimulation.

TR repetition time.

vACC ventral anterior cingulate cortex.

VBM voxel-based morphometry.

VTA ventral tegmental area.

WM white matter.

WMS working memory system.

Curriculum Vitae

Anja Kaja Ries, M.Sc., Ph.D. (c)

Technische Universität München (TUM) anja.ries@tum.de
Klinikum rechts der Isar LinkedIn
Dept. of Diagnostic & Interventional Neuroradiology +4915754613947
Ismaninger Str. 22, 81675, München

Education **Technische Universität München**
Ph.D., Medical Life Science and Technology, 2019.
Dissertation: Spectral analysis of resting-state fMRI BOLD signal in healthy subjects and patients suffering from major depressive disorder.

Ludwig-Maximilians-Universität München
M.Sc., Neuro-Cognitive Psychology (NCP), 2014.

University of Warsaw
B.Sc., Applications of Physics in Biology and Medicine
Major in Neuroinformatics, 2012.

Research **Klinikum rechts der Isar, Technische Universität München**
Research Assistant
Project: fMRI chronnectomics: electrophysiological underpinnings and impact of major depressive disorder on brain dynamics.
Supervisor: Dr. Afra Wohlschläger

Klinikum Großhadern, Ludwig-Maximilians-Universität München
Research Assistant
Master Thesis: Distinct and common brain networks recruited during human magnitude estimation: fMRI study.
Supervisor: Prof. Dr. Stefan Glasauer and Dr. Virginia Flanagan

Computational Neuroscience Group, Universitat Pompeu Fabra

Research Assistant

NCP Research Project: Large-scale modeling of resting-state BOLD activity.

Supervisor: Prof. Dr. Gustavo Deco

Psychiatric Clinic, Ludwig-Maximilians-Universität München

Research Assistant

NCP Research Project: Real-time fMRI neurofeedback training of the Anterior Cingulate Cortex in PTSD patients.

Supervisor: Prof. Dr. Kristina Hennig-Fast

Faculty of Physics, University of Warsaw

Research Assistant

Project: Designing a human-computer interface for paralysed people.

Supervisor: Prof. Dr. Piotr Durka

Languages Polish (native), German (native), English (C1), French (B1)

Skills Matlab, SPM, SPSS, \LaTeX , Python
Training in fMRI, EEG, tDCS

References Dr. Afra Wohlschläger
Dept. of Diagnostic and Interventional Neuroradiology
Technische Universität München
afra.wohlschlaeger@tum.de, +49(0)8941404665

Publications and awards related to this thesis

Awards

1. Doctoral Scholarship of the Studienstiftung des deutschen Volkes (2016–2018).

Scientific articles

1. **Anja Ries**, Catie Chang, Sarah Glim, Chun Meng, Christian Sorg and Afra Wohlschläger (2018). "Grading of frequency spectral centroid across resting-state networks". In: *Frontiers in Human Neuroscience* 12, p.436.
2. **Anja Ries**, Matthew Hollander, Sarah Glim, Chun Meng, Christian Sorg and Afra Wohlschläger (2018). "Frequency-dependent spatial distribution of functional hubs in the human brain and alterations in major depressive disorder". Manuscript submitted for publication.

Oral presentations

1. "Temporal architecture of fMRI intrinsic brain dynamics and alterations in major depressive disorder". FAPESP-BAYLAT workshop on *Multimodal approaches in experimental psychology and clinical neuroscience and psychiatry*. University of São Paulo, São Paulo, Brazil, November 2018.
2. "Frequency-resolved resting-state fMRI analysis in major depressive disorder". FAPESP-BAYLAT workshop on *Neural Basis of Stress, Fear and Anxiety*. University of São Paulo, Ribeirão Preto, Brazil, April 2018.

3. "Frequency spectrum of BOLD fluctuations and impaired synchronicity in depression". 5th HBP School on *Future Medicine: Brain Disease Neuroscience. Influencing clinical diagnoses and treatments by data mining analysis- and modelling-driven neuroscience*. Medical University Innsbruck, Obergurgl, Austria, December 2017.
4. "Spectral BOLD signal analysis" *Research Colloquium of the Neuroradiology Department*, Klinikum rechts der Isar, Munich, Germany, October 2017.
5. "Frequency spectrum of BOLD fluctuations relates to depressive symptoms". 5th Symposium of the TUM-Neuroimaging Center, Munich, Germany, July 2016.
6. "Spectral center of gravity of infra-slow BOLD fluctuations relates to symptom severity in major depressive disorder" *Research Colloquium of the Neuroradiology Department*, Klinikum rechts der Isar, Munich, Germany, June 2016.

Poster presentations

1. "Frequency-specific organization of functional hubs in the human brain and alterations in major depressive disorder". 6th Biennial Conference on Resting State and Brain Connectivity, Montreal, Canada, September 2018.
2. "Altered dynamics of fMRI intrinsic connectivity relate to changed patterns of information integration in major depressive disorder" Society for Neuroscience Conference, San Diego, California, November 2016.
3. "Dynamics of fMRI intrinsic connectivity networks dissociate between pathology markers and symptom markers in major depressive disorder" 5th Biennial Conference on Resting State and Brain Connectivity, Vienna, Austria, September 2016.

Colophon

This thesis was typeset with $\text{\LaTeX}2_{\epsilon}$. It uses the *Clean Thesis* style developed by Ricardo Langner. The design of the *Clean Thesis* style is inspired by user guide documents from Apple Inc.

Download the *Clean Thesis* style at <http://cleanthesis.der-ric.de/>.

